NEW IN-SITU EROSION TEST AND MAXIMUM ALLOWABLE SCOUR DEPTH AT BRIDGE ABUTMENTS

A Dissertation

by

MABEL CHEDID

Submitted to the Office of Graduate and Professional Studies of
Texas A&M University
in partial fulfillment of the requirements for the degree of

DOCTOR OF PHILOSOPHY

Chair of Committee,	Jean-Louis Briaud
Committee Members,	Charles Aubeny
	Cristine Morgan
	Marcelo Sanchez
Head of Department,	Robin Autenrieth

December 2018

Major Subject: Civil Engineering

ABSTRACT

Soil erosion problems present a major threat to the nation's infrastructure. These problems include but are not limited to bridge scour, levee overtopping, meander migration, dams' internal erosion, and embankments surface erosion. This research addresses two aspects of soil erosion. The first deals with quantifying soils erodibility while the second deals with the problem of bridge scour.

Many laboratory and, more recently, field tests have been proposed to measure soils erodibility. The first contribution of this research is a new in-situ erosion test, the Borehole Erosion Test (BET). This test consists of measuring the increase in the borehole diameter as a function of time for a given flow velocity during wet rotary drilling. The BET results in a soil erodibility profile along the entire depth of the borehole. BET tests are performed in clay and sand at the National Geotechnical Experimentation Sites at Texas A&M University. Computational Fluid Dynamics (CFD) simulations of the BET are conducted to determine the shear stress fields during the test. The experimental and numerical data are then used to compare soil erodibility results from the BET tests to those from the Erosion Function Apparatus (EFA) tests on soil samples extracted from the same borehole.

Bridge scour is the erosion of riverbed soils around bridge foundations at piers and abutments. Existing guidelines for maximum allowable scour are based on foundations stability criteria. An additional criterion must be considered when limiting scour depths at spill-through abutments where scour can cause slope stability failure of the embankment well before reaching

the depth endangering the foundations. The second contribution of this research consists of equations and guidelines for determining the maximum allowable scour depth at or near spill-through abutments. These guidelines are based on a combination of a review of the existing knowledge, DOT survey, analyses of different scour failure scenarios, slope stability simulations, and a study of case histories. They can be easily followed by bridge inspectors to judge the criticality of the measured or observed total scour at the abutments, including both contraction and local abutment scour.

DEDICATION

To my mother, Marie-Thérèse, because I owe it all to you.

ACKNOWLEDGEMENTS

I would like to express my utmost gratitude to my committee chair Prof. Jean-Louis Briaud for his generous support throughout my master and doctoral studies. Prof. Briaud opened up many doors for me to rewarding and challenging opportunities that, not a longtime ago, seemed completely out of reach. I believe taking on these challenges stretched my abilities and shaped me into the person I am today. I am forever grateful to him for being an exceptional leader and for making my journey in graduate school superior to any other.

I would also like to sincerely thank my committee members, Prof. Aubeny, Prof. Morgan, and Prof. Sanchez, for their contributions and guidance throughout the course of this research. Prof. Aubeny helped me addressing many issues in my research and without his contributions this PhD would not have been successful. Prof. Morgan provided insightful feedback and corrections to my research proposal and gave me valuable ideas on how to make the research findings more practical. Prof. Sanchez was and will always be my Go-To-Person in the face of any technical or personal difficulty.

A very special appreciation goes out to Prof. Garry Gregory for all the time he dedicated to guide me through his slope stability program. Despite the distance, Prof. Gregory and I visited a couple of times and spent a total of more than 10 hours on the phone during which he was always trying to debug my runs and helping me achieve accurate results effectively.

A heartfelt thank you also goes to my lifetime mentor and role model, Dr. Gebran Karam. It is impossible to count all the ways that Dr. Karam has helped me since my very first day as a

civil engineering student at the Lebanese American University. I will always be indebted to him and I hope one day I can be half the engineer he is.

I wish to thank my friends and colleagues and the Civil Engineering department faculty and staff for making my journey at Texas A&M University an enjoyable experience. I am also thankful for my friends in Lebanon for still being my supportive and cheerful friends, despite the fact that I was mostly missing in action for a long time now.

Last, but by no means least, I am the most thankful to my hardworking parents, Antoine and Marie-Thérèse, and to my golden best-friend and sister, Yara, for their unfailing encouragement and miraculous love. And here is where words fail.

CONTRIBUTORS AND FUNDING SOURCES

Contributors

This research was supported by a dissertation committee consisting of the student academic advisor and committee chair Professors Jean-Louis Briaud, and professors Charles Aubeny, and Marcelo Sanchez of the Department of Civil Engineering and Professor Cristine Morgan of the Department of Soil and Crop Sciences.

Professor Hamn-Ching Chen of the Department of Civil Engineering provided tremendous help with the computational fluid dynamic numerical simulations for the Borehole Erosion Test. The fieldwork for the Borehole Erosion Test was conducted in collaboration with Fugro and Terracon. The case histories of scoured abutments in Texas were provided by the Texas Department of Transportation, Bryan and Austin offices. The Texas department of Transportation also helped with the distribution of an introductory survey to the states' departments of transportation to identify their current guidelines and practices regarding the maximum allowable scour depth.

Funding Sources

The development of the borehole erosion test was sponsored by the Texas A&M University Transportation Institute. The work on the maximum allowable scour depth at bridge abutments was performed under the Texas Department of Transportation Project 0-6935 by the Texas A&M University Transportation Institute.

TABLE OF CONTENTS

Page

Page

Page

LIST OF FIGURES

Page

Page

Page

Page

Page

LIST OF TABLES

Page

Page

1. INTRODUCTION

1.1 Soil Erosion and Bridge Scour

Soil erosion problems present a major threat to the nation's infrastructure. These problems include but are not limited to bridge scour, levee overtopping, meander migration, dam's internal erosion, and embankments surface erosion. Any soil erosion problem is composed of three components: the soil or rock, the water and the obstacle with which the water is interacting. The soil resistance to erosion is described by its erodibility. The erodibility of a soil or rock is defined as the relationship between the erosion rate $\dot{z}$ of the soil surface and the water velocity v or interface hydraulic shear stress τ. This relationship is called the erosion function and serves as the fundamental constitutive law for soil erosion problems much like the stress strain curve is the fundamental constitutive law for deformation problems. The best way to predict the erodibility of a soil is to measure it directly on a site specific basis by in-situ testing in the field or by testing samples in the laboratory. Many tests have been proposed over the last 25 years starting with laboratory tests and more recently with in-situ tests.

Scour is the erosion of riverbed soils caused by the water flow. Two main forms of scour are general scour and bridge scour. General scour is a natural phenomenon caused by the aggradation and degradation of bed materials. This form of scour may occur at any section of the river that is subject to channel instability, regardless of whether a bridge is located in this section. On the other hand, bridge scour is the scour occurring at the bridge supports, i.e. bridge piers and abutments. Bridge scour can be contraction scour and local scour. Contraction scour is caused by the reduction of the water flow cross-sectional area at the bridge section due to the presence of

piers, abutments, approach embankments and pressure flow condition (vertical contraction). Local scour is caused by the presence of obstructions in the watercourse at the bridge section. Two types of local scour exist: pier scour and abutment scour.

Bridge scour is the number one cause of bridge failure in the United States. Between the years 1966 and 2005, there were 1502 bridge failures of which 60% can be related to scour problems. This amounts to one bridge failure due to scour every 17 days. This alarming statistic was behind the funding invested in scour research over the last 30 years estimated at 25 million dollars. As a result, the rate of bridge failure has dropped significantly to 1 bridge every 120 days. While previous research efforts mostly focus on the prediction of the scour depth at bridge supports, little to no attention was given to the determination of maximum allowable scour depth which is a key input when deciding when to implement remedial measures for existing bridges. Texas has around 9.7% of the nation's bridges over waterways. With such a large bridge population, it makes sense to assume that Texas spends a tremendous amount of money yearly in its effort to repair scour damaged bridges and install scour countermeasures at bridges where a scour damage is probable. Unfortunately, providing scour countermeasures at all existing bridges to ensure acceptable scour resistance is economically infeasible. Therefore, risk-informed decisions following a scour evaluation must be taken to ensure the greatest impact and most effective use of the state's limited resources. Here is where the maximum allowable scour depth plays a crucial role in deciding when corrective measures should be taken to ensure public safety at the minimum cost possible.

A scour evaluation program does not reflect a complete picture of the scour condition at an existing bridge if the effects of the calculated scour depth on the bridge stability was not assessed. Similarly, a bridge engineer or inspector facing a bridge with a scour problem must be able to

decide whether the measured scour depth is excessive or not. In addition, engineers must have a solid prioritization scheme allowing them to address bridges with scour problems in the order of decreasing scour criticality. Therefore, guidelines on the determination of maximum allowable limits of scour depth are needed to compare the calculated or measured scour the scour limits and subsequently judge the stability of the bridge foundations.

The Texas Department of Transportation (TxDOT) already has guidance for the determination of the maximum allowable scour depth at piers with pile or drilled shaft foundations. Scour at abutments should also be limited to prevent the potential failure of the abutment foundation due to the loss of lateral stability and/or bearing capacity. Nevertheless, scour at the abutment may cause a slope stability failure of the approach embankment and make the bridge inaccessible to traffic. Therefore, the allowable depth of scour at/near the abutment must take into consideration the abutment embankment stability in addition to the abutment foundation stability. In fact, the slope stability failure is expected to control the allowable scour depths at spill-through abutments supported by deep foundations which are the most common type of abutments in Texas.

1.2 Objectives

The objective of this research is twofold. The first is related to quantifying soils erodibility. For this purpose, a new in-situ test, the Borehole Erosion Test or BET is developed. The second is related to the specific soil erosion problem of bridge scour. It consists of developing guidelines and practical recommendations for the determination of the maximum allowable scour depth at abutments. Simplified formulations have already been developed to estimate the depth of scour at/near the abutment causing the failure of the embankment slope for uniform cohesionless soils.

This research advances the concept of failure scour depth to account for varying combinations of embankment and channel soils, abutment geometries and water conditions.

1.3 Motivation

Millions of kilometers of boreholes are drilled each year for geotechnical projects. The drilling technique primarily consists of rotating a hollow drilling bit at the end of hollow drill rods while circulating drilling fluid down the rods. The drill bit cuts the soil and the cuttings are brought back to the surface by the returning drilling fluid. It is called wet rotary drilling or WRD. This circulation of drilling fluid is an erosion test because the borehole diameter D increases as a function of the circulating water velocity v (Figure 1a). The relationship between D and v can be transformed into the fundamental erosion function used in all erosion studies (Figure 1b). The fact that millions of kilometers of erosion testing are performed each year though out the world without recording the results is the main drive of developing the Borehole Erosion Test, BET (Briaud, 2014).

The second research objective, determining the maximum allowable scour depths at bridge abutments, is mainly propelled by the frequent failures of bridge abutments in Texas due to the recent floorings and high flow events. There is a pressing need to quickly evaluate the stability of the bridge when exposed to scour at/near the abutments to minimize failures. Comparing the observed or the calculated scour depth to an allowable scour depth is the key for assessing the bridge scour condition and the need for implementing remedial measures. Yet, there is an obvious imbalance between the advancement in scour predictions and scour measurement techniques on one side, and the lack of a stability criteria to limit scour on the other side. This gap in a scour

evaluation program can be justified by the great variability of bridge site conditions. Indeed, different bridges have different

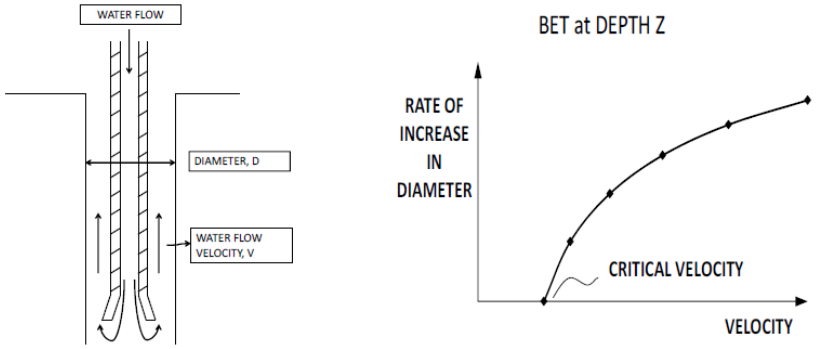

(a) (b)

Figure 1- Borehole erosion test concept (reprinted from Briaud et al. 2017, with permission from ASCE): (a) sketch of the BET; (b) erosion function obtained at one depth

structural, geotechnical and hydraulic conditions and subsequently different responses to scour. This makes it inappropriate to limit scour depth at all the sites to one absolute threshold depth. However, site-specific allowable scour depths can be determined by following systematic guidelines, just like scour depths are estimated at different sites by applying the same prediction equations. The guidelines for the determination of allowable scour depths are based on thorough stability analyses of different scour failure scenarios for different site conditions. At the same time, the final recommendations would be practical and easily used by bridge inspectors to assess the bridge condition and justify the need of seeking higher order structural analysis, when needed.

1.4 Methodology

1.4.1 The Borehole Erosion Test

First, a review of the existing erosion tests is carried out to make sure that the research idea has not been explored previously. Second, the procedure of the test is developed and the necessary equipment is selected. Pilot BET tests are then performed in cooperation with Fugro and Terracon at the National Geotechnical Experimentation Sites at Texas A&M University National (NGES-TAMU). Soil samples are retrieved from the same boreholes where the BET is performed and are brought back to the laboratory. Index properties tests and Erosion Function Apparatus (EFA) tests are conducted. Computational Fluid Dynamics (CFD) numerical simulations of the velocity and shear stress fields for the BET are performed. The experimental and numerical tests results are analyzed and the erosion functions from the EFA and the BET are constructed and compared. This comparison serves as a validation of the new BET test.

1.4.2 Maximum Allowable Scour Depth at Bridge Abutments

The approach selected to develop guidelines for allowable scour depth is based on a combination of a review of the existing knowledge, a survey questionnaire sent to state Departments of Transportation (DOTs), a study of case histories, analyses of different scour failure scenarios, slope stability simulations, and verification of the proposed method against available data. The review of existing knowledge proves that this research is sorely needed since very little information was found on allowable scour depths. The DOT survey helps in identifying the current DOT practices no scour limits. The survey responses show the lack of well-defined recommendations for allowable scour depth. The case histories were collected partly to infer possible failure mechanisms that a bridge can experience due to scour at or near its abutment. The

analyses of possible scour failure scenarios result in four different failure modes a bridge can experience due to scour at its abutment: foundation failure due to vertical loading, foundation failure due to lateral loading, embankment slope failure, and lateral erosion of embankment soils. The controlling failure mode of bridge abutments in Texas is expected to be slope stability failure of the spill-through embankment. For this reason, slope stability simulations are performed using 2D limit equilibrium methods to analyze the stability of abutment embankments when exposed to excessive scour and find the scour depths causing failures. The simulations account for the variability of the various geometry, geotechnical, scour and hydraulic parameters. As a result of these simulations, guidelines and recommendations on the maximum allowable scour at or near abutments are developed. The proposed equations and guidelines are validated using the collected case histories.

1.5 New Contributions

1.5.1 The Borehole Erosion Test

The borehole erosion test or BET is a new in-situ erosion test developed to measure soil's erodibility under the in-situ stress environment. It consists of drilling a borehole by the wet rotary method while measuring the increase in diameter of the hole as a function of depth and as a function of time. Therefore, the BET only represents an incremental work when boreholes are drilled for the purpose of soil identification. It does not require special equipment and anyone performing wet rotary drilling can carry the test. The BET is to erosion what the Cone Penetrometer Test (CPT) is to strength; each test gives a continuous soil erosion function covering all the borehole depth. This would require tests on many samples if laboratory erosion tests were

to be conducted. Overall, the BET is a routine, reliable and quick test considering the amount of data collected.

1.5.2 Maximum Allowable Scour Depth at Bridge Abutments

The guidelines for the determination of maximum allowable scour depth at bridge abutments are key components for the evaluation of the scour condition at new or existing brides. In the absence of scour limits, critical scour depths at or near a bridge abutments might go unnoticed leading to catastrophic bridge failures. On the other side, unnecessary repairs, where the observed scour is actually less than the proposed scour limit, would waste the limited state resources. Therefore, the guidelines results in an improved rating of the infrastructure condition and can be integrated into a prioritization scheme for maintaining existing bridges with scoured abutments. They also improve the resilience and sustainability of bridge abutments designs to avoid scour failures rather than trying to mitigate them. Other positive contributions from the application of the developed guidelines for the determination of maximum allowable scour at or near the abutments include an increased bridge service life, and reduced construction, operations and maintenance costs. Most importantly, these guidelines offer the drivers increased safety by reducing bridge failures and associated social, economic, and environmental consequences.

2. BACKGROUND KNOWLEDGE

2.1 Review of Existing Soil and Rock Erosion Tests

The following erosion tests are the most common tests used in research and practice today. The development of these tests has taken place in the laboratory over the last 50 years and in the field as in situ tests over the last 10 years. In the laboratory, they are the Erosion Function Apparatus (EFA) test (Briaud et al. 2001b; Briaud 2013) and similar versions (McNeil et al. 1996; Roberts et al. 2003; Trammell 2004; Crowley et al. 2012; Shan and Kerenyi 2014; Shan et al. 2015), the Jet Erosion Test (JET) (Hanson 1990; Hanson and Cook 2004; USSD 2011), the Hole Erosion Test (HET) (Wan and Fell 2004; Lefebvre et al. 1985; Wahl 2010; Benahmed and Bonelli 2012) as an evolution of the Pinhole test (ASTM 2006), and the Rotating Cylinder Test (RCT) (Moore and Masch 1962; Chapuis and Gatien 1986; Bloomquist et al. 2012). In the field, the in situ tests are the In Situ Erosion Evaluation Probe (ISEEP) (Gabr 2014), the In Situ Scour Testing Device (ISTD) (Kerenyi, personal communication, 2014), the Pocket Erodometer Test (PET) (Briaud et al. 2012), and the new Borehole Erosion Test (BET) (Briaud 2014). They all have advantages and drawbacks as well as a range of applications. The BET was developed as an in-situ test which does not require any special equipment or expertise, is relatively rapid and gives a complete soil erodibility profile. The EFA was used to evaluate the results of the BET by testing samples from the same borehole. As such, a short summary of the EFA test is given next.

The development of the EFA test (Figure 2) and associated design guidelines for bridge scour, levee overtopping, and meander migration started in 1991 and can be credited to Briaud et al. (2001b) Briaud (2013). It is a laboratory erosion test that consists of having a soil sample pushed through the bottom of a conduit only as fast as it is eroded by the water flowing over it. The erosion

rate measured as the rate of advancement of the piston is recorded for each velocity and point by point the erosion rate versus velocity or shear stress (erosion function) is measured. The shear stress is calculated based on the measured mean flow velocity and Moody's chart (Moody 1944; Briaud 2013). The erosion function (erosion rate versus velocity or shear stress) is the outcome of this test. Based on many tests performed over the last 25 years, Briaud (2008) proposed an erosion classification (Figure 3) and related the soil classification to the erosion classification by placing the dual symbols of the United Soil Classification System (USCS) in the erosion chart (Briaud 2013).

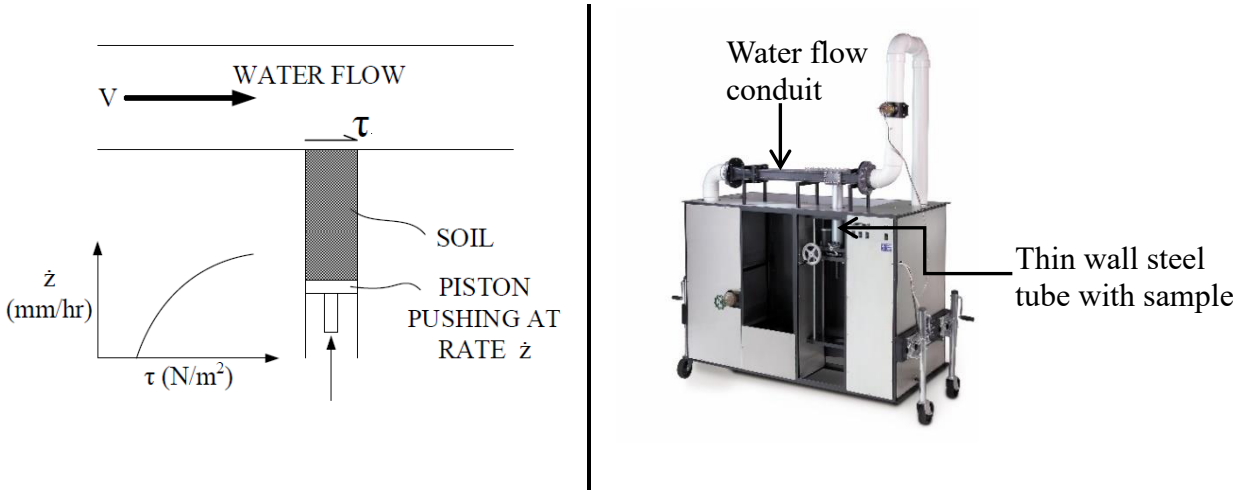

Figure 2- EFA type of test (reprinted from Briaud et al. 2017, with permission from ASCE)

2.2 Review of the Regulations and Practices related to Scour Evaluation

After the scour failures of the Schoharie Bridge in New York in 1987 and the Hatchie Bridge in Tennessee in 1989, the Code of Federal Regulations, 23 CFR 650 Subpart C- National Bridge Inspection Standards (NBIS), was reviewed to require the identification of scour critical bridges. This regulation by the Federal Highway Administration (FHWA) defines a scour critical

bridge as “a bridge with a foundation element that has been determined to be unstable for the observed or evaluated scour condition” (FHWA 2004). The revised inspection procedures also require that all scour critical bridges be monitored based on a well-developed plan of action.

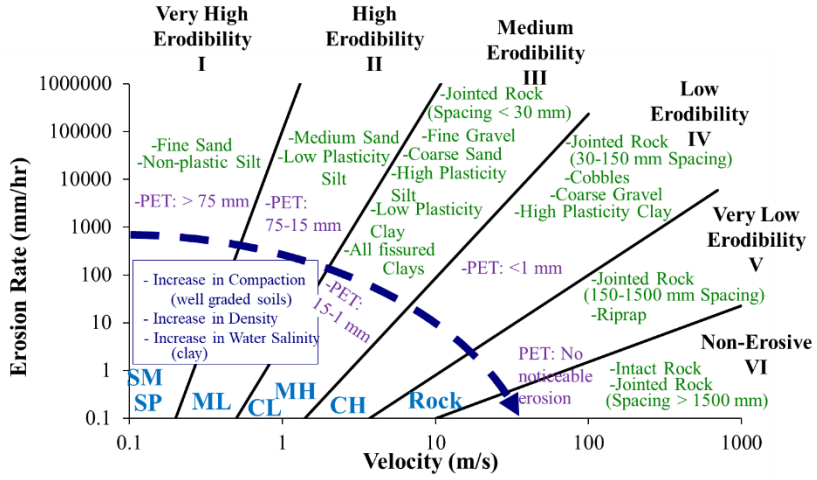

(a)

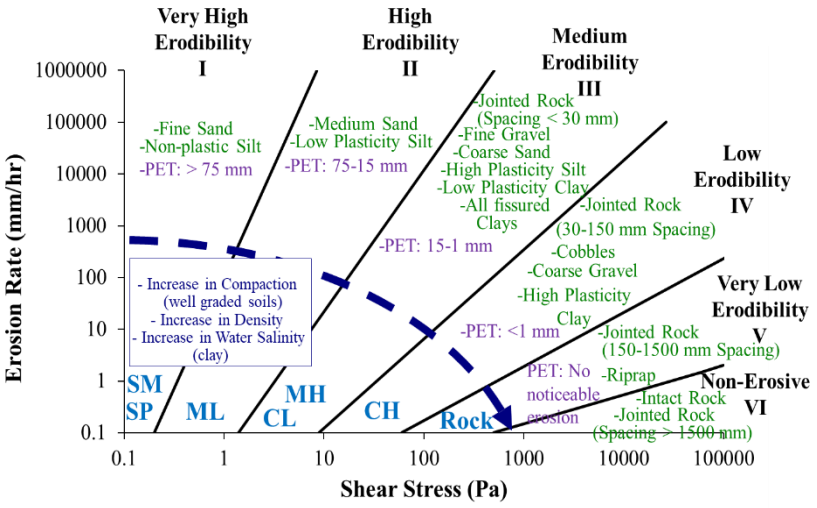

(b)

Figure 3- Erosion classification and soil types (reprinted from Briaud et. al 2017, with permission from ASCE): (a) velocity; (b) shear stress

To facilitate the compliance with this regulation, the FHWA technical advisory T5140.23 (FHWA 1991) and the Hydraulic Engineering Circular (HEC) 18 (Arneson et al. 2012) offer recommendations for the development and implementation of scour evaluation guidelines and procedures. In short, a scour evaluation program for new bridges should begin by selecting the scour design flood and the scour design check flood frequencies using a risk-based approach. Prior to this approach, new bridges were designed to resist the scour effects resulting from the 100-year flood without failing and are further checked against the 500-year flood. The hydraulic parameters studies required for scour calculations are then developed for the selected flood events using a hydraulic model. The total scour depth is then estimated using the prediction equations summarized in the next section. The stability of the designed bridge and its foundations is finally evaluated considering that all the streambed soil above the total scour depth has been removed. If the structure is found to be unstable under the scour design flood or the scour design check flood (ultimate load), the bridge design is revised and the analysis is repeated. On the other hand, existing bridges are first required to undergo an initial screening to develop a priority list of scour susceptible bridges. The list is then conveyed to an interdisciplinary team of hydraulic, structural, and geotechnical engineers, which perform the scour evaluation of the bridges on the list. As a result, scour critical bridges are identified and a plan of action including a suitable course of remedial actions is developed and implemented.

In accordance with the NBIS, each state or federal agency has to keep an inventory of all the inspected bridges in which some Structure Inventory and Appraisal data should be collected and recorded. When combined, the states' bridge inventories form the National Bridge Inventory (NBI). FHWA provided a tabulation sheet where the Structure Inventory and Appraisal data to be recorded are organized into 116 items. The bridge scour condition is recorded under Item 113-

Scour Critical Bridges. The Recording and Coding Guide for the Structure Inventory and Appraisal of the Nation's Bridges (FHWA 1995) outlines the coding guidelines for each of the items. In particular, this guide calls for the use of one digit to describe the bridge susceptibility to scour in Item 113. Table 1 presents the different single-digit codes in order of increased scour severity and their respective significance, as described in the recording and coding guide.

Table 1- Description of single-digit codes in Item 113

Code	Description
N	Bridge not over waterway.
U	Bridge with unknown foundation. Bridge not evaluated for scour. A plan of action and monitoring are required to reduce the risk of failure during a flood event.
T	Bridge over tidal waters. Bridge not evaluated for scour. Regular inspections and monitoring are required until bridge scour is evaluated.
9	Bridge foundation on dry land with no risk of scour.
8	Bridge with stable foundations for observed or calculated scour; scour depth is above the foundation top (Figure 4; the crossed line in Figure 4 refers to the estimated scour depth).
7	A previous scour problem was corrected, and bridge is no longer scour critical.
6	Scour has not been evaluated yet.
5	Bridge with stable foundations for observed or calculated scour; scour depth is within the foundation depth (Figure 5; the crossed line in Figure 5 refers to the estimated scour depth).
4	Bridge with stable foundations for calculated scour. However, field observation requires corrective measures to protect the exposed foundation from additional erosion.
3	Bridge is scour critical. Bridge foundations are found to be unstable for the assessed scour, which may be either within the depth of the foundation (Figure 5) or below the foundation bottom (Figure 6; the crossed line in Figure 6 refers to the estimated scour depth).
2	Bridge is scour critical. Field review reveals excessive scour making the bridge foundations unstable and urging for immediate corrective measures.
1	Bridge is scour critical. Field observation indicates that the bridge foundation or abutment is near failure. Bridge is closed to traffic.
0	Bridge is scour critical. Bridge failure has occurred. Bridge is closed to traffic.

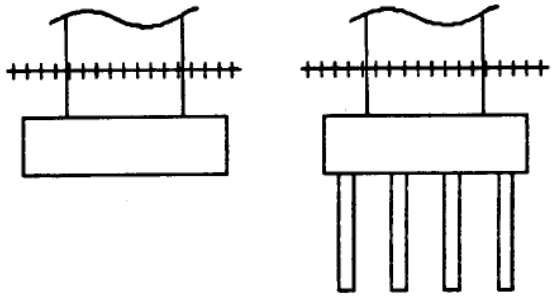

Figure 4- Scour depth above foundation top (reprinted from FHWA 1995)

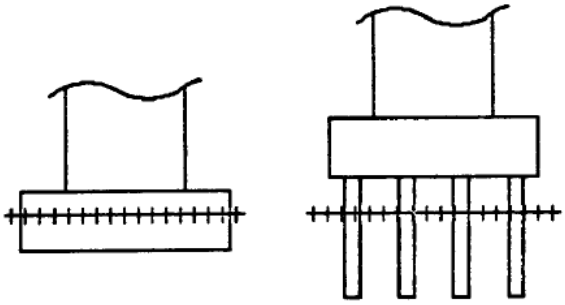

Figure 5- Scour depth within foundation limit (reprinted from FHWA 1995)

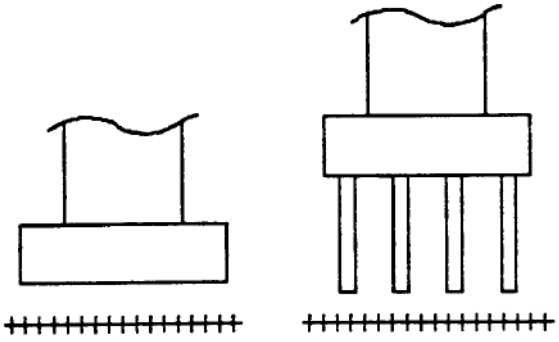

Figure 6- Scour depth below foundation bottom (reprinted from FHWA 1995)

Based on this guide, a scour depth, assessed by field review or predicted by a scour evaluation, is considered critical if it affects the stability of the bridge foundations at the piers and abutments. The item further indicates that an unstable condition may be determined by either a comparison of the calculated scour to the observed one during inspection or by an engineering analysis of the observed scour during inspection.

Following the FHWA regulations and guidelines, each DOT developed its own bridge scour evaluation program and to date more than half of the DOTs have assessed 90 percent or more of their bridges over waterways for their vulnerability to scour. In particular, TxDOT maintains the Bridge Inventory Inspection and Appraisal Program database, which can be regarded as a state-level equivalent of the NBI (Haas et al. 1999). The Bridge Inventory Inspection and Appraisal Program includes 135 fields, two of which are scour-related:

- Item 113—typical scour coding: a single-digit code rating the bridge scour condition as described previously (Table 1).
- Item 113.1—additional TxDOT coding: a single-digit code assessing the scour vulnerability of bridges with unknown foundation and bridges where a scour plan of action has been written and implemented (Table 2).

The coding is based on an evaluation of the scour depth and on a stability analysis of the bridge foundation elements. TxDOT performs bridge scour evaluations following the guidelines of HEC-18 and the Geotechnical Manual (Delphia n.d.). Chapter 5- Foundation Design, Section 5-Scour of the Geotechnical Manual indicates which prediction equation in HEC-18 to use for calculating pier and contraction scour in channels with different soil types (TxDOT, 2018). Instead of calculating abutment scour, TxDOT requires providing the appropriate protection to prevent any potential abutment scour.

Table 2- Description of single-digit codes in Item 113.1

Code	Description
A	Bridge foundation is unknown, and screening indicates a low risk of scour.
B	Bridge foundation is unknown, and screening indicates that bridge is scour critical. Plan of action is in place.
C	Bridge foundation is unknown, and screening indicates that bridge is scour critical. No plan of action is in place.
D	Bridge foundation is unknown, and bridge is closed to traffic. Plan of action is in place.
E	Bridge foundation is unknown, and bridge is closed to traffic. No plan of action is in place.
P	Bridge with a scour plan of action in place.

The Texas Secondary Evaluation and Analysis for Scour (TSEAS) can be used to ensure that existing bridges can withstand the effects of scour without failing. The TSEAS Manual includes both an observational scour analysis and an engineering scour analysis (TxDOT 1993). The observational analysis is referred to as secondary screening and contains 11 questions intended to identify the risk factors signalizing a potential stream stability problem or bridge scour problem or both (bridge scour and stream stability) problems. If this observational analysis reveals bridge scour related problems, an engineering scour analysis entitled concise analysis follows. The concise analysis estimates the maximum allowable scour depth, the maximum pier scour depth, and subsequently the maximum allowable contraction scour depth to assess whether the bridge will be stable if the contraction scour is superimposed onto the pier scour. The TSEAS concise analysis can be considered as a significant abbreviation of the standard detailed analysis. For instance, the TSEAS concise analysis uses simply derived hydraulic variables from construction plans or bridge design files while the standard detailed scour analysis requires a step backwater analysis and extensive data manipulation. In fact, the TSEAS was designed to minimize the cost, time, and effort level required to perform a detailed scour analysis, especially when the initial

screening conservatively leaves out many bridges for further evaluation. The use of the TSEAS has been restricted to low volume off-system bridges.

2.3 Scour Components and Prediction Equations

Scour is the erosion of riverbed soils caused by the water flow. Two main forms of scour are general scour and bridge scour. General scour is a natural phenomenon caused by the aggradation and degradation of bed materials. This form of scour may occur at any section of the river that is subject to channel instability, regardless of whether a bridge is in this section. On the other hand, bridge scour is the scour occurring at the bridge supports (i.e., bridge piers and abutments). Bridge scour can be contraction scour and local scour. Contraction scour is caused by the reduction of the water flow cross-sectional area at the bridge section due to the presence of piers, abutments, approach embankments, and pressure flow condition (vertical contraction). Local scour is caused by the presence of obstructions in the watercourse at the bridge section. Two types of local scour exist: pier scour and abutment scour. Figure 7 presents the contraction, pier, and abutment scour components. This figure indicates that abutment scour already includes contraction scour, but that pier scour and contraction scour are cumulative.

2.3.1 Pier Scour

Pier scour is the erosion of bed material at the pier base due to the acceleration of the flow and the formation of vortices around the pier. Various pier scour equations were developed based on extensive laboratory studies. Most of the prediction equations apply solely for cohesionless bed material. Ultimately, scour of cohesive materials may be as deep as scour of cohesionless sand-bed. However, cohesive materials erode at a much slower rate, which is strongly related to the

geotechnical and physical properties of the cohesive soils. For this reason, pier scour equations for cohesionless soils would overestimate the scour depth when applied on cohesive beds. The most commonly used pier scour equations for cohesionless soils are presented next and an equation for the maximum pier scour in cohesive materials is also presented.

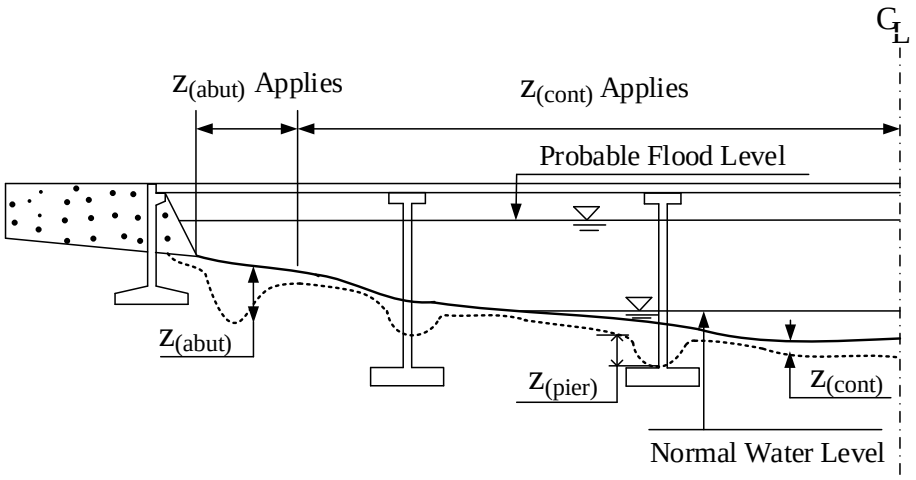

Figure 7- Scour components

The HEC-18 equation (Eq. 2-1) is based on the Colorado State University equation with some modifications to account for the effect of bed condition, size of bed soil, and wide piers:

$$\frac{y_s}{a} = 2.0 K_1 K_2 K_3 \left(\frac{y_1}{a}\right)^{0.35} Fr_1^{0.43} \qquad \text{(Eq. 2-1)}$$

where y_s is the scour depth, y_1 is the flow depth upstream of the pier, K_1 is the correction factor for pier nose shape, K_2 is the correction factor for angle of attack, K_3 is the correction factor for bed condition, a is the pier width, Fr_1 is the Froude number upstream of the pier ($Fr_1 = \frac{V_1}{(gy_1)^{1/2}}$, with V_1 being the mean approach velocity and g the acceleration of gravity).

As a result of comparing the calculated pier scour depths using Eq. 2-1 with field and laboratory data, HEC-18 recommends the following limiting ratio for circular piers aligned with the flow:

$$\frac{y_s}{a} \leq 2.4 \text{ for } Fr \leq 0.8$$

$$\frac{y_s}{a} \leq 3.0 \text{ for } Fr > 0.8$$

The Florida Department of Transportation (FDOT) pier scour analysis methodology is based on a National Cooperative Highway Research Program (NCHRP) study that improved the Sheppard and Miller equation. The NCHRP equation includes all the factors considered in the HEC-18 equation and also accounts for particle size. This equation has been incorporated in all the versions of HEC-18 and is widely used for bridge scour evaluations and design. The FDOT has expanded the NCHRP equation into a pier scour analysis methodology described by Eqs. 2-2, 2-3, and 2-4:

$$\frac{y_s}{a^*} = 2.5 f_1 f_2 f_3 \qquad \text{for } 0.4 \leq \frac{V_1}{V_c} < 1.0 \qquad \text{(Eq. 2-2)}$$

$$\frac{y_s}{a^*} = f_1 \left[2.2 \left(\frac{\frac{V_1}{V_c} - 1}{\frac{V_{lp}}{V_c} - 1} \right) + 2.5 f_3 \left(\frac{\frac{V_{lp}}{V_c} - \frac{V_1}{V_c}}{\frac{V_{lp}}{V_c} - 1} \right) \right] \qquad \text{for } 1.0 \leq \frac{V_1}{V_c} \leq \frac{V_{lp}}{V_c} \qquad \text{(Eq. 2-3)}$$

$$\frac{y_s}{a^*} = 2.2 f_1 \qquad \text{for } \frac{V_1}{V_c} > \frac{V_{lp}}{V_c} \qquad \text{(Eq. 2-4)}$$

with:

$$f_1 = \tanh\left[\left(\frac{y_1}{a^*} \right)^{0.4} \right]$$

$$f_2 = \left[1 - 1.2 \left[\ln\left(\frac{V_1}{V_c} \right) \right]^2 \right]$$

$$f_3 = \left[\frac{\left(\frac{a^*}{D_{50}} \right)^{1.13}}{10.6 + .04 \left(\frac{a^*}{D_{50}} \right)^{1.33}} \right]$$

where y_s is the scour depth, a^* is the effective pier width combining the effects of pier shape and angle of attack, V_1 is the approach mean velocity, V_{lp} is the velocity of the live-bed pier scour estimated as $5V_c$ or $0.6\sqrt{gy_1}$ (whichever is greater), V_c is the critical velocity calculated as a function of D_{50} and y_1, D_{50} is the median particle size of the bed material, and y_1 is the flow depth upstream of the pier.

The FDOT scour methodology divides scour into four regions (Figure 8):

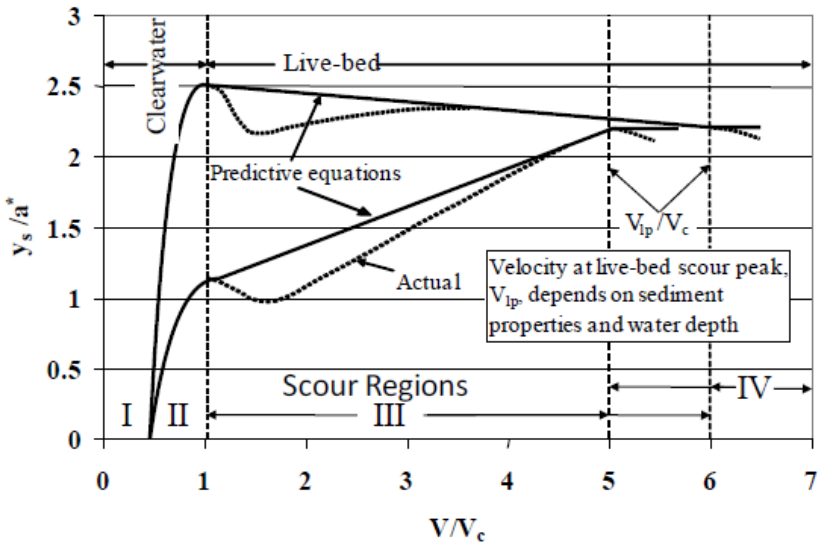

Figure 8- FDOT scour analysis methodology (reprinted from Arneson et al. 2012)

- Scour Region I: $V_1 < 0.4V_c$, clear water conditions with no scour.
- Scour Region II: $0.4V_c < V_1 < V_c$, clear water conditions with pier scour calculated using Eq. 2-2. In fact, the scour depth in this region can be seen as a fraction of the scour depth at the critical velocity y_{s-c}; $y_s = f_2 y_{s-c}$ where $y_{s-c} = 2.5 f_1 f_3 a^*$.

- Scour Region III: $V_c < V_1 < V_{lp}$, live-bed scour conditions with pier scour depth calculated by Eq. 2-3, which is essentially a linear interpolation between the scour depth at critical velocity y_{s-c} and the scour depth at live-bed peak velocity $y_{s-lp} = 2.2 f_1 a^*$;

  $$y_s = y_{s-c} + \frac{(V_1 - V_c)}{(V_{lp} - V_c)}(y_{s-lp} - y_{s-c}).$$

- Scour Region IV: $V_1 \geq V_{lp}$, live-bed scour conditions with pier scour depth assigned the value of the maximum live-bed scour y_{s-lp} (Eq. 2-4).

Briaud et al. (2011) developed an equation for the maximum pier scour depth based on flume test results and dimensional analysis. This equation is included in the latest version of HEC-18. While it is described as an equation for pier scour in cohesive materials, it is actually applicable to both cohesionless and cohesive soils as demonstrated in the NCHRP study, which led to:

$$y_s = 2.2 K_1 K_2 a^{0.65} \left(\frac{2.6 V_1 - V_c}{\sqrt{g}}\right)^{0.7} \quad \text{(Eq. 2-5)}$$

where y_s is the maximum pier scour depth, y_1 is the flow depth upstream of the pier, K_1 is the correction factor for pier nose shape, K_2 is the correction factor for angle of attack, a is the pier width, V_1 is the mean approach velocity, V_c is the critical velocity, and g the acceleration of gravity. The maximum pier scour is the maximum depth of the hole that can form around the pier. For cohesive materials characterized by low erosion rates, this depth is not normally reached during a single flood event. Once the maximum pier scour depth is computed, the SRICOS (Scour Rate In COhesive Soil) method (Briaud et al. 2011) can then be used to perform a time dependent analysis and predict the scour versus time for cohesive soils.

2.3.2 Contraction Scour

Contraction scour is the lowering of the river bed across the bridge section due to the reduction in the area available for the flow at this section. Computation of contraction scour involves two regions of the river: the approach or uncontracted zone (zone 1) and the contracted zone (zone 2). Contraction scour can either be live-bed scour or clear-water scour. Live-bed condition occurs when the eroding flow transports bed materials from the approach section into the bridge section. Clear water contraction occurs when the shear stress in the approach section is under the critical shear stress of the bed material in that section, so no sediments are transported into the contracted area. The clear water condition includes the case where sediments are transported through the bridge section in suspension mode. As the scour depth increases, the flow area increases and the shear stress decreases. Live-bed scour ends when the shear stress decreases to a point such that the sediment transport into the contracted bridge section is equal to the sediment transport out of this section. On the other hand, clear water contraction ends when the shear stress decreases to the critical shear stress of the bed material in the contracted section.

HEC-18 recommends the use of the following modified version of Laursen's equation to estimate the average live-bed contraction scour depth, y_s:

$$\frac{y_2}{y_1} = \left(\frac{Q_2}{Q_1}\right)^{6/7} \left(\frac{W_1}{W_2}\right)^{k_1} \qquad \text{(Eq. 2-6)}$$

$$y_s = y_2 - y_0$$

where y_1 is the average flow depth in the approach main channel, y_2 is the average flow depth in the bridge contracted section after scour, y_0 is the flow depth in the contracted section prior to scour, Q_1 is the flow in the approach channel transporting sediment, Q_2 is the flow in the contracted channel, W_1 is the bottom width of the approach channel, W_2 is the bottom width of the main

channel in the contracted section excluding the width of the piers, and k_1 is an exponent depending on the mode of bed material transport.

Contraction scour calculated using Eq. 2-6 may be limited by the presence of coarse sediments armoring the bed material. In this case, HEC-18 recommends the calculation of both live-bed and clear water contraction scour depths and the use of the smaller calculated depth.

The maximum clear water contraction scour depth is calculated using the following equation, which is also based on Laursen's work:

$$y_2 = \left[\frac{K_u Q^2}{D_m{}^{2/3} W^2}\right]^{3/7} \qquad \text{(Eq. 2-7)}$$

$$y_s = y_2 - y_0$$

where Q is the discharge through the bridge section or on the set-back overbank area at the bridge associated with the width W, D_m is the diameter of the smallest non-transportable particle in the bed material in the contracted area ($1.25D_{50}$), W is the bottom width of the contracted area excluding the pier widths, $K_u = 0.0077$ for English units or 0.025 for SI units, and the other parameters are as previously defined.

Eqs. 2-6 and 2-7 are applicable to cohesionless soils. Briaud et al. (2011) developed Eq. 2-8 for the ultimate contraction scour, y_{s-ult}, based on the analysis of flume tests results:

$$y_{s-ult} = 0.94 y_1 \left(\frac{1.83 V_2}{\sqrt{g y_1}} - \frac{K_u \sqrt{\frac{\tau_c}{\varphi_w}}}{g n y_1^{1/3}} \right) \qquad \text{(Eq. 2-8)}$$

where y_1 is the average water depth in the main channel at the approach section, V_2 is the average flow velocity in the main channel at the bridge in the contracted zone, τ_c is the critical shear stress, n is Manning coefficient, and K_u is 1.486 for U.S. units and 1.0 for S.I. units.

Eq. 2-8 is applicable to both cohesionless and cohesive soils. However, y_{s-ult} is not likely to be reached during the bridge life in erosion-resistant cohesive soils. The SRICOS method can be applied to find the final contraction scour depth during the bridge-life flow hydrograph.

2.3.3 Abutment Scour

Abutment scour is the erosion of bed material around the abutment due to the acceleration of the flow and the formation of vortices caused by the abutment and the approach embankment obstructing the flow. Various equations have been developed to predict the depth of the abutment scour hole. Most of these methods are based on laboratory research that has not been successful in replicating the complex combination of field conditions. Consequently, these methods usually result in over predicting the abutment scour depth. HEC-18 presents three methods for calculating abutment scour: Froehlich's equation, Highway In the River Environment (HIRE) equation, and the recently developed NCHRP project 24-20 approach.

Froehlich's equation (Eq. 2-9) is based on regression analysis using 170 laboratory measurements of live-bed scour:

$$\frac{y_s}{y_a} = 2.27 K_1 K_2 \left(\frac{L'}{y_a}\right)^{0.43} Fr^{0.61} + 1 \qquad \text{(Eq. 2-9)}$$

where y_s is the scour depth, y_a is the average depth of the flow on the floodplain, K_1 is the abutment shape coefficient, K_2 is the embankment orientation angle coefficient, L' is the length of active flow obstructed by the embankment, and Fr is the Froude Number of the approach flow.

HIRE equation (Eq. 2-10) is based on scour field data at the base of spurs in the Mississippi River collected by the U.S. Army Corps of Engineers:

$$\frac{y_s}{y_1} = 4 Fr^{0.33} \frac{K_1}{0.55} K_2 \qquad \text{(Eq. 2-10)}$$

where y_1 is the depth of flow at the abutment and the other parameters are as defined previously.

HIRE equation is only applicable to abutments where $\frac{L}{y_1} \geq 25$ (L being the length of the embankment normal to the flow) and where other conditions are similar to the field conditions from where the data were collected.

Ettema et al. (2010) established new equations for estimating the abutment scour depth in cohesionless soils. The method considers abutment scour as a short contraction scour and therefore calculates the total scour depth at the abutment by amplifying the scour depths estimated for flow through a long contraction. The amplification factor considers the non-uniform flow distribution around the abutment and the turbulence developed when the flow contracts at the abutment. This amplification is large where the contraction is small and decreases as the contraction increases in severity. This is because a large contraction increases the flow velocity and uniformity through the contracted waterway. Furthermore, the study distinguished between three abutment scour conditions, as observed during the flume experiments:

1. Condition A (Figure 9).

- The abutment is in or at a close proximity to the main channel.
- The ratio of the embankment projected length L to the floodplain width B_f is equal to or greater than 75 percent ($L/B_f \geq 0.75$).
- Abutment scour occurs only in the main channel and the erosion of the floodplain, if any, is negligible.
- The contraction scour depth is calculated using the live-bed condition equation.

- The abutment scour depth is then calculated by applying an amplification factor for live-bed condition α_A, which is found graphically as a function of the unit discharge ratio ($\frac{q_2}{q_1}$) and the abutment type:

$$y_{max} = \alpha_A y_c \quad \text{(Eq. 2-11)}$$

$$y_s = y_{max} - y_0$$

where y_{max} is the maximum flow depth including abutment scour, α_A is the amplification factor for condition A, y_c is the flow depth after live-bed contraction scour, y_s is the abutment scour depth, and y_0 is the flow depth before scour.

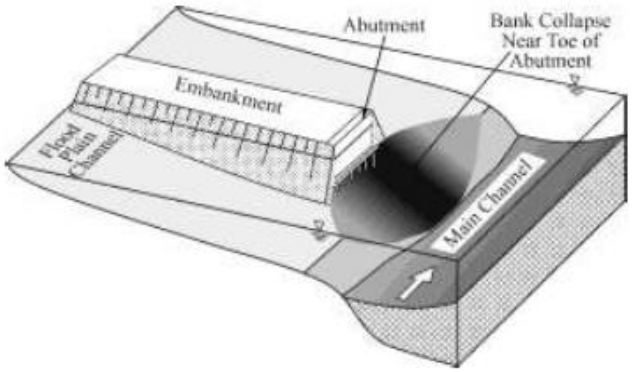

Figure 9- Abutment scour condition A (reprinted from Ettema et al. 2010)

2. Condition B (Figure 10).

- The abutment is set back from the main channel.

- The ratio of the embankment projected length L to the floodplain width B_f is less than 75 percent ($L/B_f < 0.75$).
- Abutment scour occurs only in the floodplain around the abutment.
- The contraction scour depth is calculated using the clear water condition equation.
- The abutment scour depth is then calculated by applying an amplification factor for clear water condition α_B, which is found graphically as a function of the unit discharge ratio ($\frac{q_2}{q_1}$) and the abutment type:

$$y_{max} = \alpha_B y_c \quad \text{(Eq. 2-12)}$$

$$y_s = y_{max} - y_0$$

where y_{max} is the maximum flow depth including abutment scour, α_B is the amplification factor for condition B, y_c is the flow depth after clear water contraction scour, y_s is the abutment scour depth, and y_0 is the flow depth before scour.

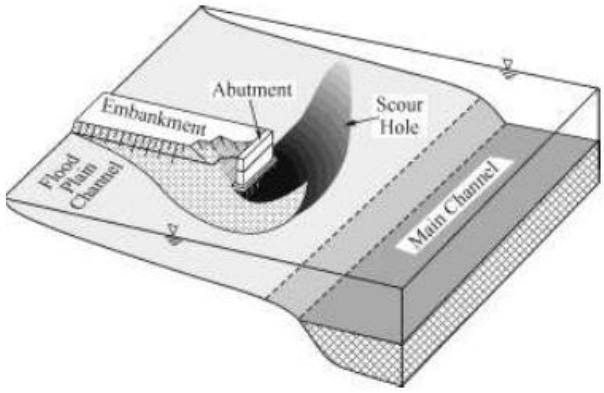

Figure 10- Abutment scour condition B (reprinted from Ettema et al. 2010)

3. Condition C (Figure 11).

- The abutment approach embankment is breached.
- Local scour depth at the exposed abutment column is estimated similarly to pier scour.

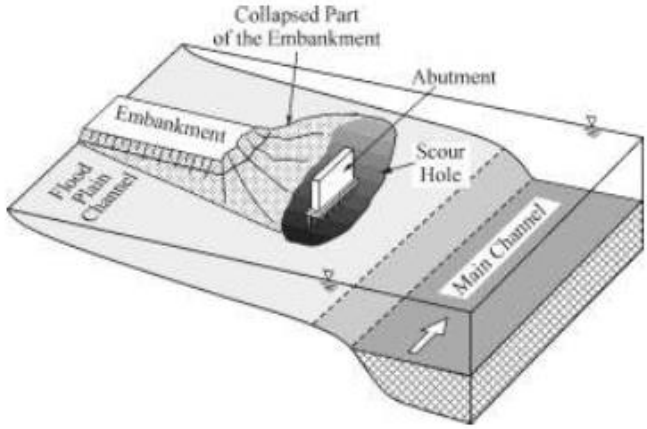

Figure 11- Abutment scour condition C (reprinted from Ettema et al. 2010)

2.4 Maximum Allowable Scour Depth at Bridge Piers

TxDOT defines the maximum allowable scour depth at piers supported by deep foundations, y_a, as the maximum scour depth where the criteria of both lateral stability and bearing capacity of deep foundations are satisfied:

$$y_a = \text{minimum}(y_{al}, y_{ab}) \quad \text{(Eq. 2-13)}$$

where y_{al} is the maximum allowable scour depth based on lateral stability and y_{ab} is the maximum allowable scour depth based on bearing capacity.

y_{al} is calculated by subtracting the actual unsupported length y from the allowable unsupported length y_u, $y_{al} = y_u - y$. The allowable unsupported length y_u can be estimated depending on the

deep foundation type, it is 18 times the diameter of a column/drill shaft, 24 times the diameter of a trestle pile and 24 times the nominal section depth of an H pile or a square pile. y_{ab} is assumed to be 50 percent of the original pile embedment length. The sum of pier scour and contraction scour is required to be less than the maximum allowable scour to avoid scour failure. The pier and contraction scour are calculated using HEC-18 scour prediction equations and the Geotechnical Manual guidelines.

TxDOT is currently testing the use of a progressive severity rating to judge the stability of the bridge and determine when to take action. This scaled approach is based on the maximum allowable pier scour as follows:

1. $0 < y < y_a/3$; acceptable, no action required.
2. $y_a/3 < y < 2y_a/3$; scour critical, start planning remedial measures.
3. $2y_a/3 < y < y_a$; immediate repair needed.

where y is the measured or calculated total scour at the pier.

As mentioned previously, the TSEAS presents a simplified analysis to assess the scour criticality of low volume and off-system bridges exposed to pier and contraction scour. According to the TSEAS, the maximum allowable contraction scour depth y_c for each region of the bridge (left overbank, main channel, right overbank) is calculated by subtracting the maximum pier scour from the maximum allowable scour ($y_c = y_a - y_{ps}$). The type of the contraction scour (live-bed scour or clear-water scour) in each region under the bridge is then determined by comparing the maximum velocity in the uncontracted regions upstream of the bridge (main channel and floodplains) to the critical velocity of the bed material. Typically, clear-water scour occurs in the floodplain where the approaching velocity is less than the critical velocity and live-bed scour occurs in the main channel where the approaching velocities are higher. For clear water contraction

scour, the contraction scour depth y_{cs} is calculated using Eq. 2-7 and then compared to the maximum allowable contraction scour depth y_c for each applicable area of the bridge. For live-bed contraction scour, the allowable discharge ratio q_a is determined using a nomograph based on Eq. 2-6. q_a is defined as the ratio of the main channel flow in the contracted area, Q_t, to the main channel flow upstream of the contracted area, Q_c, when the contraction scour depth equal to the allowable contraction depth, y_c. The stability of the bridge is assessed by comparing the allowable discharge ratio q_a to the actual discharge ratio q estimated using Eq. 2-14:

$$q = \left(\frac{n_b}{n_u}\right) \times \left(\frac{V_b}{V_u}\right)^{\frac{5}{3}} \times \left(\frac{P_b}{P_u}\right)^{2/3} \quad \text{(Eq. 2-14)}$$

where n_b is weighted Manning's roughness coefficient through the bridge opening, n_u is the weighted Manning's roughness coefficient in the unconstricted area, V_b is the average velocity through the bridge opening, V_u is the average velocity through the unconstricted area, P_b is the estimated total wetter perimeter through the bridge opening, and P_u is the estimated total wetter perimeter in the unconstricted area.

Minnesota Department of Transportation (MnDOT) issued a memo in 1995, entitled "Guidelines for Evaluation of Stability of Existing Pile Foundations When Exposed by Scour." These guidelines were incorporated in the MnDOT bridge scour evaluation procedure (MnDOT 2009). The scour depth calculated based on the lesser of overtopping or 500-year flood is compared to the maximum allowed scour to evaluate the structural stability of the bridge. Similar to TxDOT guidelines, MnDOT guidelines define the maximum allowed scour at a bridge substructure unit supported by deep foundations as the lesser of the maximum allowed scour based on lateral stability and the maximum allowable scour depth based on bearing capacity. The maximum allowed scour based on lateral stability is the one causing a total unsupported length of 24 times

the diameter of a cast-in-place concrete pile, 24 times the nominal section depth of an H pile, or 16 times the average diameter of a timber pile. The maximum allowed scour based on bearing capacity depends on the type of the piles. For friction piles, this depth is at 50 percent of the original embedment depth. For end bearing piles, this depth is determined such as 5 ft of the pile will remain embedded in dense soil. MnDOT uses these guidelines to limit scour not only at piers but also at abutments and therefore does not take into account the slope stability of the abutment embankment. Many approach embankments at bridge sites in Minnesota failed during the flooding of April 1997 (Mueller and Hitchcock, 1998).

Current guidelines on allowable scour adopted by other DOTs were surveyed and presented later.

2.5 Abutment Components and Geotechnical Limit to Scour

Two types of bridge abutments are commonly used in the United States. These are spill-through abutments and vertical wall abutments with or without wing walls (Figure 12). Both types have the following design components:

- Abutment embankment: formed by a compacted earth-fill with side slope and spill slope (in the case of spill-through abutments) depending on the soil type and shear strength. This spill-through slope is the most important abutment component when studying scour allowable limits as it may be erodible and/or subjected to geotechnical instability due to abutment scour as explained next.
- Abutment column: supporting the bridge deck. A spill-through abutment column is located at the top of the unconfined approach embankment and is known as standard-stub column. On the other hand, a wing-wall column is composed of a central vertical wall with angled side wings confining the end of the embankment.

- Abutment-column foundation: Piles or drilled shafts foundation are commonly used to support the abutment column, especially when the abutment is located in or near the main channel where the bed material is usually erodible. Nonetheless, spread footing supported columns can be found on more erosion resistant soils and rocks that may be present in the channel banks and floodplains.

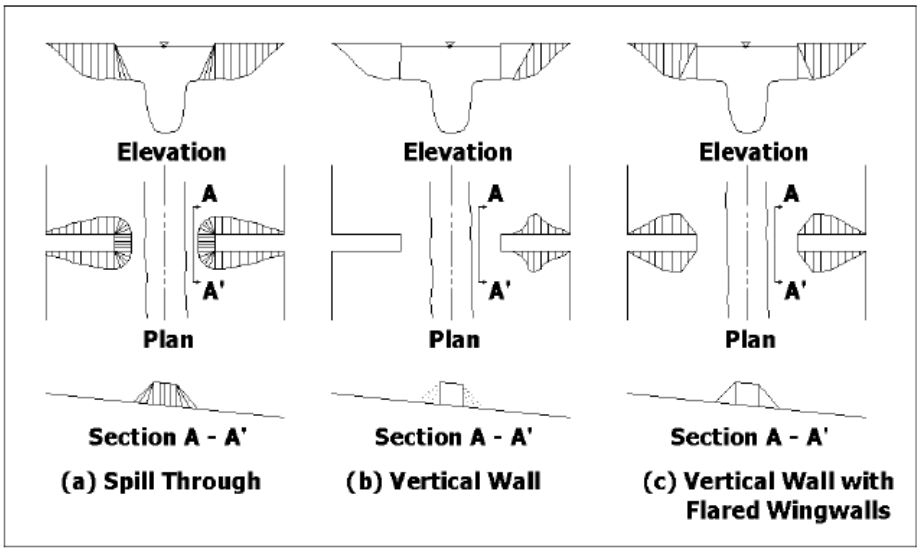

Figure 12- Abutment types (reprinted from Arneson et al. 2012)

However, the difference in structure between the spill-through abutment and the vertical wall abutment leads to different allowable scour limits. In fact, the two abutment types are shown to have different erosion processes, different time durations to breach, and different scour depths. Analysis of the flume experiments data show that the wing-wall abutment takes a longer time to breach and results in a deeper bed scour hole than the spill-through abutment. Flume experiments with model spill-through and wing-wall abutments conducted by Ettema et al. (2016) show that

both abutment types undergo erosion during a flood event. For both abutment types, the embankment erosion initiates at the upstream corner due the highest velocity, flow contraction, and turbulence structures and then progresses toward downstream. However, the breaching process of the spill-through abutments is found to be different than that of the wing-wall abutments where the wings confine the embankment and prevent any erosion at the water level. The erosion cycle of spill-through abutments starts at the face of the unconfined slope and consists of formation of tension cracks followed by undercutting and block toppling. On the other hand, embankment erosion behind the wing wall abutments starts at the base under the pile cap of the upstream wing and the center column. The erosion sequence in this case consists of soil settlement, which causes the development of a cavity behind the wing-wall. Subsequent undercutting and toppling of soil blocks from the unstable side slopes follow until the embankment is breached and the abutment wing-wall is exposed.

In addition to the erosion of the embankment soil, embankment slope failure is a potential failure mode of spill-through abutments exposed to scour at the abutment toe. However, the embankment of a wing-wall abutment is confined by the central vertical panel and the wing-walls. This confinement provides a certain level of protection against both slope instability and embankment erosion. As a result, the problem of maximum allowable scour depth at vertical wall abutments is similar to that at piers; the scour causing failure in this case would be the depth exposing the foundation elements to the extent where the vertical or horizontal bearing capacity is exceeded. The types of deep foundations of vertical wall abutments are shown to affect the scour limit and the failure process. Scour data show that models of vertical wall abutments with wing-walls supported on sheet piles exhibit longer times to breach the embankment and withstand deeper scour holes compared to those supported by circular piles. This is because the solid foundation

protects and retains the abutment base soil. The breach process takes place at a very slow rate due to the sliding of the soil at the abutment side slopes (Yorozuya and Ettema 2015).

Nevertheless, bridges with vertical walls abutment are becoming rare and the majority of the new bridges have spill-through abutments where slope stability failure is expected to control the maximum allowable scour depth. This is particularly true at spill-through abutments supported by deep foundations. When the abutments are supported by spread footings, scour may expose the footing before causing any geotechnical instability of the approach embankment and subsequently the limit scour depth may be controlled by the foundation capacity rather than slope stability. However, spread footing are not typically used to support abutments except on erosion resistant channel beds and floodplains.

It has been recognized that scour at spill-through abutments eventually would reach a depth causing the failure of the embankment slope. This depth is defined as "geotechnical limit to scour" because the geotechnical slope failure of the approach embankment would increase the flow area and subsequently limit the extent and depth of scour. The geotechnical limit to scour also called the "limiting scour depth" is associated with the equilibrium slope θ_S of the embankment material (Ettema et al. 2010). Figure 13 shows a sketch of a spill-through abutment at which the limiting scour depth, d_{Smax} , is derived in Eq. 2-15.

$$\tan\theta_S = \frac{(d_{Smax}+E_H)}{R}$$

$$d_{Smax} = R\tan\theta_S - E_H \qquad \text{(Eq. 2-15)}$$

where θ_S is the equilibrium slope reached when the scour hole depth is d_{Smax} , E_H is the embankment height, and R is the radial distance between the abutment column and the scour hole

bottom. If the scour depth exceeds d_{Smax}, the embankment slope exceeds the equilibrium slope θ_S, the slope face will collapse and eventually the embankment will be breached.

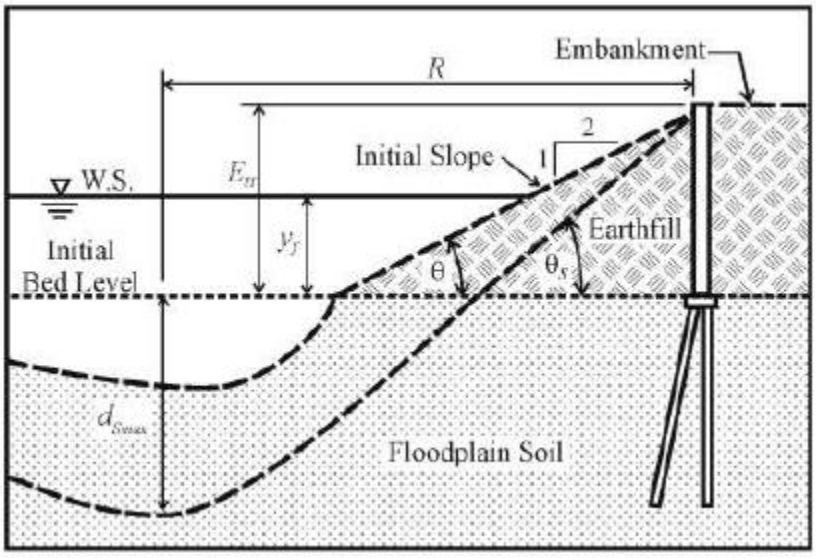

Figure 13- The limiting scour depth (reprinted from Ettema et al. 2010)

Flume experiments by Ettema et al. (2010) and Melville et al. (2006) show that the radial distance R varies with the ratio $\frac{L}{B_f}$ where L is the abutment length, and B_f is the floodplain width (Eq. 2-16 and Figure 14). Essentially, R is positively correlated to the discharge ratio q_2/q_1 with q_2 being the flow rate in the main channel at the bridge section and q_1 being the flow rate in the main channel upstream of the bridge. Indeed, when the ratio q_2/q_1 increases and the bridge waterway is severely contracted, the scour caused by the highly contracted flow will be much larger than the local scour caused by the turbulence structures at the abutment. In this case, the maximum scour depth will not be localized at the abutment column but will occur at a radial distance R away from the abutment where the bed shear stress exerted by the contracted flow is maximum:

$$R = 4\left(\frac{L}{Y_f}\right)^{0.2} Y_f \quad \text{(Eq. 2-16)}$$

where Y_f is the flow depth in the floodplain.

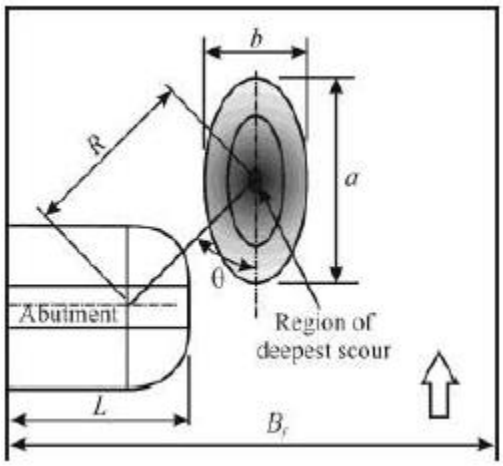

Figure 14- Scour radial distance (reprinted from Ettema et al. 2010)

Combining Eqs. 2-15 and 2-16 results in the following equation for d_{Smax} suggested by Ettema et al. (2010):

$$d_{Smax} = 4\left(\frac{L}{Y_f}\right)^{0.2} Y_f \tan\theta_S - E_H \quad \text{(Eq. 2-17)}$$

where all the variables are previously defined.

The geotechnical limit of scour is found to be dependent on the embankment shear strength (Ettema et al. 2010; Yorozuya and Ettema 2015; Ettema et al. 2016; Feliciano et al. 2014). Indeed, as the soil shear strength increases, the embankment critical height increases and the embankment critical slope θ_S becomes steeper leading to a higher value of d_{Smax} (Eq. 2-17). The effect of the shear strength of the abutment embankment on the limiting abutment scour depth was studied by Ng et al. (2015) who conducted a series of flume experiments with spill-through abutment models of various shear strengths. The shear strength of the abutment embankments was controlled by

controlling the compaction of the soil while constructing the abutment model. Three types of soils were tested: uniform sand, clayey sand, and a mixture of clay and sand. However, the findings of the study apply to abutments made of uniform sand where the shear strength was correlated to the penetration resistance measured on top of the compacted spill-through abutment embankment by using a needle penetrometer. In addition, one test was conducted with a non-erodible spill through abutment made with an aluminum plate. The development of scour during each experiment was recorded using a camera. The scour bathymetry was also measured using an acoustic transducer mounted on a beam above the model and connected to a data acquisition system. The collected results show that embankments of higher shear strength took a longer time to fail and breach, which increased the time of bed scour and consequently the maximum scour depth, which was defined as the geotechnical limit to scour. As expected, the non-erodible aluminum spill-slope model gave the highest scour depth, which was 2.5 times greater than the maximum scour depth obtained from the sand abutments model.

The use of the simplified formulation in Eqs. 2-15 and 2-17 is limited to the case of uniform cohesionless soils where the equilibrium slope can be taken as the soil effective friction angle. The current research extends this simple principle to account for varying combinations of embankment and channel soil types, abutment geometries, and critical hydraulic conditions.

2.6 Slope Stability Methods

Since the developed guidelines for the determination of the maximum allowable scour at spill-through abutments rely heavily on slope stability simulations of the spill-through embankment, a review of the commonly used slope stability methods is presented herein.

Slope stability problems are typically solved in two dimensions by assuming a plane strain condition and a cylindrical sector shape for the failing soil mass. Limit Equilibrium Methods have been the most frequently used methods for studying slope stability due to their ability to account for all the external and internal forces acting on the soil mass and to partially or completely satisfy the representative constitutive and fundamental equations. Particularly, the methods of slices are the most common because they can be applied to complex failure slip failure geometries, variable soil strength, and complex water pressure conditions. These methods are numerous but they all define the factor of safety (FS) as the ratio between the available shear strength of the soil on the potential failure plane and the mobilized shear stress on this plane to keep the soil mass in a state of limiting equilibrium. A simplified shape of the failure surface, typically a circular arc, is selected. The soil mass is then divided into slices and assumptions are made to make the problem statistically determined. Next, the forces acting on each slide are resolved and the FS is finally determined. Different methods of slices have been developed over time. The difference between these methods lies in the equations of equilibrium explicitly satisfied and in the assumptions made about the inter-slice forces (Fredlund and Krahn, 1977). The review of the most common methods shows the evolution sequence starting in 1927 from the Ordinary Methods of Slices with coarse assumptions and progressing with time toward more refined assumptions and a complete satisfaction of the equilibrium conditions.

The Ordinary Methods of Slices assumes that the direction of the inter-slice forces is parallel to the base of the slice, which results in a linear equation for a rapid estimation of the FS. However, this method does not satisfy force equilibrium conditions nor Newton's third law. Janbu's simplified method assumes horizontal inter-slice forces and accounts for the influence of the shear inter-slice forces by using a correction factor f_0 to correct the FS derived from the force

equilibrium conditions. His rigorous method assumes a line of thrust that defines the direction and point of application of the inter-slice forces. However, both his methods fail to satisfy the moment equilibrium condition.

Bishop (1955) developed a rigorous method that incorporates the inter-slice forces and satisfies both force and moment equilibrium conditions. The approach consists of first computing the FS by assuming zero shear side forces. This initial value of the FS is then used to find a distribution of shear forces satisfying force equilibrium conditions. However, it was found that the variation of the initial FS, based on the assumption of horizontal inter-slice forces, and the final value obtained from the complete rigorous procedure, is insignificant. Due to its accuracy, the simplified Bishop method gained a lot of acceptance even though it does not satisfy the horizontal force equilibrium condition.

The Morgenstern-Price method requires making an assumption about the shape of the potential failure surface as this method can deal with any arbitrary shape. In addition, a second assumption on the distribution of the inter-slice forces is also required as this approach considers that the direction of the inter-slice forces varies across the different slices as a function of position. Hence, an arbitrary function is required to relate the position of each slice to the angle of the corresponding resultant inter-slice force: $X=\lambda f(x)E$ where X represents the shear inter-slice force, E the horizontal inter-slice force, f(x) the assumed function, and λ an unknown constant. This method solves for the FS and for the constant λ by satisfying vertical force equilibrium, horizontal force equilibrium, and moment equilibrium. Morgenstern and Price (1965) concluded that the FS is insensitive to the variations in the assumed position function f(x).

When the assumed position function is a constant, this method becomes equivalent to Spencer's method, which assumes that the inter-slice forces are parallel and satisfies both forces

and moment equilibrium conditions (Spencer, 1967). Spencer's approach considers a range for the angle θ, which defines the direction of the resultant inter-slice force with respect to the horizontal. For each value of θ, two FSs are obtained: FS_f based on the overall force equilibrium equation and FS_m based on the overall moment equilibrium equation. The curves showing the variations of FS_f and FS_m as a function of θ are then plotted on the same graph. The point of intersection of these two curves gives the factor of safety FS_i and the corresponding inter-slice forces θ_i direction satisfying all equilibrium conditions. Using this approach, the FS by the simplified Bishop method is FS_{m0}, the intercept of the curve FS_m where the FS only satisfies the moment equilibrium condition and the inter-slice forces are horizontal (θ=0). Spencer found that the FS satisfying the moment equilibrium is insensitive to the angle θ, which explains how the Simplified Bishop method can be accurate without even satisfying the horizontal force equilibrium condition.

Each of these different methods of slices gives the FS for an assumed location of the failure surface. However, the critical failure surface is the one having the lowest possible FS and can be found by iteration. Computer programs search for the critical failure surface by using either an automatic search approach or a grid approach. The first approach consists of mapping the value of the lowest FS at the location of the corresponding center of the failure circle with coordinates x and y. The slope of the resulting surface FS=F(x,y) is then used to move toward the centers with lower FS values until the minimum value is found. Using this approach can lead to an erroneous critical surface with a local minimum of the FS instead of the absolute minimum. The user can overcome this problem by starting a new search with at a different location for the center. The grid search pattern was adopted by Spencer (1967). It consists of setting a rectangular grid of center locations and determining the FS at each grid intersection. The critical surface is then found by graphical interpolation. The user can start with a coarse grid then refine it for a precise

identification of the critical surface and the associated FS. According to Spencer, the location of the critical circle center is in the uphill area near the bisector of the slope.

In reality, all slope failures are three-dimensional (3D) problems where the failing soil block has the shape of a spoon. However, performing a 3D analysis is not common since a 2D analysis is simpler and leads to a more conservative FS (Briaud 2013). Most of the 3D limit equilibrium methods do not satisfy all equilibrium conditions in 3D and lack general methods for finding the location of the most critical 3D failure surface. Nevertheless, sophisticated 3D analyses can be performed using several computer programs. One approach for 3D slope stability analysis consists of decomposing the slope into a series of circular failure surfaces each of which is analyzed in 2D. A better approach uses the Finite Element Method to determine the stress field in the soil mass and predict the displacements by a stress-strain constitutive model. Therefore, the Finite Element Method automatically satisfies all equilibrium conditions. It uses a Strength Reduction Factor (SRF) to reduce the effective cohesion and friction angles. The analysis is repeated with increasing values of SRF until failure occurs. The FS is equal to the value of SRF at failure, which can be defined by one of the following three criteria: bulging of the slope surface, shear strength reached on the failure surface, or non-convergence of the solution. However, finite element slope stability analyses require the knowledge of several additional parameters describing the stress-strain behavior of the soil. To avoid making unnecessary assumptions, finite element methods were not used. The slope stability analyses performed during this project are based on two 2D limit equilibrium methods, namely the Simplified Bishop Method and Spencer Method.

2.7 Survey of DOTs

Since little information could be found in the literature on allowable scour, an early task for the project entailed conducting a survey of DOTs to identify what maximum scour depths is allowed in each state before corrective actions are taken. The survey questionnaire was distributed by TxDOT to the American Association of State Highway and Transportation Officials (AASHTO) Subcommittee on Bridges and Structures. Survey replies were received from 24 states including two responses from New Mexico Department of Transportation (NMDOT). Figure 15 shows the respondent states on the map. The survey consisted of four questions and focused on the maximum allowable depths for pier scour, contraction scour, and abutment scour. The survey questions, a synthesis of the answers, and survey concluding remarks are presented next. Detailed survey answers are tabulated by state in the Appendix (Table 37, Table 38, Table 39, and Table 40).

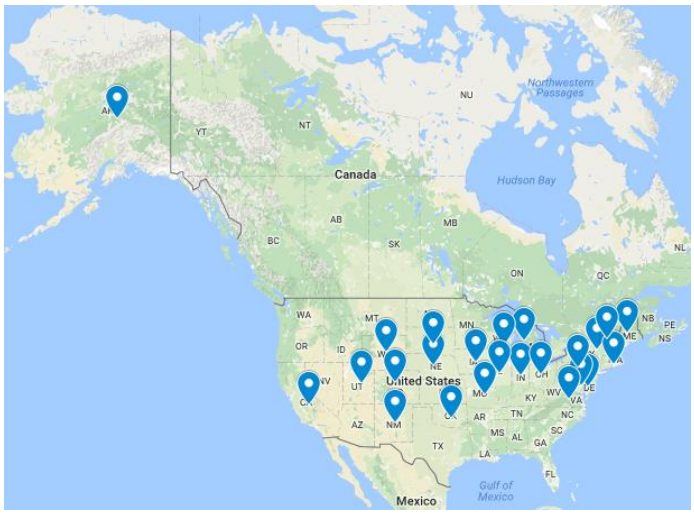

Figure 15- Respondent states

Question 1—What Maximum Scour Depth Do You Allow for Abutment Scour before You Take Action? Please Explain

None of the respondent states gave a specific depth or depth range for maximum abutment scour. While all the answers imply that a case by case evaluation is required due to numerous site-specific factors affecting the analysis, some of these answers further provided general guidelines on when to take action. Nebraska department of roads sets the maximum allowable abutment scour for the 100-year storm event at or above the critical berm elevation defined as 2/3 down the length of the steel sheet pile. Half of the respondents (50 percent) agreed that action is triggered by some level of footing exposure (any exposure, substantial exposure, footing bottom exposure, or moderate exposure, 20 percent of the footing length or area under the footing). Caltrans, Delaware Department of Transportation, NMDOT, and Pennsylvania Department of Transportation further differentiated between the scour limits of spread footing supported abutments and piles supported abutments. For the latter case, the four respondents said that allowable scour depends on the piles structural stability and the remaining embedment depths. Missouri Department of Transportation and Wisconsin Department of Transportation are the only respondents whose answers consider the slope stability of the roadway as one of the factors affecting the allowable abutment scour limits. NMDOT, Wisconsin Department of Transportation, and New York State Department of Transportation (NYSDOT) also take action when abutment protection features are damaged. Indiana Department of Transportation (INDOT) and Iowa DOT require scour protection as per HEC-23 on all their abutments and do not perform any further scour evaluation.

Question 2—What Maximum Scour Depth Do You Allow for Contraction Scour before You Take Action? Please Explain

Seventy-one percent of the responses to this question are exactly the same as to the responses to question 1. While INDOT and Iowa DOT control abutment scour by providing required protection per HEC-23, both DOTs have established limits for total scour, which is calculated as the sum of pier and contraction scour depths. INDOT takes action when the total scour has reduced the pile embedment length to 10 ft or less whereas Iowa DOT takes action when the total scour exceeds 50 percent of the pile embedment length or the maximum unbraced length for pile bent. The DOTs of New Mexico, Vermont, and Wyoming said that contraction scour trigger action only when it impacts the bridge substructure foundations. South Dakota DOT stated that when contraction scour is considerable, measures to armor against scour are taken well before foundations exposure. NMDOT and NYSDOT considered that contraction scour, when measured in the field, would be classified as either abutment scour or pier scour and addresses as per the answers to questions 1 and 3, respectively.

Question 3—What Maximum Scour Depth Do You Allow for Pier Scour before You Take Action? Please Explain

Seventeen out of 24 states DOTs answered this question on pier scour limit similarly to question 1 on abutment scour limit. This indicates that these states do not differentiate between the scour components making up the measured or predicted total scour depth when assessing the structure vulnerability at the cumulative scour depth. Ohio DOT claimed that most of its bridge piers are supported by deep foundations, which makes them invulnerable to sudden scour failure and allows for addressing scour holes before they become a problem. INDOT and Iowa DOT

consider the total scour depth as the sum of contraction and pier scour depths and therefore gave the same answers as the answers to question 2. DOTs of Alaska, Missouri, Nebraska, New Mexico, and Wisconsin have different allowable pier scour depths controlled by the structural stability of the bridge (i.e., buckling and bearing capacity).

Question 4—Please Share Any Publications or Additional Information that Would Be Helpful to the Project by Directly Contacting Professor Jean-Louis Briaud at briaud@tamu.edu.

The received publications, manuals, guides, and documents are presented in the Appendix, Table 40.

The survey led to the following conclusions on DOTs practices related to the allowable scour limits:

- States DOTs do not have unique scour depth limits for any of the three scour components. In addition, some of the comments denote that a threshold scour depth applicable to all bridges is impossible to determine due to several variables (abutment details, foundation type, soil characteristics, and structure and embankment stability). This confirms the approach selected to solve the problem. The proposed guidelines lead to site-specific allowable scour depth rather than a unique threshold depth for scour limits. In fact, the site-specific factors stated in the survey answers had been deduced by the review of literature. The effects of these factors are captured by the proper selection of independent variables in performing the analysis and developing the guidelines for the maximum allowable scour limits.

- The majority of the respondents repeated the same answers for questions 1–3. This highlights the fact that the total scour depth (observed or measured) near or at the bridge substructures (abutments or piers) should be limited based on foundation and abutment embankment stability criteria, rather than setting different limits for each of the three scour components. Therefore, the scour process and scour components involved (abutment scour, pier scour, and/or contraction scour) are not important when it comes to determining the allowable scour depth at bridges.
- The scour limit at piers is better defined than that at abutments; while the answers to the first two questions are qualitative and descriptive (inspection, monitoring, subjective evaluation, case by case analysis, criticality of the particular scour depth, etc.), answers to question 3 included some quantitative established limits.
- More than half of the respondent states DOTs define the limiting abutment scour depth by some level of footing exposure, which poses a very important problem: What if foundation exposure occurs during a flood event when it is impossible to arrest scour? The stability of the structure would be jeopardized. This stresses the importance of using the proposed maximum allowable scour depths as to limit the sum of any observed scour depth plus the predicted scour depth associated with a design flood event.
- Survey answers show the lack of systematic and practical procedures for the determination of allowable scour at abutments to assess the bridge scour condition and justify the need of implementing corrective measures or seeking higher order structural and geotechnical analyses.

3. THE BOREHOLE EROSION TEST*

3.1 Test Procedure

The Borehole erosion test was invented by Briaud (2014). It is a field test which consists of drilling a hole approximately 100 mm in diameter to a depth covering the zone of interest for the erosion problem at hand. For example for a scour problem at a bridge pier, the depth of interest may be conservatively estimated as a depth equal to 3 times the width of the bridge pier. Once the hole is drilled, the rods and drill bit are removed and a borehole caliper is lowered to the bottom of the hole. The diameter of the borehole is logged by pulling the borehole caliper up the hole to obtain the zero reading borehole diameter profile. Note that it is best to repeat this diameter profiling step several times to minimize the error possibly associated with borehole cross section irregularities. The caliper is now out of the borehole and the rods and drill bit are re-inserted to about 25 mm from the bottom of the borehole. Water is circulated at a chosen velocity down the rods, around the bottom of the drill bit, and up the annulus between the rods and the wall of the borehole (Figure 16). This erodes the walls of the soil borehole if the water velocity is larger than the critical velocity. After a set time (say 10 minutes), the flow of water is stopped and the drill bit and rods are removed from the hole. The borehole caliper is reinserted to the bottom of the borehole and the diameter of the borehole is logged again to obtain the eroded borehole diameter profile

(Figure 17). Again, several caliper profiles are recommended. The increase in radius which occurred during the flow divided by the flow duration is the erosion rate associated with the flow velocity. It gives one point on the erosion function curve . The caliper is removed from the borehole and the rods and bit are reinserted to the bottom of the borehole. A higher velocity is chosen and the flow is maintained during the set time (10 minutes) to repeat the process. Velocity after velocity, the erosion functions of all soil layers within the borehole depth including the critical velocity profile are obtained. One advantage of the BET is that it gives a complete profile of erosion rates and allows for the evaluation of all soil layers within the depth of the borehole in one single test. By comparison a large number of soil samples would have to be collected and tested in the laboratory to give the same amount of information.

Figure 16- Flow during BET

Figure 17- Diameter logging after flow

The BET erodes the side walls of the borehole but it also erodes the bottom of the borehole because of the water flowing out of the bottom of the drill bit. The caliper also gives the depth of the eroded bottom of the borehole. The primary BET is associated with the lateral erosion; it will be called BET in general and LBET or lateral borehole erosion test when it is necessary to distinguish it from the BBET or bottom borehole erosion test.

The LBET is very similar in concept to the early pinhole tests (ASTM 2006) which was later developed into the Hole Erosion Test or HET (Wan and Fell 2004). The HET is a laboratory test on a 100 mm diameter 100 mm long sample where the hole is small (6 mm in diameter) and the flow is horizontal. By comparison the hole for the BET is much larger (e.g., 100 mm) and the flow is vertical. As such structural anisotropy may create a difference in result between the two tests. The BBET on the other hand is very similar in concept to the Jet Erosion Test or JET (Hanson 1990). The JET is a laboratory test which can also be performed in the field; in both cases the jet is vertical as in the BBET. The JET is limited to surface testing however while the BBET is performed at any desired depth.

3.2 Test Equipment

One of the advantages of the BET is that it only requires the use of commonly available equipment (Briaud et al. 2016). Indeed, it requires a commonly used drilling rig for wet rotary boring, and a commonly used borehole caliper (Figure 18). The water circulation part of the BET relies on the pump from the rig, an in line flow meter and a stop watch (Figure 19).

The borehole caliper can be a mechanical caliper with radial arms which extend horizontally in a cone shape (Figure 18) or an acoustic caliper which uses sound waves to scan the distance from the instrument to the borehole wall. The advantage of the acoustic caliper is that it

gives a complete scan of the diameter by rapid rotation scanning of the wave propagation beam. An acoustic caliper was used in the tests reported here but it was found that the precision with which the diameter was measured was much worse than that of the mechanical calipers. The reason was that the signal of the return wave was fuzzy and difficult to interpret because the interface at the wall of the soil borehole did not provide a sharp enough stiffness discontinuity. Acoustic calipers work well for rock borehole profiling because of the sharp stiffness discontinuity at the borehole wall but in the case of soils, the tests carried out here showed that mechanical calipers are to be favored.

Figure 18- Borehole mechanical caliper

Figure 19-Flow meter

Mechanical calipers come with imitations as well. One issue is that the caliper hangs from a cable and not from a rod; thus it is not possible to control the orientation of the caliper which might spiral as it comes up by following grooves left by the drilling bit. The caliper is calibrated

just before testing to ensure that the readings are correct but the borehole may not be perfectly cylindrical and a minimum of three arms is recommended. Calipers with up to 8 arms do exist and would give a better definition of the borehole cross section but such calipers are typically much larger in diameter with a body diameter in the unexpanded arms position larger than 100 mm. Drilling a larger diameter borehole would thus be desirable however the pump from the drilling rig would not typically be able to generate sufficient flow capacity for the range of velocity of interest for most erosion studies. In the end a three arm mechanical caliper hanging from rods to control angular direction is recommended as well as repeating the logging of the hole a minimum of two times in different directions to gage the precision of the measurements.

3.3 Field Tests and Soils Tested

A series of BET tests were undertaken at the National Geotechnical Experimentation Sites at Texas A&M University (NGES-TAMU, Briaud 1997). There are two sites: a clay site (NGES-TAMU Clay) and a sand site (NGES-TAMU Sand). The clay is a very stiff clay with an average shear strength of 110 kPa within the top 4 m. It is overconsolidated by desiccation and of relatively high plasticity because it was deposited in a very low energy environment through a series of geologic transgressions and regressions of the Gulf of Mexico over Texas. The sand is a medium dense silty sand with an average Standard Penetration Test (SPT) blow count equal to 15 blows per 0.3 m within the top 4 m. It was deposited by an ancient meander of the Brazos River and contains a significant amount of fine particles. More soil properties were obtained for the BET by collecting samples from the very borehole that would be BET tested. These samples were brought back to the laboratory where index and engineering properties tests were conducted. The results of these tests are presented in the two following sections.

3.3.1 Stiff Clay

For the clay, the samples collected ranged in depth from 0.61 and 3.6 m and the following tests were conducted: unit weight, water content expressed on a gravimetric or mass basis, sieve analysis, hydrometer tests, Atterberg limits, pycnometer tests. The results of these tests are presented in Table 3 and Figure 20.

Table 3- Clay samples classification

Depth (m)	Bulk density (Mg/m^3)	Water content (%)	G_s	Liquid limit (%)	Plasticity index (%)	USCS
0.6-1.2	1.97	20.53	2.47	47.3	27.7	CL
1.2-1.8	2.14	21.76	2.47	55.52	36.47	CH
1.8-2.4	2.08	22.75	2.54	38.07	21.54	CL
2.4-3.0	2.01	22.52	2.58	40.07	23.17	CL
3.0-3.6	—	22.70	2.55	52.99	33.21	CH

3.3.2 Medium Dense Sand

Standard penetration tests were conducted in the two sand boreholes, SBH6 and SBH7. Split spoon samples were collected and used to determine the water content of the sand at different depths in both boreholes. Table 4 shows the results of the blow count N expressed in blows per foot (bpf) and the water content for boreholes SBH6 and SBH7. These samples were then dried and sieve analyses were performed to obtain the gradation curves (Figure 20). The sand in both boreholes can be classified as poorly graded silty sand (SM).

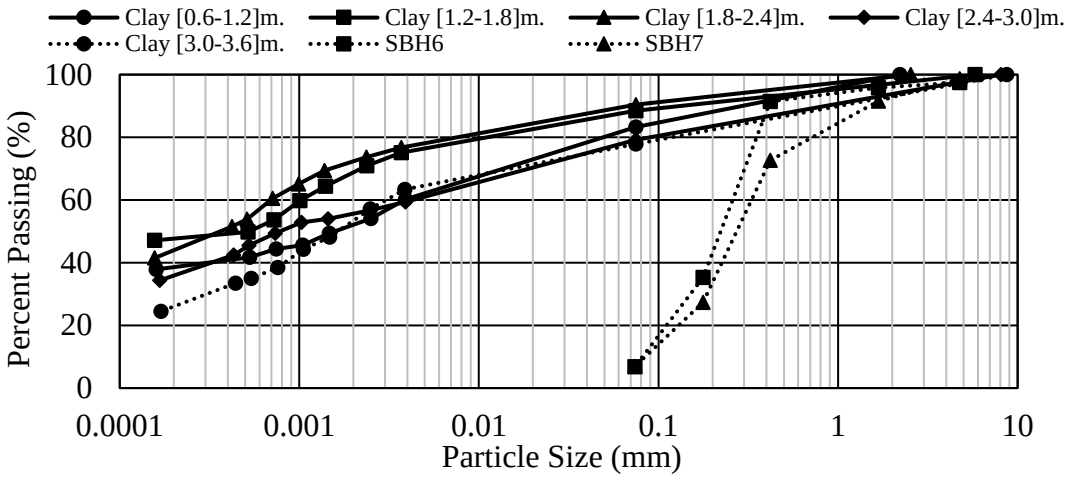

Figure 20- Gradation curves for the clay and sand samples

Table 4-Sand sample tests results

Depth range (m)	Sand borehole SBH6		Sand borehole SBH7	
	Blow count N (bpf)	Water content (%)	Blow count N (bpf)	Water content (%)
0-0.45	13	8.89	11	8.35
0.6-1.05	16	21.24	11	15.15
1.2-1.65	11	11.99	8	14.55
1.8-2.25	11	11.27	10	16.38
2.4-2.85	12	21.81	14	18.44
3.0-3.45	14	14.75	22	19.32

3.4 Test Results in Clay

Three sets of BETs were conducted at the clay site, one in November 2014, one in June 2015, and one in July 2018. The BET borehole of November 2014 is designated CBH1, the two BET boreholes of June 2015 are designated CBH 3 and CBH5, and the BET borehole of July 2018 is designated CBH8. The results of these four BETs in terms of diameter profiles are shown in Figures 21-24. Considering Figure 21 for example, the initial borehole was completed with an 89

mm three wing drill bit to a depth of 3.35 m. After removing the drill bit and the rods, the borehole caliper was inserted and readings were taken as the caliper was pull up the borehole. This gave the zero diameter reading profile (C-0 on Figure 21, C is for caliper). Inspection of this initial profile reveals two layers which are more erosion resistant than the rest of the soil profile, one at a depth of 1.2 m and one at 2.5 m. The average initial diameter drilled with the 89 mm bit was about 95 mm on the average. This enlargement could be due to drilling rod wobble and/or to erosion of the clay during the circulation of the drilling mud. Then the caliper probe was removed and the drill bit - drilling rods assembly reinserted. The drilling mud was circulated and the flow rate was measured to be 0.00142 m^3/s with an inline flowmeter. This test is designated C-1 in Figure 21.

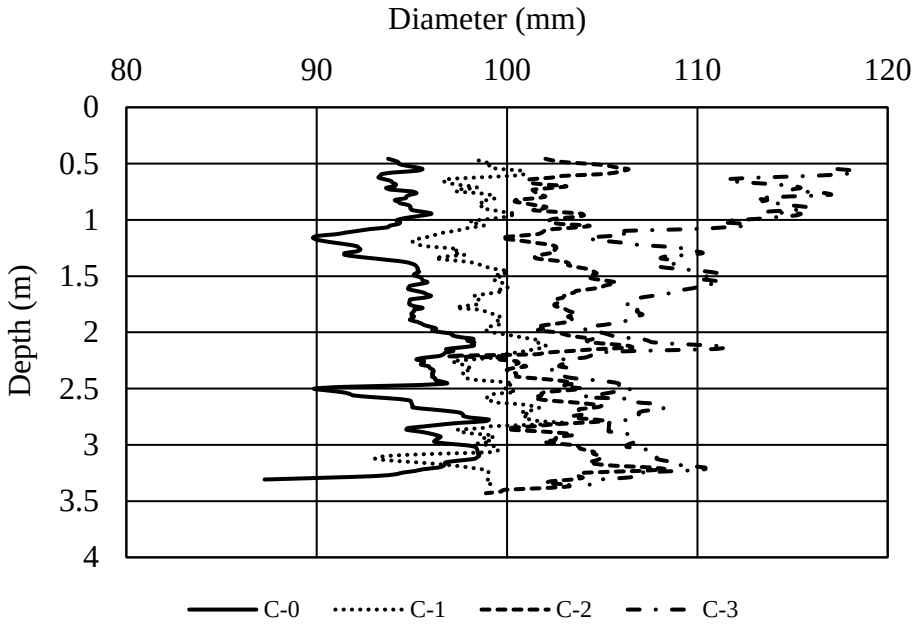

Figure 21- BET diameter profiles for CBH1 at the clay site

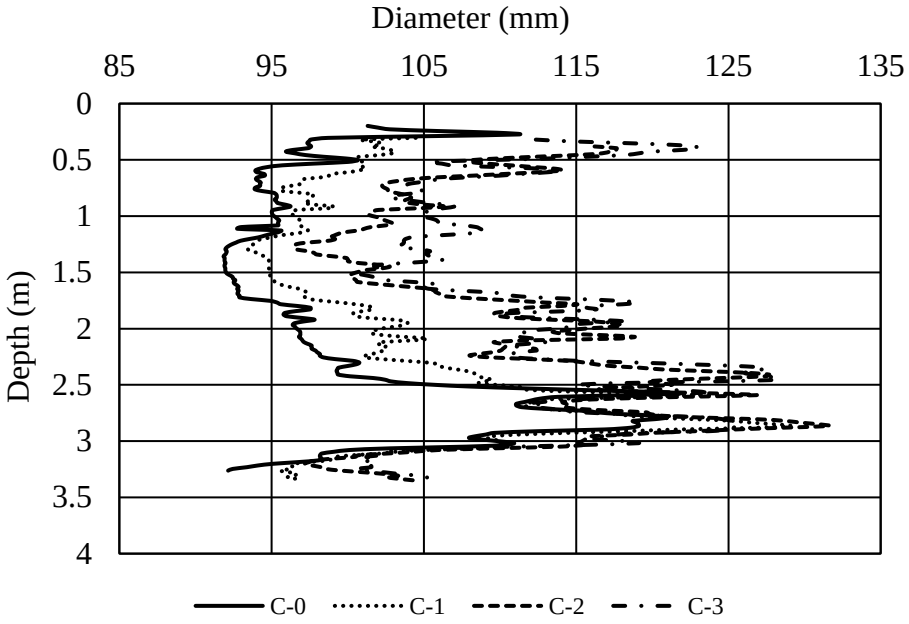

Figure 22- BET diameter profiles for CBH3 at the clay site

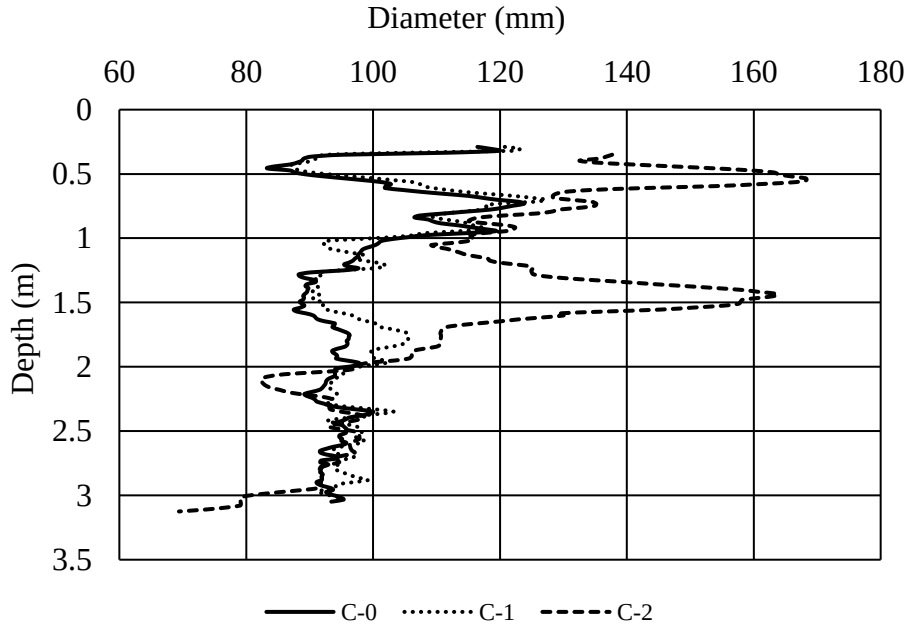

Figure 23- BET diameter profiles for CBH5 at the clay site

The mean flow velocity in the annulus between the rods and the borehole wall was calculated by using the equation:

$$Q = vA \qquad \text{(Eq. 3-1)}$$

where Q is the discharge, v is the velocity, and A is the cross section area between the outside wall of the rods and the borehole walls as measured with the caliper.

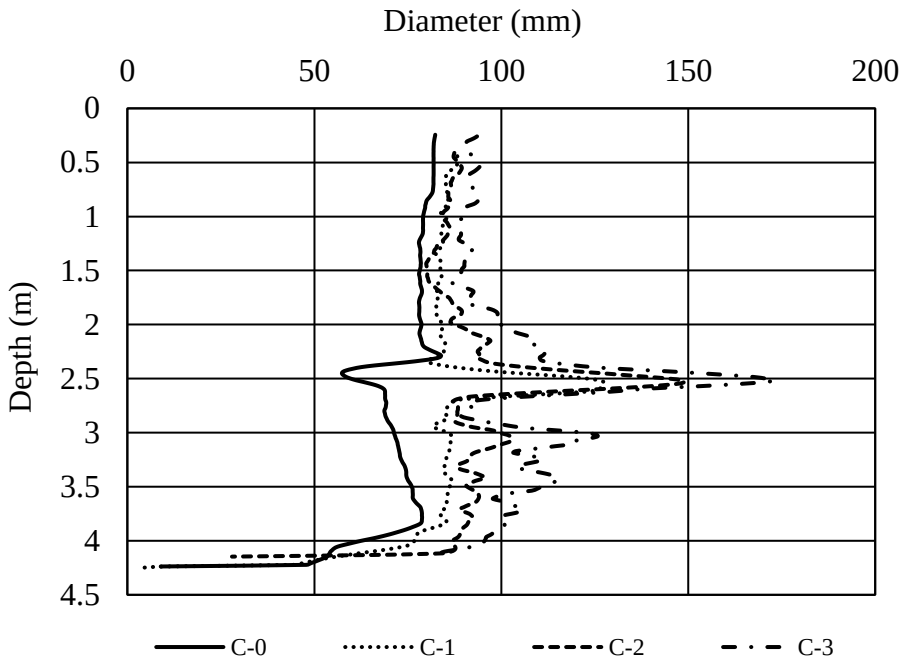

Figure 24- BET diameter profiles for CBH8 at the clay site

The average diameter for each caliper profile was used to transform the flow Q into the velocity v for that test. In the future it is recommended that software be developed to use the actual diameter at any depth as measured with the caliper to obtain v from Q. The time-average velocity during test C-1 was 0.4 m/s which was maintained for 10 minutes. As can be seen during those 10

minutes of flow at 0.4 m/s (Figure 21 from C-0 to C-1), the average borehole diameter increased from about 95 mm to about 99 mm as measured by the mechanical caliper. The corresponding average erosion rate calculated as increase in radius divided by the time of flow is 12 mm/h. Combined with the flow velocity of 0.4 m/s, this gives a first point on an erosion function curve similar to the one in Figure 1b (Briaud, 2013). A second BET was conducted in the same hole by reinserting the rods, increasing the flow velocity to 1.36 m/s and maintaining it for 10 minutes. Table 5 gives the flow rates, velocities, and time of application of each velocity for all the BETs.

Table 5- Flow, velocity, and time for the BETs at the clay NGES-TAMU site

Borehole Designation	Flow (m^3/s)	Velocity (m/s)	Duration (min)	Change in profile
CBH1	0.00142	0.40	10	Figure 21, C-0 to C-1
	0.00562	1.36	10	Figure 21, C-1 to C-2
	0.00568	1.19	10	Figure 21, C-2 to C-3
CBH3	0.00850	1.73	10	Figure 22, C-0 to C-1
	0.00907	1.69	10	Figure 22, C-1 to C-2
	0.00545	0.83	10	Figure 22, C-2 to C-3
CBH5	0.00519	1.15	10	Figure 23, C-0 to C-1
	0.00848	1.74	7	Figure 23, C-1 to C-2
CBH8	0.00221	1.26	10	Figure 24, C-0 to C-1
	0.00132	0.75	10	Figure 24, C-1 to C-2
	0.00208	0.79	10	Figure 24, C-2 to C-3

The erosion rate calculations can be performed at any depth by using the two borehole diameter profiles and the time of constant flow application leading to the erosion rate profile. As an example, the erosion rate profiles of CBH3 are shown in Figure 25. These profiles show that not all layers erode at the same rate; they also show that in some layers the erosion is negative which means that the hole became smaller after the water circulation. This may be due to the fact

that the borehole cross section is not circular but elliptical or at least irregular in such a way that the caliper gives the long axis prior to the test and the short axis after the test. One of the lessons learned from this testing is that there is a need to run the calipers in two perpendicular directions if possible or to control the orientation of the caliper or to develop a caliper with more arms. Another possibility is that the end of the caliper arms may penetrate into the soil and impact the readings; this problem can be minimized by using soft springs on the caliper arms and enlarged ends on the arms so as to decrease the average pressure on the soil. An acoustic caliper gives a complete circumference of the borehole by sweeping an acoustic vibration beam around the borehole. An acoustic caliper was tried during the field tests but did not give good results. The reason is that the interface between the drilling fluid and the borehole wall is not very sharp and the arrival of the return wave is not well defined. This leads to significant uncertainty on the measured diameter of the borehole.

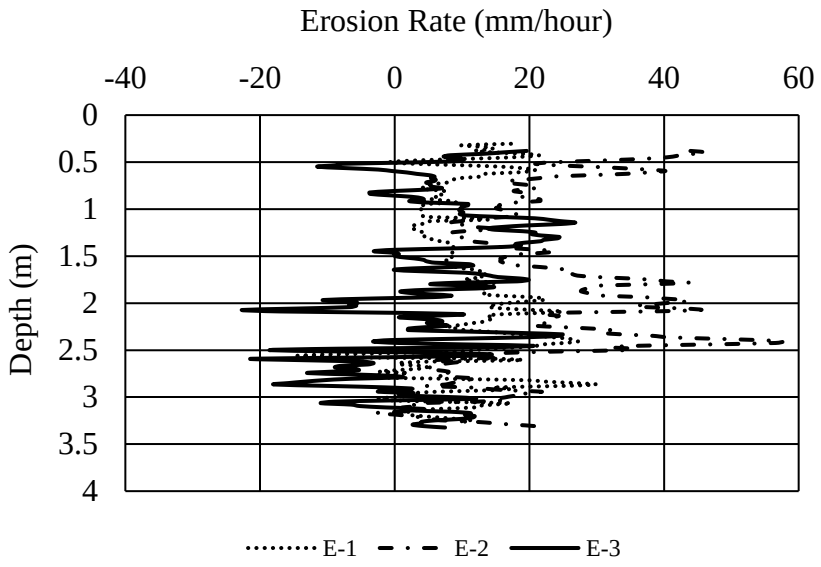

Figure 25- BET erosion rate profiles for CBH3 at the clay site

3.5 Test Results in Sand

Three sets of BETs were conducted at the sand site, one in November 2014, one in June 2015, and one in July 2018. The BET borehole of November 2014 is designated SBH2, the two BET boreholes of June 2015 are designated SBH6 and SBH7, and the BET borehole of July 2018 is designated SBH9. The results of these three BETs in terms of diameter profiles are shown in Figures 26-29. The nomenclature for the profiles on those figures is the same as the nomenclature for the clay BETs profiles; for example C-0 is the zero reading for the diameter profile (C stands for caliper) and C-1 is the diameter profile after the first flow rate was applied.

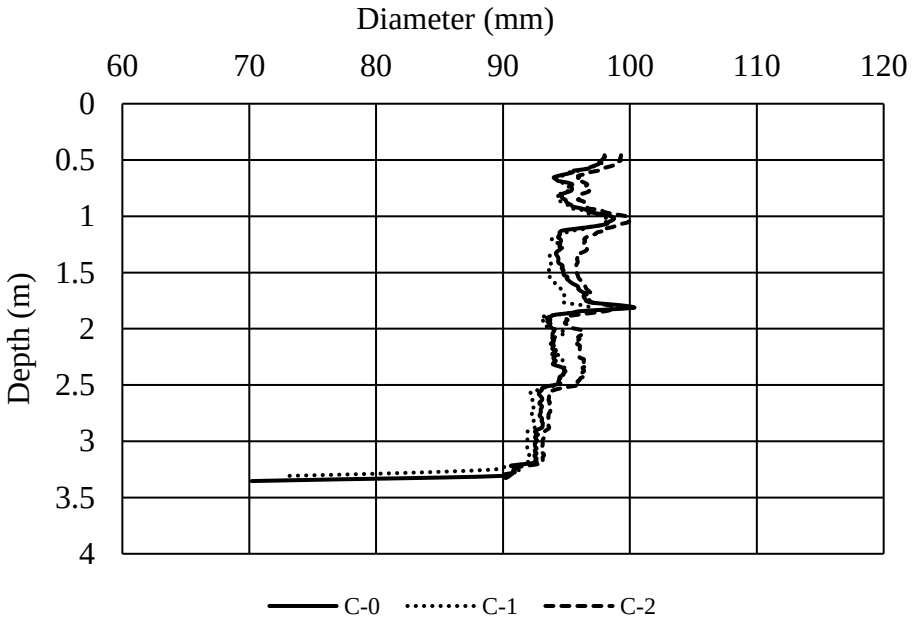

Figure 26- BET diameter profiles for SBH2 at the sand site

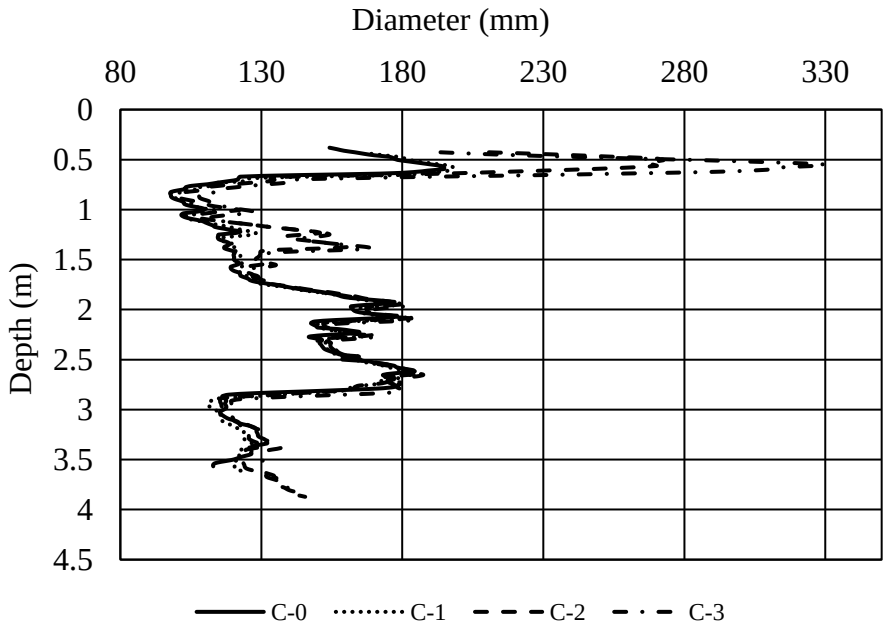

Figure 27- BET diameter profiles for SBH6 at the sand site

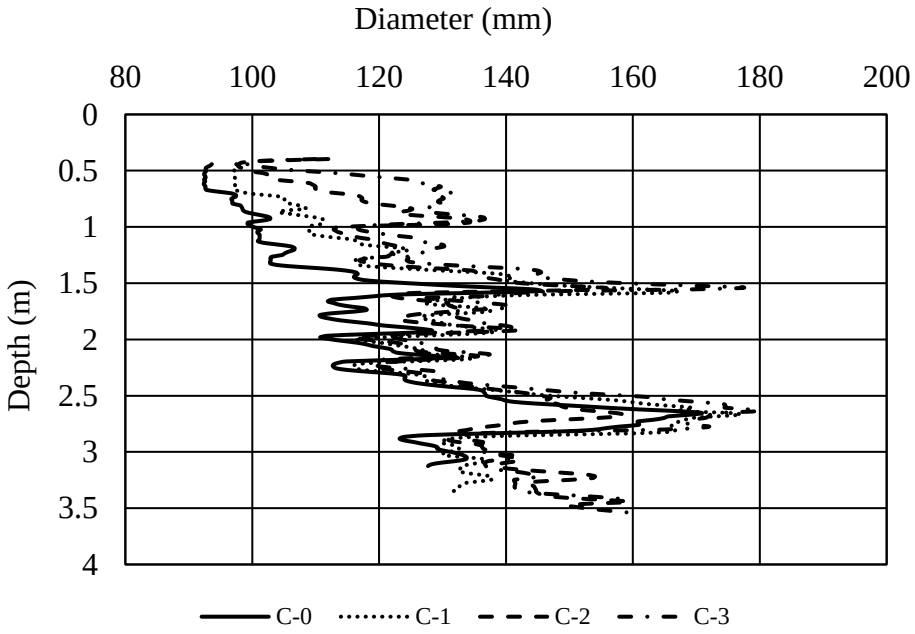

Figure 28- BET diameter profiles for SBH7 at the sand site

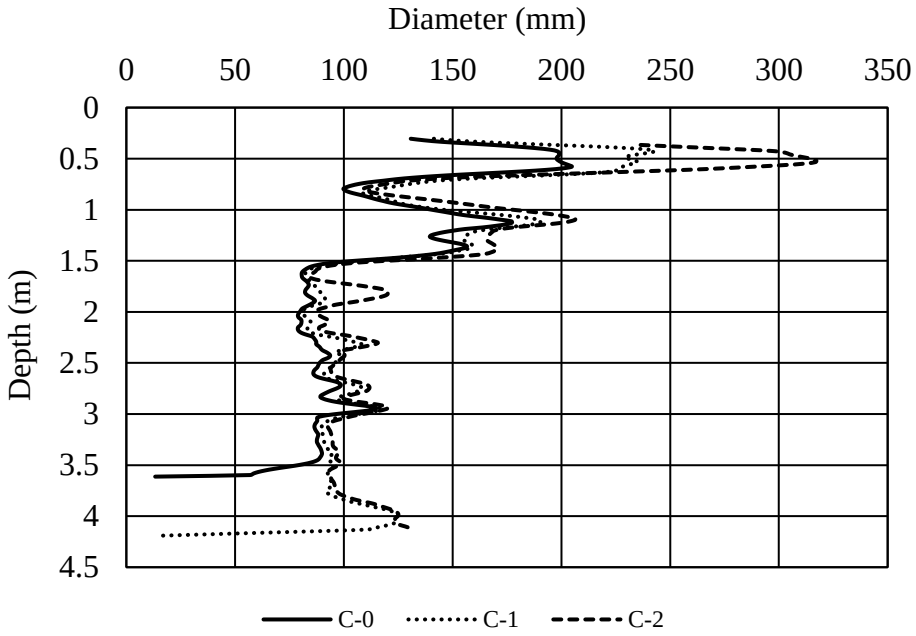

Figure 29- BET diameter profiles for SBH9 at the sand site

Table 6 gives the flow and velocity conditions for all BETs. The erosion rate calculations can be performed at any depth by using the two borehole diameter profiles and the time of velocity application. The erosion rate profiles for SBH6 are shown in Figure 30 as an example (E in the figure stands for erosion rate). These profiles show the same tendencies as at the clay site.

During the interpretation of the BET results it is important to realize that there could be some irregularities in the borehole diameter due to sloughing in addition or instead of erosion. This is particularly true in gravel and sand deposits. Good judgement is necessary to make the distinction between borehole collapse and erosion of the borehole soil. In that sense the BET is more suited to fine grained soils than coarse grain soils.

As can be seen in Figure 30, the erosion rate profile varies significantly more than the diameter profile. This is due in part to the fact that the erosion rate is related to an increment of the

diameter profile and as such it magnifies the errors on individual measurements. One way to smooth the data is to use an average in each major layer within the soil horizon.

Table 6- Flow, velocity, and time for the BETs at the sand NGES-TAMU

Borehole Designation	Flow (m^3/s)	Velocity (m/s)	Duration (min)	Change in profile
SBH2	0.00172	0.50	10	Figure 26, C-0 to C-1
	0.00513	1.49	10	Figure 26, C-1 to C-2
SBH6	0.00385	0.32	5	Figure 27, C-0 to C-1
	0.00738	0.61	8	Figure 27, C-1 to C-2
	0.00808	0.58	8	Figure 27, C-2 to C-3
SBH7	0.00874	1.07	8	Figure 28, C-0 to C-1
	0.00477	0.47	8	Figure 28, C-1 to C-2
	0.00528	0.50	9	Figure 28, C-2 to C-3
SBH9	0.00215	0.39	7	Figure 29, C-0 to C-1
	0.00240	0.34	7	Figure 29, C-1 to C-2

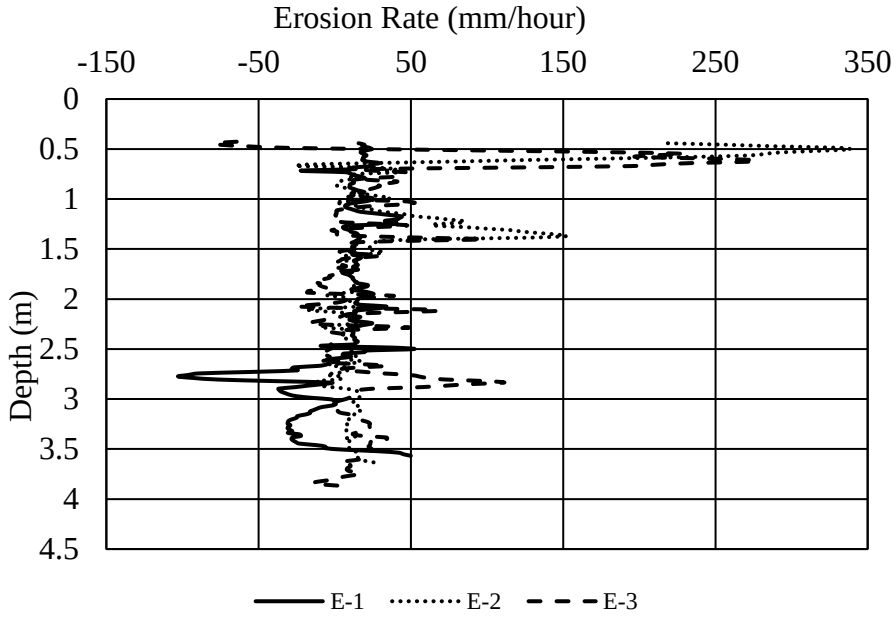

Figure 30- BET erosion rate profiles for SBH6 at the sand site

Also in Figure 30, there are negative values of the erosion rate. The likely reason for this surprising result is that the caliper did not go through the same path before the erosion test and after the erosion test and that at the depth showing a negative erosion rate the borehole cross section was not cylindrical but oblong or ellipsoidal. The caliper measured mostly the long axis prior to the erosion test and mostly the short axis after the erosion test, thus giving a negative erosion rate at that location. It is suggested that several borehole caliper profiles be taken to minimize this problem. This is part of the lessons learned during this work.

3.6 Numerical Simulations

Computational fluid dynamics numerical simulations were performed for the Borehole Erosion Test (BET), assuming a non-erodible soil. The purpose of these simulations was to obtain estimates of the shear stress generated on the walls of the borehole for a given borehole diameter as well as to better understand how the flow develops around the bottom of the borehole. The Finite-Analytic Navier-Stokes (FANS) numerical method of Chen et al. (1990) and Pontaza et al. (2005) was employed for the prediction of shear stresses on the soil surfaces along the bottom and side walls of the BET. The FANS code solves the unsteady, incompressible Navier-Stokes equation in conjunction with the near-wall two-layer k-ε turbulence model of Chen and Patel (1988). The effect of soil surface roughness is taken into account by using the modified two-layer k-ε model of Patel and Yoon (1995). The FANS code has been employed extensively for the simulation of bridge scour in cohesive soils (Chen 2002; Briaud et al. 2001a), sediment transport around abutments in channel bends (Kim and Chen 2014), and scour infilling in sand (Kim et al. 2016).

The geometry of the drilling rods and borehole are shown in Figure 31. The borehole was 100 mm in diameter and approximately 3.35 m deep; the outside diameter of the rods was 70 mm and the inside diameter of the rods was 40 mm. Two flow rates through the inside of the drill rods were considered (1.45×10^{-3} m3/s and 5.68×10^{-3} m^3/s) because they correspond to the range of flow rates that were possible with the pump of the drill rig used in the field. Also, three distances between the discharge point at the bottom of the drill rods and the bottom surface of the borehole were considered (gap = 25 mm, 75 mm, and 150 mm). Figure 31 shows an example of the velocity distribution results at four different times after initiation of the flow. In this example, the gap between the bottom of the rods and the bottom of the borehole is 25 mm, the flow rate is 1.45×10^{-3} m^3/s and the soil roughness is 5%. The vertical distance shown on the diagrams in Figure 31 is 235 mm and the diameter is 100 mm. The roughness is defined here as the standard deviation σ of the diameter values along the borehole depth divided by the initial diameter D of the borehole. For the BET tests reported here, this roughness varied from 2 to 19%; an intermediate value of 5% was used in the simulations. As can be seen on Figure 31, the velocity vectors range in magnitude from 0 to 6 m/s at the bottom of the borehole, and from 0 to 2 m/s in the annulus between the rods and the borehole wall. These velocities are within the range of interest for velocities in bridge scour for example.

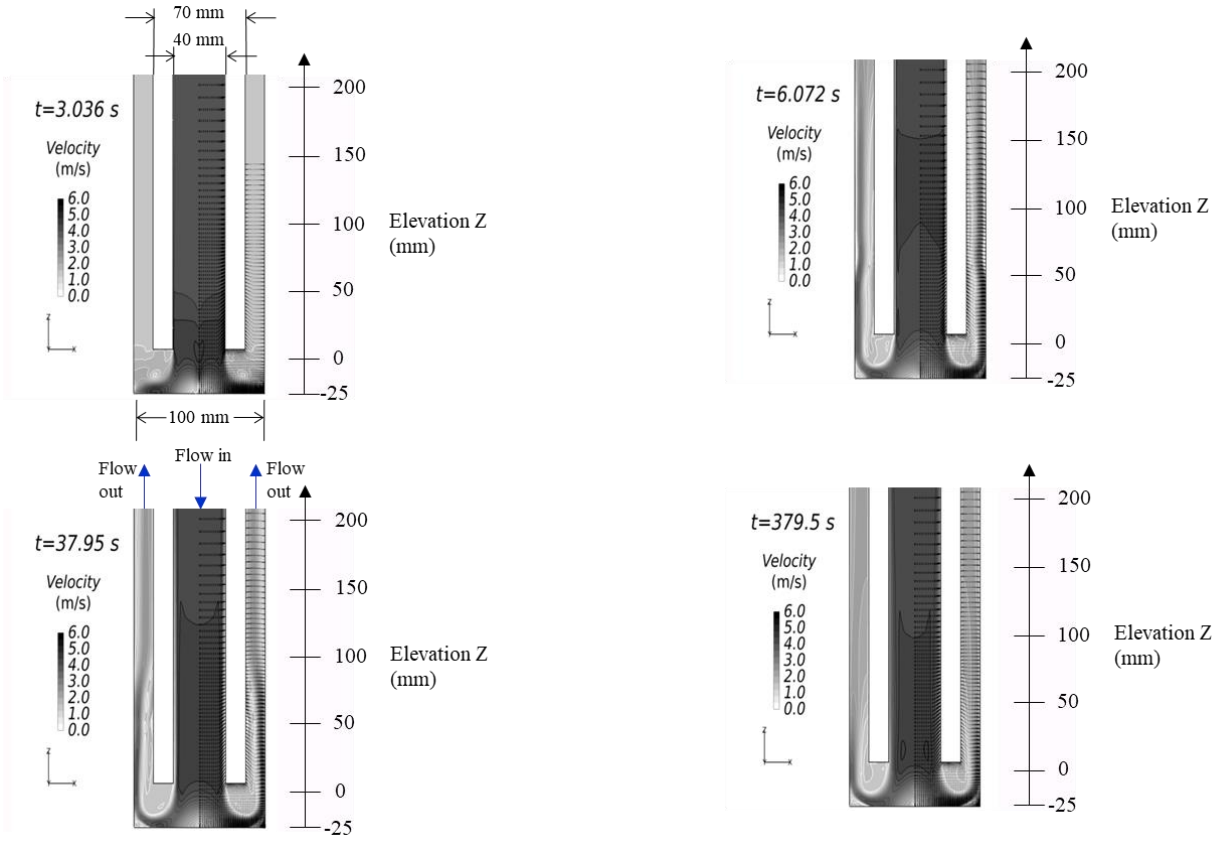

Figure 31- Velocity patterns as a function of time as the flow is established around the BET: (a) time step=400; (b) time step=800; (c) time step=5,000; (d) time step=50,000 (flow=5.68 x 10^{-3} m^3/s; gap= 25 mm; soil roughness = 5%)

Figure 32(a and b) show the shear stress distribution along the vertical wall of the borehole for the high and the low flow values, respectively. An expanded view of these side shear stress distributions from a height of 0.4 m above the borehole bottom to the top of the borehole are presented in Figure 32(c) for the high flow rate and Figure 32(d) for the low flow rate. As expected the shear stress is much higher for the high flow rate. As expected also, the shear stress values for the cases with 5% roughness are well above those corresponding to the case with 0% roughness.

One unexpected observation is that the maximum side shear stress in the transition zone near the bottom of the borehole is reached for the intermediate gap of 75 mm.

Figure 33(a and b) show the shear stress distribution along the horizontal bottom of the borehole for the high and the low flow values, respectively.

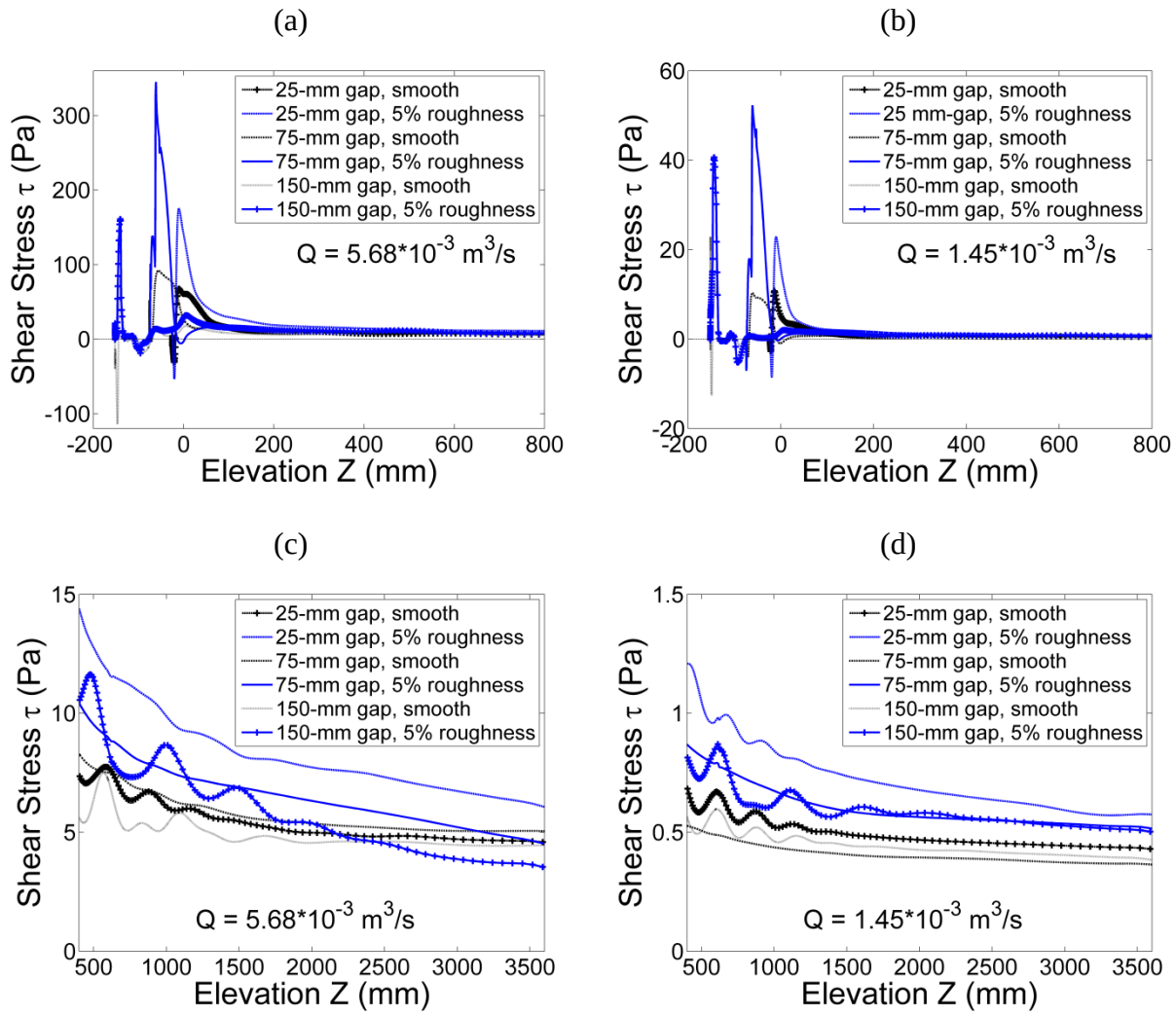

Figure 32- Shear stresses distribution on the borehole wall: (a) flow = 5.68 x 10^{-3} m^3/s; (b) flow = 1.45 x 10^{-3} m^3/s

The effects of the roughness and of the gap between the discharge orifice and the bottom surface of the borehole on the bottom shear stress are similar to those observed for the side shear stresses. Figure 33(a and b) indicate that the maximum shear stress at the bottom of the borehole can be 10 times larger than the steady state shear stress along the sides of the borehole. The rapid variation in shear stress along the bottom of the borehole makes the Bottom BET (BBET), a jet test, much more difficult to interpret precisely than the Lateral BET (LBET).

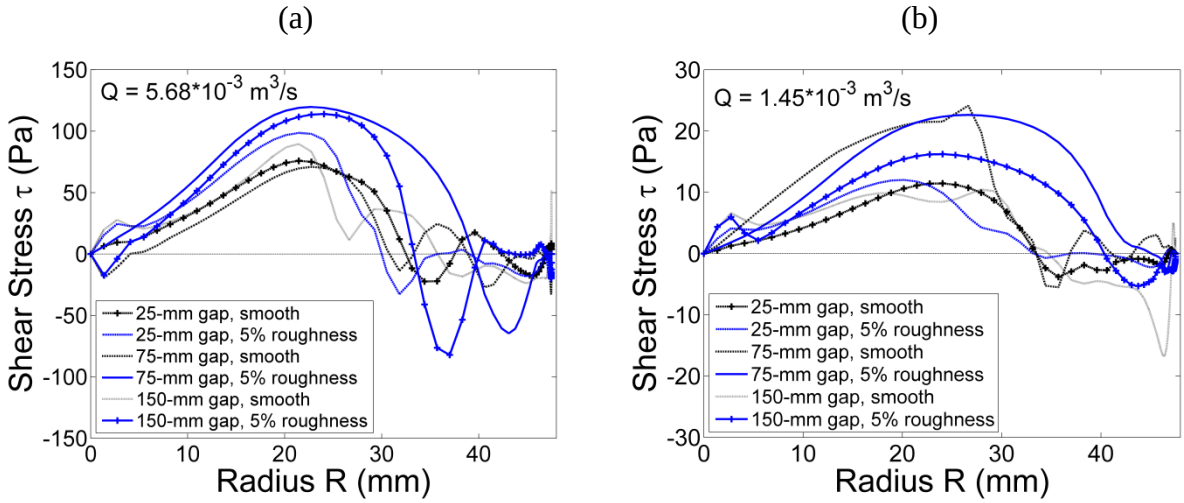

Figure 33- Shear stresses distribution on the bottom surface of the borehole: (a) flow = 5.68 x 10^{-3} m^3/s; (b) flow = 1.45 x 10^{-3} m^3/s

3.7 Validation of the Proposed Test

Samples were collected as part of the preparation of the BET boreholes. At the clay site the samples were obtained by pushing thin wall steel tubes, bringing the tubes back to the surface, leaving the samples in the steel tubes, bringing the tubes and samples back to the laboratory and testing them in the EFA. At the sand site they were obtained by sampling with the split spoon sampler, bringing the sampler back to the surface, splitting the sampler open, and placing the disturbed sand in plastic bags. All the material collected from the split spoon samples in one

borehole was used to reconstruct one sand sample representative of that borehole. Each of the sand samples was reconstructed to its natural moisture content and compacted in layers in a Shelby tube. The compaction process consisted of forming 50 mm thick layers and applying 7 blows per layer to achieve a total unit weight of 20 kN/m^3; this unit weight had been measured in previous projects at the National Geotechnical Experimentation Site (Briaud 1997).

The EFA tests followed the procedure described earlier (Briaud 2013). The EFA results can be presented as erosion rate versus velocity or erosion rate versus shear stress. While it is easier to get a feel for the value of a velocity, it is more theoretically satisfactory to use the shear stress because the velocity near the interface with the soil is not a unique quantity and is in fact theoretically zero at that interface. For that reason all results are plotted as erosion rate versus shear stress. This shear stress was calculated using the mean flow velocity and Moody chart (Moody 1944; Briaud 2013).

For the BET the interface shear stress is obtained from the numerical simulations. These numerical simulations were developed to match the dimensions and flow conditions in borehole CBH1 and gave the shear stresses for the BET in borehole CBH1. Because of the rapid variation of the shear stress along the side of the borehole near the bottom of the drilling rods, the average shear stress from 0.6 m above the bottom of the drilling rods to the top of the borehole (3.5 m) was used in the data reduction. These shear stresses were extrapolated to obtain the shear stress for all other BETs including the side shear stress for the lateral BETs (LBET) and the bottom shear stress for the bottom BET (BBET). The extrapolation scheme was as follows. First, the values of the steady state side shear stress τ_{side} and the maximum bottom shear stress τ_{bottom} corresponding to the flow rates used in CBH1 (Q_1= 1.45x10^{-3} m^3/s and Q_2=5.68x10^{-3} m^3/s), were determined using the simulation results shown in Figures 32 and 33. The side shear stress τ_{side} was taken

from Figure 32 as the average of the values between 0.6 m and 3.5 m along the borehole. The maximum bottom shear stress τ_{bottom} was taken as the maximum value on Figure 33. It is well known (Munson et al, 2009) that the shear stress is proportional to the square of the velocity or square of the flow rate since the cross section does not vary significantly. The average ratios of $\frac{\tau_{side}}{Q^2}$ and $\frac{\tau_{bottom}}{Q^2}$ were calculated for the numerical simulations matching the case of CBH1. These average ratios were then used together with the different flow values Q for other boreholes to estimate τ_{side} and τ_{bottom} for any value of Q. Furthermore, the case of 5% roughness and 25-mm bottom gap was used because it corresponds more closely to the actual field case. Table 7 shows the shear stresses obtained for the LBETs and the BBETs.

Table 7- Side shear stresses and bottom shear stresses calculated for the BETs.

Borehole Designation	Q_1 (x 10^{-3} m^3/s)	Q_2 (x 10^{-3} m^3/s)	Q_3 (x 10^{-3} m^3/s)	τ_{side1} (Pa)	τ_{side2} (Pa)	τ_{side3} (Pa)	$\tau_{bottom1}$ (Pa)	$\tau_{bottom2}$ (Pa)	$\tau_{bottom3}$ (Pa)
CBH1	1.42	5.62	5.68	0.64	9.76	9.76	9.27	141.87	141.87
SBH2	1.72	5.13	—	0.88	7.91	—	12.77	114.92	—
CBH3	8.50	9.07	5.45	21.97	24.99	8.91	319.21	363.19	129.54
CBH5	5.19	8.48	—	8.10	21.64	—	117.77	314.50	—
SBH6	3.85	7.38	8.08	4.48	16.50	19.75	65.17	239.76	286.97
SBH7	8.74	4.77	5.28	23.29	6.96	8.50	338.41	101.17	123.59
CBH8	2.21	1.32	2.08	1.48	0.53	1.31	21.46	7.72	19.07
SBH9	2.15	2.40	—	1.39	1.74	—	20.25	25.29	—

The average erosion functions resulting from the EFA tests and the BETs in the clay boreholes CBH1 and CBH3 are shown on Figure 34 and Figure 35, respectively. Figures Figure 36 and Figure 37 show the average erosion functions from the BETs and the EFA in the sand boreholes SBH2 and SBH6, respectively. In both cases, clay and sand, the comparison between the two

types of erosion tests is reasonable and the trend is similar. The scatter in the results gives an indication of the precision which can be expected. It is also noted that the LBET and the BBET are reasonably consistent since they approximately line up on the same erosion function curve. The BBET does generate much larger shear stresses than the LBET thus the erosion rate associated with the BBET are much higher. Also, the shear stresses calculated assumed that the fluid was water. This is not exactly correct as, at the clay site, the water mixed with the natural clay to form a drilling mud while at the sand site it was purposely mixed with bentonite clay to form the drilling fluid. Drilling mud has a higher viscosity than water; if the viscosity of water is 10^{-6} kPa.s, the drilling mud viscosity is typically anywhere from 1.3 to 2.5 times higher than that. No correction factor was applied for this difference as the mud viscosity was unknown. In the future the mud viscosity should be measured for example with the Marsh Funnel test to improve on the precision with which the shear stresses are calculated. Overall, the comparison of BET with EFA tests proves the new BET concept and validates its results.

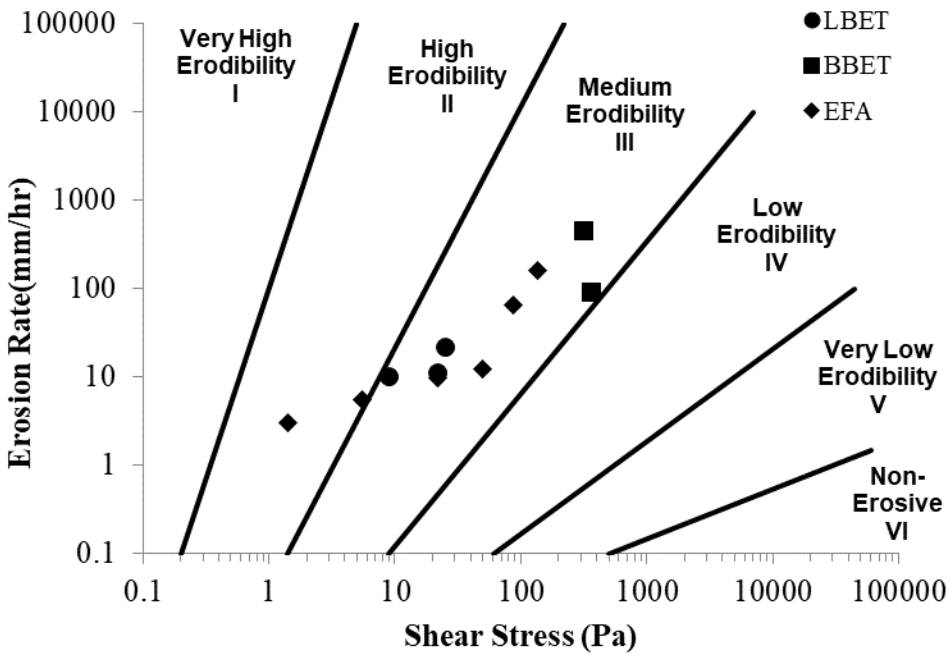

Figure 34- EFA, LBET and BBET results for clay borehole CBH3

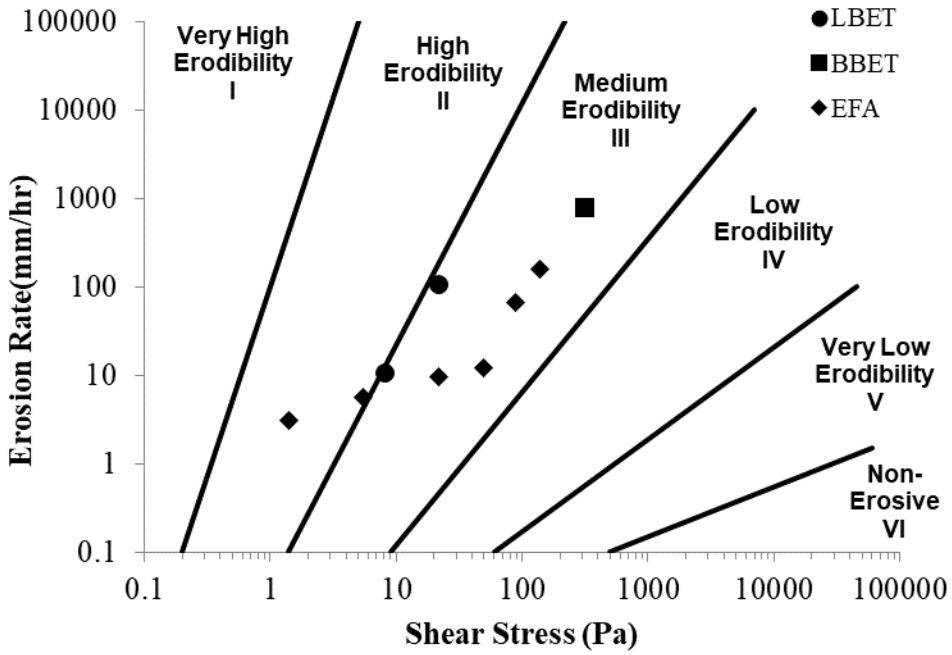

Figure 35- EFA, LBET and BBET results for clay borehole CBH5

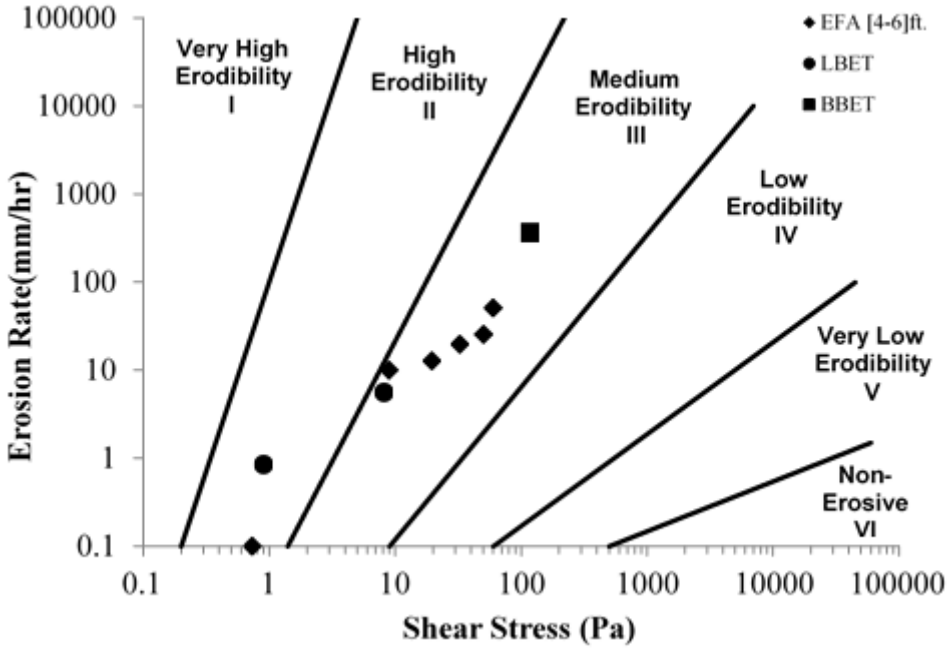

Figure 36- EFA, LBET and BBET results for sand borehole SBH2

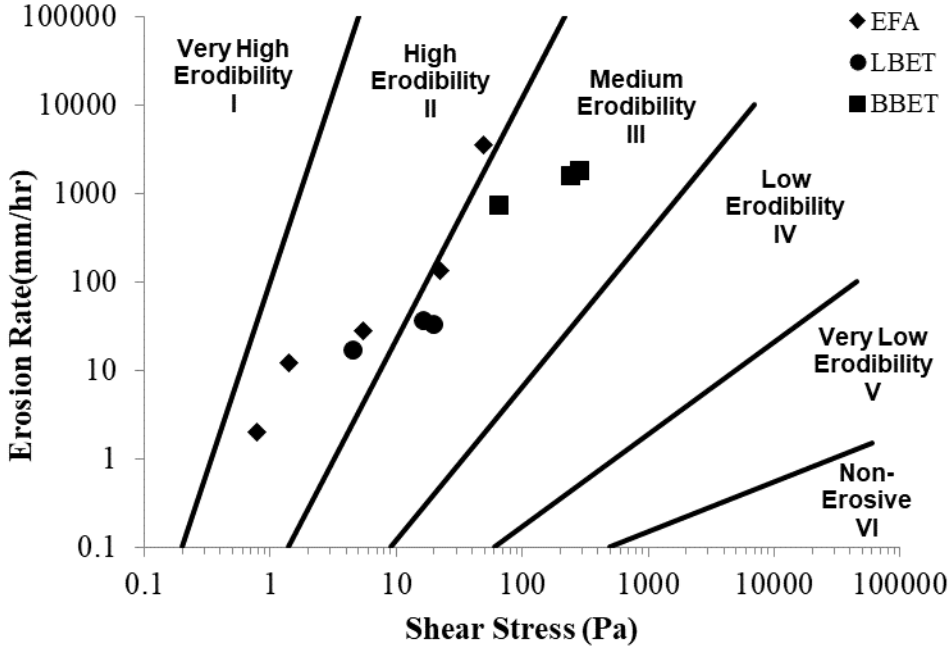

Figure 37- EFA, LBET and BBET results for sand borehole SBH6

3.8 Advantages and Limitations of the Borehole Erosion Test

The BET test has several advantages

- It does not require that any special equipment be built and as such anyone can carry the test.
- Boreholes are drilled for soil identification on many jobs where erosion is a concern. Running a BET only represents incremental work rather than a new set of tests.
- It tests the soil under its in situ stress environment and is a quick test considering the amount of data collected.
- Each test gives the erosion function for all layers traversed since a complete borehole diameter profile is obtained from the calipers. This would require many tests on many samples if laboratory tests were to be conducted.
- It has two component tests: the lateral erosion test associated with the increase in diameter of the borehole or LBET and the bottom erosion test associated with the increase in depth below the bottom of the drilling rods during the flow or BBET. The LBET is much like an in situ HET and the BBET is much like an in situ JET.
- Given the flow rate that the pump on the drill rig can generate, the diameter of the drill bit can be adjusted so that the velocity in the annulus between the rods and the borehole wall is in the right range.

The BET test has limitations as well

- If the borehole is unstable, any collapse maybe interpreted as erosion. This can be minimized by using the proper weight of drilling mud.

- The fluid circulating is drilling mud instead of the river water. This difference in chemistry and viscosity may influence the results and should be accounted for. Many erosion tests face the problem of the eroding fluid having a different chemistry from the river water.
- The arms of the mechanical caliper could penetrate into the wall of the borehole thus giving erroneous readings. Therefore it is important to have soft springs on these arms and larger areas at the tip of the arms to minimize the pressure on the wall of the borehole while maintaining contact.
- If the horizontal cross section of the borehole is not round and if the borehole calipers are not inserted in the same position, inconsistent readings will be obtained. This can be remedied by lowering the caliper several times, each time recording the diameter profile, and using the average of all diameter profiles.

4. CASE HISTORIES OF BRIDGES WITH SCOUR AT ABUTMENTS

4.1 Objectives of Case Histories Collection

Case histories of scoured abutments serve to:

- Make sure that the variables ranges, used to perform the slope stability simulations and hence to develop the guidelines for the maximum allowable scour depth, cover their actual values at bridge sites.
- Infer the possible failure modes of abutments due to scour.
- Validate the equations developed to predict the failure scour at/near spill-through abutments.
- Prepare application examples using the proposed guidelines.

The search was not only limited to failure cases but also included the cases where the abutment remained stable even when exposed to significant scour. Both the failure and non-failure cases are equally valuable for the validation of the developed equations for the failure scour depth; the calculated failure scour depth would be smaller than the observed scour depth for the failure cases and larger than the observed scour depth for the cases were the abutment remained stable.

Overall, case histories associated with scoured abutments are not infrequent. However, case histories where all the desired information is documented were extremely difficult to find. This is because most of the field scour studies only report the depths of the different scour components at bridge sites (pier, contraction, and abutment scour), which is not sufficient for the determination of the total scour depth at/near the abutment and the validation of the proposed methods.

4.2 Sources of Field Scour Measurements

The main sources of field scour data are the result of cooperative programs between the United States Geological Survey (USGS), FHWA, NCHRP, and some state DOTs. These cooperative studies mainly aimed to assess the applicability of scour prediction equations for the geometry, soil, and hydrology conditions at bridge sites throughout the United States. Another objective was to develop methods to monitor scour in the field.

Four sources of scour measurements near/at the abutments are found and studied. These are: the National Bridge Scour Database (NBSD), the South Carolina Bridge Scour Database (SCBSD), abutment scour data in Maine, and contraction scour data in Alabama (Table 8).

Table 8- Summary of field scour data

	Number of bridge sites	Abutment type	Scour depth at/near the abutment (ft)	
			Minimum	Maximum
NBSD	96	Spill-through and vertical-wall	0	18*
SCBSD	146	Spill-through	0	23.6
MAINE	50	Vertical-wall	0	6.8*
ALABAMA	25	Not stated. Field measurements focused on clear water contraction scour.	1.4	10.5

*This might be not the total scour at/near the abutment as the reference for measurement was the ambient bed elevation and consequently contraction scour component might be excluded from the measurement.

The NBSD contains bridge sites located in 20 states in the United States. Three of which had experienced abutment damages due to scour. These failure cases along with other NBSD cases were retrieved and analyzed. The remaining three sources (SCBSD, Maine, and Alabama) present scour measurements at typical bridge sites in each of the three states and result in empirical scour prediction methods specific to each state. Even though these three sources are state-specific and do not contain any limiting or critical scour data, they provide field insights about the shape, location, and depth ranges of scour at or near the abutments. These field observations are useful for modeling the scour hole.

4.2.1 National Bridge Scour Database

The NBSD is a result of three rounds of national scour field data collection. The database was established because of the first USGS national scour field data collection in 1996 to evaluate and improve the existing physical and numerical scour models and prediction equations. The second USGS national study (Mueller and Wagner, 2005) expanded the database from 56 to 79 sites. The NCHRP project 24-14 (Wagner et al., 2006) added 15 sites to the database. Today the database contains a total of 93 sites compiled in the Bridge Scour Data Management System (BSDMS), which is made accessible online through the website of the USGS Office of Surface Water (USGS, n.d.). The BSDMS summarizes each bridge site, which consists of information about the bridge location and specifications, channel geometry, measured scour components (abutment, pier, and contraction), hydraulic or flood characteristics, and bed sediment data.

The different scour components are determined by analyzing the collected bathymetric data and defining reference surfaces corresponding to each component of scour. For contraction scour, the reference surface is the average elevation of the uncontracted sections upstream and

downstream of the contracted bridge section. When determining the average bed elevation of the contracted section, the local scour holes due to pier or abutment scouring processes are excluded. Contraction scour is therefore determined by subtracting the average contracted elevation from the average uncontracted elevation. As for the local pier and abutment scour, the reference surface is the concurrent ambient bed surface near the pier or the abutment but outside the extent of the local scour hole. Local pier or abutment scour is calculated as the difference in elevation between the bottom of the scour hole and the concurrent bed surface near the hole. This way of separating local abutment scour from contraction scour makes it difficult to assess whether the total scour at/near the abutment should be equal to the abutment scour component only or to the summation of the abutment scour and contraction components. In addition, the summary report does not include information about the location of the reported scour depths. However, some cases in the NBSD are supported by files containing additional data such as the bridge plan, channel cross-section data, hydrograph, etc. The supporting files for two case histories are retrieved and the raw data are analyzed to determine the maximum observed scour depth near the abutment and the location of this scour relative to the abutment toe.

4.2.2 South Carolina Bridge Scour Database

Measurements of abutment and contraction scour are collected by the USGS and the South Carolina Department of Transportation at 146 bridge sites in the Coastal Plain and Piedmont of South Carolina. Bridge sites in the Coastal Plain and Piedmont sites consist of either low flow main channels with set-back abutments in the floodplain or shallow swampy channel on the floodplain (Figure 38). In total, 209 abutment scour measurements and 76 contraction scour measurements were collected during this field study. These observations are used to verify the

applicability of scour prediction equations and to develop an improved method to predict scour in South Carolina.

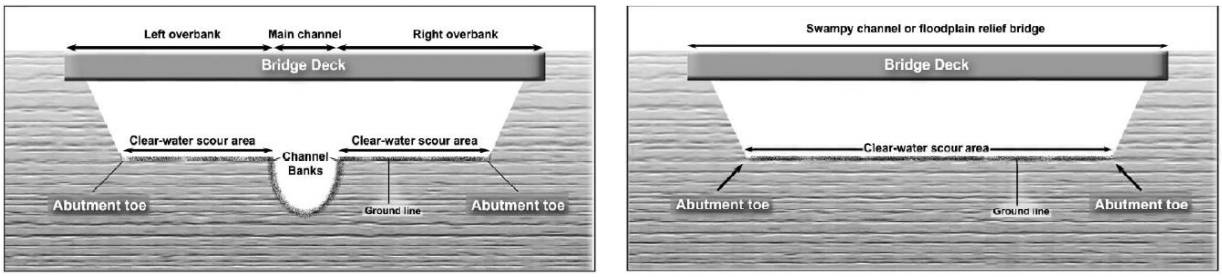

Figure 38- Common configuration of abutments at Coastal Plain bridge sites in South Carolina (reprinted from Benedict 2016)

During the October 1990 flood in South Carolina, 79 bridges failed due to abutment embankment washout. The severe flow contraction at the abutment caused bank mass failures. The resulting channel widening undermined the stability of the abutment structure located in the overbank at a close proximity to the main channel bank. Deemed outside the scope of the study, 114 bridge sites experiencing channel widening were not included in the SCBSD. In fact, none of the bridge sites selected for this study are experiencing critical scour conditions.

The conclusions drawn from the study are limited to spill-through abutments as only 3 out of the 146 selected bridges have vertical-wall abutments. The scour measurements reflect the maximum scour depth at each studied site since the bridge construction and are not associated with a particular flood event. The reference for measuring contraction and abutment scour depths is the average undisturbed floodplain elevation near the scour hole. The scour depth is assessed as either contraction or abutment scour as these two scour components are considered mutually exclusive.

In other words, contraction scour is not considered as a component of total scour in the area of the abutment. This is justified by the fact that contraction scour equation is derived based on the assumption of rectilinear flow patterns, which does not hold in the area of the abutment.

The South Carolina field scour observations provide valuable guidance on the abutment scour hole longitudinal and lateral locations, width, and shape. The study reveals that 68 percent of the measured abutment scour holes are located at the abutment toe and 22 percent are located at a lateral distance between 0.3 and 4.6 m from the abutment toe. The remaining scour holes, located farther away from the toe, are shallow (less than 1.3 m) and have no effect on the abutment stability. Small bridges having a length of 73 m or less show a single hole covering the bridge section. This scour pattern can be caused by the overlap of the curvilinear flow streams of the right and the left abutment at short bridges. At longer bridges, this overlap does not occur, which explains why a separate scour hole was formed at each abutment. However, the breakpoint of 73 m does not apply for bridge sites in other states as stated in the NCHRP 24-14 report. This might be because the lateral location of the scour hole is a function of the contraction at the bridge rather than the bridge length. When the bridge waterway is severely contracted, the scour caused by the highly contracted flow is much larger than the local scour caused by the turbulence structures at the abutment. As a result, the maximum scour occurs at a certain distance from the abutment where the bed shear stress exerted by the contracted flow is maximum. Therefore, the lateral location of abutment scour is best correlated with the contraction ratio and subsequently the ratio of the embankment length to the floodplain width. As for the longitudinal location of the scour, the field investigation shows that scour holes at long bridges are located in the area under the bridge while scour holes at short bridges are found upstream or downstream of the bridge section. This is explained by the interaction of flow from the left and right abutment for small bridges causing

complex flow patterns and subsequently variable longitudinal locations of scour. The field observations show that the scour hole shape is similar to a parabola and can be best approximated using a trapezoid rather than a rectangle.

The measured abutment scour ranges from 0 to 7.2 m at the sandy Coastal Plain sites and from 0 to 5.5 m at the cohesive clayey piedmont sites. This measured abutment scour represents the total scour and not only the abutment scour component. In the coastal plain, infill is measured by taking core samples from the bottom of the scour hole. Infill ranges from 0 to 1.4 m. Infill is added to the maximum scour hole depth to determine the total scour depth. No infill is measured at the Piedmont sites as the scour occurred over the banks, in the clear water scour area. These abutment field measurements show that the scour prediction equations largely overestimate abutment scour depths. The major reason behind the large discrepancies is the difference between the lab and the field conditions and the variables influencing each of these conditions. The collected field data indicate that many factors that control abutment scour in laboratory studies, do not have a significant effect on the abutment scour process under the field conditions in South Carolina. In fact, field data reflect the importance of four variables on abutment scour: embankment length, geometric-contraction ratio, flow velocity, and soil cohesion. Given the poor performance of the scour prediction equations, another method is developed to estimate abutment scour depth for the studied regions in South Carolina. This method consists of envelope curves representing the upper bound abutment scour depths, for the Coastal Plain and Piedmont sites, as a function of embankment length or geometric-contraction ratio. The envelope curves give an estimation of the maximum potential scour for a certain embankment length or geometric contraction ratio at a bridge in the same region and of similar conditions as the bridges in the study.

In addition to abutment scour, clear water contraction scour is measured on the clayey overbanks at Piedmont sites. Contraction scour depths range from 0 to 1.4 m. Contraction scour holes are shown to have the shape of a shallow parabola perpendicular to the direction of the flow. The lateral extent of the contraction scour encompasses most of the area under the bridge, which is unaffected by the abutment scour process. Similar to the case of abutment scour, theoretical values of clear contraction scour excessively overestimate the actual contraction scour depths. An envelope curve of the maximum observed contraction scour as a function of the geometric contraction ratio is proposed to more accurately estimate the depth of clear water contraction at bridges in Piedmont.

The scour data and soil gradation at bridge sites from this study is compiled into the SCBSD, which can be accessed through Microsoft Access. In addition to the clear water scour data, the SCBSD also includes live-bed pier and contraction scour data measured in the main channel of bridge openings during a subsequent investigation conducted in 2009. Even though it does not include failure case histories, the SCBSD is a potential source for case histories. However, no cases are retrieved from the SCBSD because the scour distance from the abutment and abutment geometry are not reported.

4.2.3 Abutment Scour Data at Selected Bridges in Maine

Abutment scour is measured at 50 bridge sites in Maine by the USGS in cooperation with Maine DOT to evaluate 5 abutment scour prediction methods: Froehlich/Hire method, Sturm method, Maryland method, Melville method, and the envelope curves approach. The abutments at the study sites are vertical wall abutments with wing walls and are mainly located near the main channel (Figure 39). The abutment scour holes are surveyed with a total station theodolite or

measured from the surveyed water surface elevation. The measured scour depths represent the maximum historical scour depths and are not related to any particular flood event. The reference surface for measuring the abutment scour is the concurrent streambed surface outside the abutment scour zone. Therefore, the measured scour depths do not include contraction scour, which is assumed to cover all the bridge section.

Figure 39- Typical abutment configuration and location at the studied bridge sites in Maine (reprinted from Hodgkins 2008)

Since most of the abutments in the study protrude into the main channel, live-bed abutment scour is expected, and the evaluation of the infilled scour depth is necessary to determine the total scour depth. A ground penetrating radar is introduced in scour holes deeper than 0.3 m to determine the infilling depth. The field investigations also included the collection of soil samples from the approach section for grain size analysis and the determination of D_{50} and D_{max} to be used in some of the tested prediction equations.

The study indicates that the four tested prediction equations highly over-predict the abutment scour. In addition, no correlations existed between the observed scour and any of the considered variables (D_{50}, abutment skew angle, length of active flow blocked by the abutment embankment, contraction ratio, flow depths, velocities, and discharges in the main channel or floodplain). Therefore, envelope curves giving the maximum observed abutment scour at bridges in Maine as a function of these variables could not be developed. However, none of the abutment scour measurements exceeds 2.1 m. An FS can be applied to this maximum value to estimate the abutment scour depths at bridge sites in Maine sharing similar conditions (bridge opening, drainage area, abutment types, abutment, and embankment skew angles) with the studied sites. There are many limitations of using a single number as a maximum abutment scour depth. First, the maximum scour depth is based on a limited number of abutment scour observations (100 observations). Second, scour depth in excess of 2.1 m could have occurred at bridges that were replaced, or could have been masked by any undetected infilling.

The reported total observed scour (calculated as the sum of visible observed scour and scoured measured with ground penetrating radar) at the left and right abutment of each bridge is reported. This depth ranges from 0 to 2.1 m with an average of 0.24 m. The abutments at all the 50 surveyed bridge sites are stable. However, none of the studied bridges have spill through abutments. In addition, the contraction scour depths and the scour hole locations are not reported, and the bridge plans are not made accessible. For these reasons, none of these sites can be used as a case history.

4.2.4 Contraction Scour Data at Selected Bridges in Alabama

Clear water contraction scour measurements are made at 25 bridge sites in the Black Prairie Belt of the Coastal Plain of Alabama by the USGS and the Alabama DOT. The Black Prairie Belt is in the north half of the Coastal Plain, which constitutes 59 percent of the total area of Alabama. The Black Prairie district was selected for the field measurements because previous scour investigations by Alabama DOT showed that theoretical scour depths in this area were unrealistic and excessive. The field study aims at developing a more reliable method of scour assessment in this area (Lee and Hedgecock 2008).

The soil type at the studied bridge sites consists of highly cohesive, consolidated, and organic clay. This fertile soil type explains the presence of grasslands and vegetated floodplains. Both the cohesive soil and the presence of vegetation justify the assumption of clear scour condition in the overbank areas of a bridge or under a relief bridge. Since this study focuses only on clear water scour, the scour holes considered were the ones located in the overbanks, swampy channels, or under a floodplain relief bridge. The measured clear water scour is not related to a particular flood event and can be considered as the maximum historical scour during the life of the bridge. Scour depth measurements are made using an electronic total station. The reference for defining the clear water scour depth was considered to be the unscoured surface at the bridge section and was estimated by linear interpolation between the upstream and downstream surfaces in the approach and exit sections of the bridge, respectively. The maximum scour depth is then found as the difference between the elevation of the scour hole bottom and the reference surface elevation. While this measured clear scour has three separate components (abutment scour, contraction scour, and pier scour), the main component at the selected sites is judged to be

contraction scour based on the location and the shape of the scour hole. As a result, the scour database at the surveyed sites includes only clear water contraction scour.

The study concludes that Laursen's equation severely overestimates the scour depths by around 475 percent. Following the same approach outlined by Benedict (2016) for South Carolina, the correlation between the observed scour depth and variables deemed to be important in laboratory investigations in addition to several other hydraulic variables are examined. These variables include D_{50}, bridge velocity, critical velocity, approach velocity, velocity index, channel contraction ratio, hydraulic ratios, geometric contraction ratios, depth variables, and other variables. None of the examined variables provide a good statistical correlation with the observed scour depth (with $R^2>0.8$). However, graphical analysis shows that the measured contraction scour correlated best with the channel contraction ratio and index velocity. As a result, envelope curves relating these variables to the maximum values of observed scour are developed. These curves are used as a more reliable method for assessing clear water contraction scour at bridge sites of cohesive soils in the Black Prairie Belt. The larger value of scour depth obtained from both envelopes should be used and an FS may be applied to this value. These envelopes are only applicable where the flood events do not exceed the 100-year flood and where the values of velocity index and channel contraction ratio are in the range of the corresponding values used to develop the envelopes.

The only reported scour by this field study is the contraction scour in the overbanks, swampy channels, or under relief bridges. The depth of this scour varied from 0.4 to 3.2 m. Although the location of the scour hole is not reported, it is stated that deepest observed scour was in the middle of the bridge span and not at the piers or the abutments. However, the abutments

type is not indicated, and the bridge plans are not made available. Consequently, none of the 25 selected bridge sites in Alabama can be used as a case history for this study.

4.3 Criteria for Selection of Case Histories

The selection of quality case histories from the four sources (Table 8- Summary of field scour data) is controlled by the availability of the required data. Very few cases provide all the information needed to validate the developed equations for failure scour and proposed guidelines for allowable scour. Since FHWA does not require the abutment scour to be computed in the cases where appropriate scour protection is provided, the validation of abutment scour equation becomes less important than that of pier scour equation. This explains why pier scour measurements are much more abundant than abutment scour measurements. Besides, the data collected at each bridge site are limited to the variables needed to apply the scour equations: scour depth, hydrologic and hydraulic data, and soil gradation. Therefore, it has been a challenge to find case histories where all the following criteria are met:

- Abutment type is spill-through.
- Abutment geometry information are reported, or bridge plan is made available.
- Total scour depth at/near the abutment is reported or bridge channel-cross section measurement records are made available.
- Scour location is reported or bridge channel-cross section measurement records are made available.
- Soil strength information (in-situ test results, soil description, pictures showing the slope of scour hole walls) is available.

- Possible water conditions in the channel are described (rapid draw-down, dry condition, steady state water level). If failure occurred, water conditions at the time of the failure are specified.

4.4 The Bridges Selected as Case Histories

Seven cases meeting the above requirements were identified. Two cases were retrieved from the NBSD. Both cases were supported by their raw data files, which were studied to determine the required information. The other five cases were obtained by direct contact with the TxDOT offices in Bryan and Austin. Each of the seven cases is analyzed to determine the parameters related to abutment geometry, scour depth and location, soil shear strength, and hydraulic conditions in the river channel. The abutment geometry variables are mainly the total height of the abutment H and the slope of the abutment spill-through embankment β. In addition, the presence of any erosion protection feature is mentioned. These geometry parameters are determined using the bridge plans for each case. The scour hole depth Z is measured as the difference in elevation between the abutment toe and the bottom of the scour hole. The scour hole location D is the horizontal distance between the abutment embankment toe and the nearest edge of the scour hole. The scour hole wall slope angle θ is the angle that the nearest wall of the hole makes with the horizontal. These scour variables are calculated based on the channel cross-section measurements for each case. Information about the soil type and geotechnical properties are extracted from soil description found in reports, in-situ test results recorded on boring log sheets, and/or any additional reported sampling and testing of the channel soil. For Texas case histories, the undrained shear strength S_u of the channel bed soil is estimated using the blow count N from the in-situ Texas Cone Penetrometer (TCP) test. The hydraulic condition or flooding event mainly

responsible for scouring the abutment is determined. In the cases where a slope stability failure occurred, the water condition at the time of the failure is described. For the cases where the water elevation is measured, the Water Level (WL) is expressed as a percentage of the embankment height. Abutments are described as right or left abutments with reference to the downstream flow (i.e., looking downstream).

4.4.1 Case No.1: CR 22 over Pomme De Terre River

This case is retrieved from the NBSD. Supporting files for this case (Site ID 73) consist of a plot of the bridge plan, photos taken during the flood and various channel cross-sections measurements. The bridge is in a rural/agricultural area in Swift County, Minnesota. The bridge channel was surveyed on three days during a flood in April 1997 and then after the flood in July 1997. During the flooding event, scour progressed near the right abutment (Figure 40). During the visit on 9 April 1997, a slope failure of the right abutment (looking downstream) was observed.

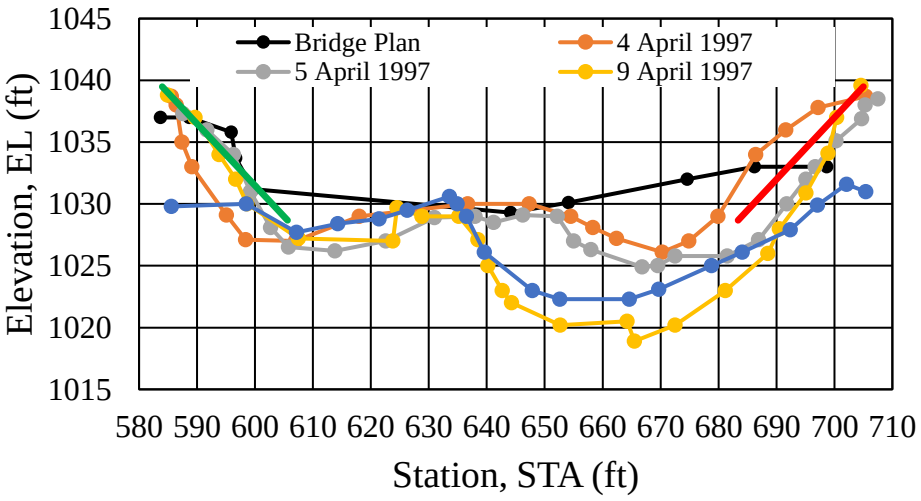

Figure 40- Channel profiles for CR 22 over Pomme de Terre River

The bridge plan (Figure 41) shows that the total height of the abutment is H= 5 m, and the slope angle of the abutment spill-through embankments is β= 26.6°. The right and left embankments are protected with stone riprap.

As previously mentioned, the reference adopted by the USGS for computing abutment scour is the concurrent bed elevation. The abutment scour depths reported in the USGS case summary report for 4, 5, and 9 April 1997 are 1.2, 1.3, and 3 m for the right abutment and 0.9, 0.85, and 0.6 m for the left abutment, respectively. The abutment scour component is then added to the contraction scour component, which is calculated as the difference in the average elevations of the uncontracted and contracted sections. In this case, no measurements were taken at the uncontracted section. Contraction scour is assumed to be the change in elevation of the main channel not affected by abutment scour (i.e., the change in elevation of the highest point in the center of the cross-section). In this way, a contraction scour of 0.3 m is reported and added to abutment scour.

To validate the guidelines developed by this research, the scour depth is defined as the total depth of the scour hole at the abutment and can be measured as the difference in elevation between the abutment toe and the bottom of the scour hole. The channel profiles (Figure 40) show that the scour depth on the failure day (9 April 1997) is Z_{Right}= 3 m at the right abutment and Z_{Left}= 0.46 m at the left abutment. The distance D between the abutments and nearest edge of the scour hole is zero.

While no information is given about the embankment soil, the channel bed soil is classified as silty sand SM. The boring logs in Figure 41 indicate that the channel bed is mostly sand with few peaty loam layers. Soil samples collected from the upstream bridge face are comprised of non-cohesive fine sand and silt. Standard Penetration Test N results at the bottom of the abutment,

reported on the boring logs (Figure 41), are used to estimate the channel bed friction angle φ'_c, which is found to be 30°.

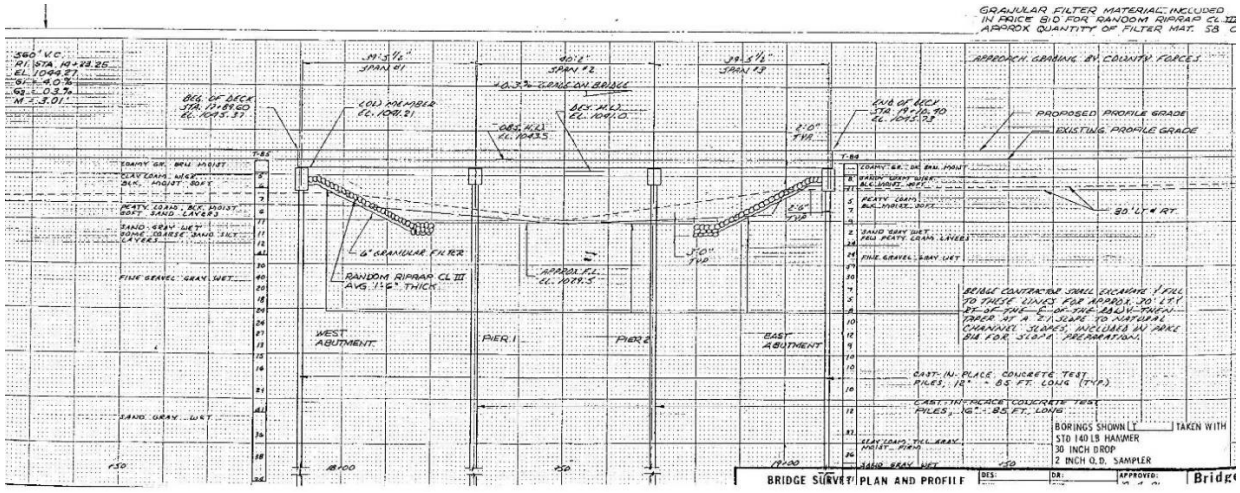

Figure 41- Profile plot of CR 22 over Pomme de Terre River from bridge plan

Regarding the hydraulic condition at the bridge, the WL was measured during the flood and was found to submerge the entire height of the abutment embankment without overtopping the bridge (i.e., WL=100 percent).

Table 9 summarizes the geometry, scour, geotechnical, and hydraulic parameters for this case.

Table 9- CR 22 over Pomme de Terre River

	Abutment Geometry			Scour Data			Channel Bed Geotechnical Info		Hydraulic Info.
Abutment	H (m)	β (°)	Scour Protection Feature	Z (m)	D (m)	θ (°)	Soil Type	Shear Strength info	Flood event, WL
Right	5	26.6	Stone Riprap	3	0	-	SM	Friction angle φ'_c = 30°	April 1997 Flood, WL=100%
Left				0.46	0	-			

4.4.2 Case No. 2: SR 37 over James River

This case is retrieved from the NBSD. Supporting files for this case (Site ID 83) consist of photos and channel cross-sections measurements during and after the flood, and bed soil grain size distribution. The bridge is in a highly rural/agricultural area near the town of Mitchell in South Dakota. The James River received the upper Midwestern flooding in spring 2001. Figure 42 and Figure 43 show the bridge condition during and after the flood of April 2001, respectively. The channel at the bridge section was surveyed during the flood on 15 April 2001 (Figure 44). The left abutment experienced some scour but remained stable (Figure 45) while no scour occurred at the right abutment.

The bridge plan is not provided. However, the channel survey at the bridge cross-section (Figure 44) shows that the total height of the left abutment is H_{Left}= 6.3 m while the total height of the right abutment is H_{Right}= 9.8 m. Figure 44 also indicates that the left spill-through embankment has a slope angle of β_{Left}= 18.4° while the right spill-through embankment has a slope angle of β_{Right}= 26.6°. The abutments are not protected against scour.

Figure 42- SR 37 over James River during the flood—looking downstream

Figure 43- SR 37 over James River after the flood—looking at the left abutment from the downstream

The case summary report by the USGS estimates contraction scour at the bridge to be 0.9 m. In addition, abutment scour depths of 1.2 m and 0 m are reported for the left and right abutment, respectively. Based on the channel profile in Figure 44, the scour depth at the left abutment is Z_{Left}= 1.2 m while no scour is observed at the right abutment. The abutment scour component

reported by the USGS is found to be equal to the total scour at the abutment. Hence, contraction scour is not located near the abutment and should not be considered. Figure 44 also shows that the slope of the scour hole at the left abutment is 1.8H:1V, which translate into a scour hole slope angle of $\theta = 29.1°$.

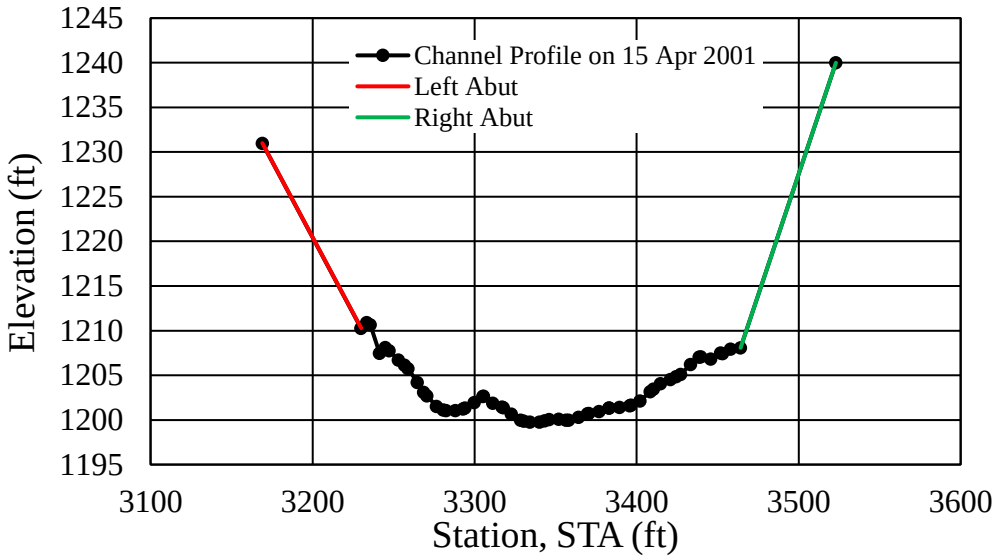

Figure 44- Channel profile for SR 37 over James River

Figure 45- Scour at the left abutment of SR 37 over James River during the flood

Bed material samples show that the upper 3–4.5 m of the channel bed is comprised of sandy silt, followed by 3–6 m of silty clay. The cohesion of the channel bed soil is described as mildly cohesive. No information is given on the soil type of the embankments.

Water surface elevations were measured during the flood using a wire-weight gage located on the upstream bridge face. These elevations are found to cover 81 percent of the abutment total height at the left abutment (WL_{Left}= 81 percent) and 57 percent at the right abutment (WL_{Right}= 57 percent).

Table 10- SR 37 over James River summarizes the geometry, scour, geotechnical, and hydraulic parameters for this case.

Table 10- SR 37 over James River

	Abutment Geometry			Scour Data			Channel Bed Geotechnical Info		Hydraulic Info
Abutment	H (m)	β (°)	Scour Protection Feature	Z (m)	D (m)	θ (°)	Soil Type	Shear Strength info	WL (%)
Right	9.8	26.6	None	0	0	-	Sandy silt	Mildly cohesive	57
Left	6.3	18.4		1.2	0	29.1			81

4.4.3 Case No. 3: FM 692 over McGraw Creek

FM 692 over McGraw Creek is in Newton County, Texas. The bridge has been closed to traffic due to damage sustained during Hurricane Harvey (August–September 2017). The information needed to analyze the case is provided by the TxDOT office in Austin. The flooding

caused significant scour in the bridge channel and caused the failure of the left abutment (Figure 46- Left abutment failure at FM 692 over McGraw Creek).

Figure 46- Left abutment failure at FM 692 over McGraw Creek

The bridge layout (Figure 47) shows that the total embankment height at the left abutment is H_{Left}= 2.5 m and at the right abutment is H_{Right}= 2.8 m. Both embankments have a 2H:1V slope (β= 26.6°). The abutments are protected by concrete riprap. The channel profiles before and after Harvey are presented on the bridge layout (Figure 47) in blue and red, respectively. The observed scour depth at toe of the left abutment after Harvey is around Z_{Left}=2.3 m, and no significant scour is observed at the right abutment.

The borehole logs indicate that the bed soil is slightly silty sand at the left abutment and very clayey silt at the right abutment. The borehole logs also show the results of TCP test. The TCP blow counts, N_{TCP}, at the bottom of the left and right embankments are 15 and 10, respectively. The undrained shear strength S_u values are calculated using N_{TCP} values and the linear

relationship S_u (tsf)= N_{TCP}/40 (TxDOT, 2018). It follows that the undrained shear strength of the channel bed soil at the left abutment is S_{uLeft}= 35.9 kPa and at the right abutment is S_{uRight}= 23.9 kPa. No information is given on the soil type of the embankments nor on the water elevation at the time of the failure.

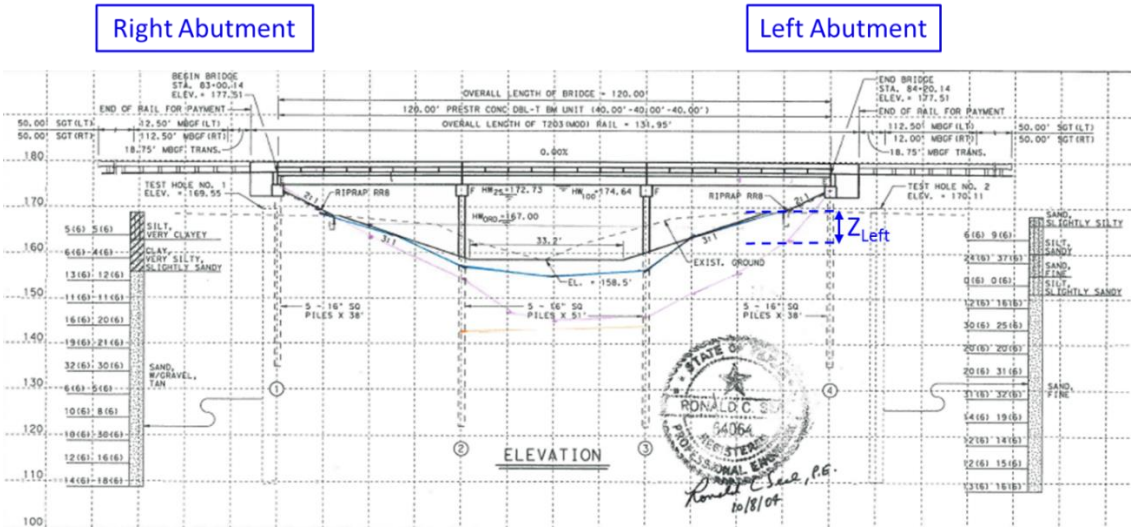

Figure 47- Bridge layout of FM 692 over McGraw creek showing the channel profiles before and after Harvey

Table 11 summarizes the geometry, scour, geotechnical, and hydraulic parameters for this case.

Table 11- FM 692 over McGraw Creek

	Abutment Geometry			Scour Data			Channel Bed Geotechnical Info		Hydraulic Info
Abutment	H (m)	β (°)	Scour Protection Feature	Z (m)	D (m)	θ (°)	Soil Type	S_u (kPa)	Flood Event
Right	2.8	26.6	Concrete Riprap	0	0	-	Clayey silt	23.9	Hurricane Harvey
Left	2.5			2.3	0	-	Silty sand	35.9	

4.4.4 Case No. 4: FM 937 over Montgomery Creek

FM 937 over Montgomery Creek is a single span bridge located in Limestone County, Texas. The bridge was closed to traffic in October 2013 due to the Halloween flash flood event. Figure 48 shows the slope stability failure of the left abutment embankment.

Figure 48- Left abutment failure at FM 937 over Montgomery Creek

The slope of the right embankment did not fail, but the concrete riprap was damaged (Figure 49).

Figure 49- Damaged concrete riprap at the right abutment of FM 937 over Montgomery Creek

The abutment geometry parameters are determined using the bridge plan, provided by the TxDOT office in Austin. The abutments are protected by concrete riprap and have a total height H of 5.3 m and a slope angle β of 26.6°.

The channel profiles at the bridge section are not provided. However, the post flood scour depth was Z_{Left} =2.4 m at the left abutment toe and Z_{Right} =1.7 m at the right abutment toe.

The borehole logs on the bridge layout show that the bed soil beneath the abutments is reddish brown silty clay with sand layers. N_{TCP} values at the bottom of the left and right embankments are 7 and 16, respectively. These values are used with the linear relationship for low plasticity clay (CL) soil type, S_u (tsf)= N_{TCP}/30 (TxDOT, 2018) to estimate the channel undrained shear strength. It is found that S_{uLeft}=22.3 kPa and S_{uright}=51.1 kPa. Embankment soil is a mixture of silty and clayey sand (SM-SC). The WL was not measured during the flood. In addition, the

water condition at the failure time is unknown. Table 12 shows the geometry, scour, geotechnical, and hydraulic parameters for this case.

Table 12- FM 937 over Montgomery Creek

Abutment Geometry				Scour Data		Channel Bed Geotechnical Info		Embankment Geotechnical Info	Hydraulic Info
Abut-ment	H (m)	β (°)	Scour Protection Feature	Z (m)	D (m)	Soil Type	S_u (kPa)	Soil Type	Flood Event
Right	5.3	26.6	Concrete Riprap	1.7	0	CL	51.1	SM-SC	2013 Halloween Flood
Left				2.4	0		22.3		

4.4.5 Case No. 5: CR 309 over Rocky Creek

CR 309 over Rocky Creek is in Washington County, Texas. On 19 April 2016, the bridge was closed to traffic due to Tax Day Flooding. While the concrete riprap remained in place and the abutment embankment did not fail, the soil composing the left embankment was scoured out and washed away (Figure 50). As a result, the abutment drilled shafts were exposed and a large void was formed under the concrete riprap (Figure 51).

The geometry parameters are estimated based on the bridge layout plan, provided by the TxDOT office in Bryan. The abutment embankments have a total height H=2 m and a slope β=26.6°. The abutments are protected against scour by concrete riprap.

Figure 50- Scour at the left abutment of CR 309 over Rocky Creek

Figure 51- Voids under the left abutment concrete riprap of CR 309 over Rocky Creek

The scour parameters are determined using the channel cross-section measurement records (Figure 52), which show no significant changes until the year 2017 (i.e., after the 2016 Tax Day

Flooding). The scour depth at the toe of the left abutment is around 0.9 m, and no scour occurs at the right abutment (Figure 52).

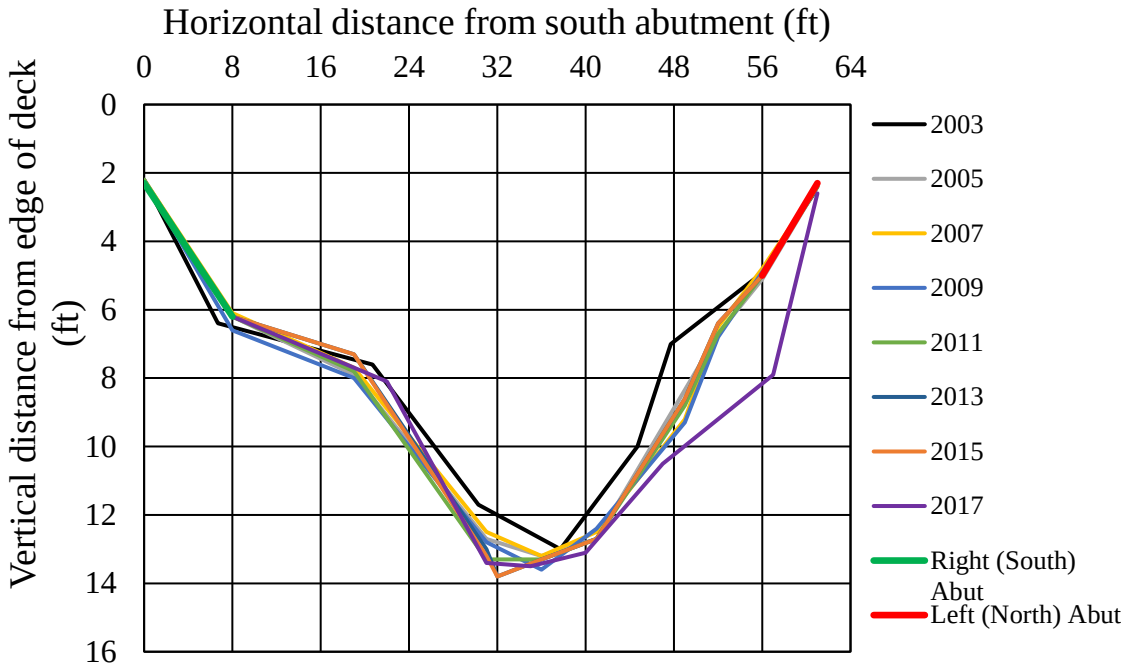

Figure 52- Channel profiles at CR 309 over Rocky Creek from 2003 to 2017

The borehole logs presented on the bridge layout plan indicate that the channel soil directly under the abutment embankment is tan sandy clay. TCP blow counts, N_{TCP}, are reported on the borehole logs. The N_{TCP} values at the bottom of the left and right embankments are 9 and 13, respectively. The linear relationship between the undrained shear strength S_u and N_{TCP} for low plasticity clay (CL) soils, S_u (tsf)= $N_{TCP}/30$ (TxDOT, 2018) is used to estimate the undrained shear strengths of the channel bed at the left and right abutments.

Table 13 presents these geotechnical parameters, in addition to the geometry and scour parameters.

Table 13- CR 309 over Rocky Creek

	Abutment Geometry			Scour Data			Channel Bed Geotechnical Info		Hydraulic Info
Abutment	H (m)	β (°)	Scour Protection Feature	Z (m)	D (m)	θ (°)	Soil Type	S_u (kPa)	Flood Event
Right	2	26.6	Concrete Riprap	0	0	-	CL	41.5	2016 Tax Day Flood
Left				0.9	0	-		28.7	

4.4.6 Case No. 6: SH 105 over Rocky Creek

SH 105 over Rocky Creek is also located in Washington County, Texas. The bridge was closed to traffic in April 2017 due to Tax Day Flooding. Large scour holes formed during the flooding and caused the failure of the right abutment (Figure 28). Pictures from the inspection of the bridge site after the flood showed that the right abutment, where the failure occurred, was not protected against scour while the left abutment was protected by a gabion mattress.

The bridge plans provided by TxDOT office in Bryan are used to determine the abutment geometry parameters. The left abutment height is found to be H_{Left}= 4.4 m, and the right abutment height H_{Right}= 4.9 m. Both abutments have a 3H:1V slope (i.e., β=18.4°).

The channel cross-section was not surveyed during the post-flood inspection. However, the inspector was contacted and asked about the scour that happened in front of the right abutment. It is estimated that the deepest point of the scour near that location was approximately 0.9–1.2 m deep.

Figure 53- Right abutment failure at SH 105 over Rock Creek

The boring log sheet indicates that the channel bed soil consists of clay with some sand. The N_{TCP} values at the bottom of the left and right embankments are 17 and 10, respectively. Using the linear relationship for CL soils in Texas S_u (tsf)= N_{TCP}/30 (TxDOT, 2018), the channel bed undrained shear strength values are found to be at the left and right abutments are found to be S_{uLeft}= 54.3 kPa and S_{uRight}= 31.9 kPa.

Table 14 summarizes the case.

Table 14- SH 105 over Rocky Creek

	Abutment Geometry			Scour Data			Channel Bed Geotechnical Info		Hydraulic Info
Abutment	H (m)	β (°)	Scour Protection Feature	Z (m)	D (m)	θ (°)	Soil Type	S_u (kPa)	Flood Event
Right	4.9	18.4	None	~ 1.2	0	-	CL	31.9	2017 Tax Day Flood
Left	4.4		Gabion mattress	-	-	-		54.3	

4.4.7 Case No. 7: US 90 over Nueces River

This bridge is in Uvalde County, Texas. In 1998, a major flooding scoured the right abutment of the bridge and nearly took out the abutment embankment (Figure 54). The embankment was promptly repaired, and stone riprap was placed at the end of the embankment to prevent future failure due to scour (Figure 55).

Figure 54- Right abutment failure at US 90 over Nueces River

Figure 55- Right abutment repair at US 90 over Nueces River

The 1998 cross-section profile of Nueces River at US 90 shows how the right (west) abutment slope became vertical after the embankment failure due to scour at the abutment (Figure 56). This profile indicates that the total abutment height is around H= 4.3 m, and the abutment slope angle is β= 26.6°. The scour depth at the right abutment is calculated as the vertical distance

between the embankment toe and the bottom of the scour hole (Figure 56) and is found to be Z_{Right}= 2.1 m. The channel bed is comprised of gravel and the embankment soil type is unknown.

Table 15 presents the parameters of this case.

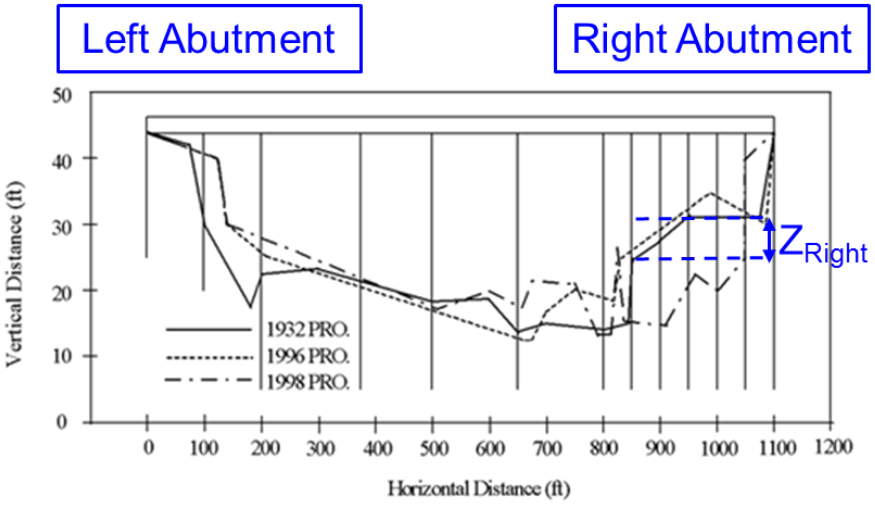

Figure 56- Channel profiles at US 90 over Nueces River

Table 15- US 90 over Nueces River

	Abutment Geometry			Scour Data			Channel Bed Geotechnical Info	Hydraulic Info
Abutment	H (m)	β (°)	Scour Protection Feature	Z (m)	D (m)	θ (°)	Soil Type	Flood Event
Right	4.3	26.6	Concrete riprap	2.1	0	-	Gravel	Major flooding in 1998
Left				0	0	-		

5. CALCULATION FOR SCOUR LIMITS AT ABUTMENTS

5.1 Failure Modes of Spill-Through Abutments

To determine the possible failure mechanisms of bridge abutments due to scour, failure is defined by any abutment damage resulting in the bridge to be closed to traffic. In this context, abutment failure is not limited to the structural failure of the abutment foundation elements. Possible failure modes due to scour at/near the abutment include:

- **Failure mode 1**: Abutment foundation failure by vertical loading (Figure 57).
- **Failure mode 2**: Abutment foundation failure by horizontal loading (Figure 58).
- **Failure mode 3**: Slope stability failure of the abutment embankment (Figure 59).
- **Failure mode 4**: Lateral channel migration and erosion of the embankment soil (Figure 60).

Vertical scour at/near the abutment can expose the abutment foundation elements, ultimately leading to failure mode 1 or 2 where the vertical or horizontal loading capacity of the abutment foundation is exceeded. In addition, scour at the abutment may affect the slope stability of the abutment embankment. This would result in failure mode 3 where soil mass failures occur at the side slopes and/or the spill slope in the case of a spill-through abutment. Failure mode 4 is more likely to happen when the abutment embankment is erodible. This is the case where the embankment soil has not been appropriately protected or where the protection has been damaged. The erosion of the soil making up the embankment creates large voids and cavities under the bridge ends. Although failure modes 3 and 4 will not affect the structural stability of the bridge, they can eventually cause the failure of the approach slab and make the bridge inaccessible to traffic.

Figure 57- Abutment foundation failure by vertical loading

Figure 58- Abutment foundation failure by horizontal loading

Figure 59- Slope stability failure of the abutment embankment

Figure 60- Erosion of the embankment soil

While failure mode 4 can be avoided by adequately protecting the embankment with concrete or stone riprap, failure modes 1, 2, and 3 can be prevented by limiting the depth of vertical scour at/near abutments. This vertical scour may be contraction scour, local scour at the abutment, long-term degradation, or most commonly a combination of these components. According to HEC-18, abutments are designed to handle the long-term degradation and contraction scour and are protected with countermeasures to prevent local abutment scour.

The minimum scour depth causing slope failure is referred to as failure scour depth. The mode of failure controlling the failure scour depth depends on the abutment type. For vertical wall abutments, the central panel and wing walls confine the abutment and provide some protection against failure modes 3 and 4. As a result, the failure scour depth would be the depth exposing the foundation elements to the extent where the vertical or horizontal bearing capacity is exceeded. On the other hand, failure mode 3 is expected to control the failure scour depth at spill-through abutments. This is particularly true where the abutment is supported by deep foundations; the scour depth needed to trigger failure modes 1 and 2 in this case is much larger than that causing the slope failure of the embankment. Most of the bridges in Texas have spill through abutments supported by drilled shaft or piling. Shallow foundations are only used wherever the abutments lay on competent rock or highly erosion-resistant cohesive soils. Therefore, failure mode 3 is expected to be the most critical mode for the determination of the failure scour depth at bridge abutments in Texas. This abutment failure scenario was observed at many bridges in Texas, as described in Chapter 4.

Determining the failure scour depths for modes 1 and 2 can be based on the TxDOT stability criteria used to limit scour depth at piers. The determination of the failure scour depth for failure mode 3 is developed by this project. Once the failure scour depth is known, it can be divided by a desired FS to obtain the allowable scour depth. Because the analyses leading to the failure scour depth are based on conservative assumptions, the maximum allowable scour depth in this research is considered to be equal to the failure scour depth. Whenever the computed or observed scour depth at the abutment exceeds the maximum allowable scour depth, action should be taken (redesign of new bridges and repair or protection of existing bridges) to prevent a potential failure. The resulting recommendations and guidelines do not account for the lateral erosion of the

embankment soil (failure mode 4). Hence, an FS needs to be applied on the failure scour depth obtained from the findings of this project to account for this erosion process whenever it is not prevented by properly protecting the embankment material against erosion.

5.2 Scour Forms at Abutments

Scour at abutments can take one of the two forms:

- Abutment scour or local scour at abutments.
- Contraction scour.

In reality, these two components are not independent. Sturm et al. (2011) recognize that the processes of abutment and contraction scour are linked and occur simultaneously during flood events. Their research, sponsored by NCHRP, presents a new view of abutment scour and considers contraction scour as a reference scour depth for calculating abutment scour. Consequently, abutment scour is defined as the total scour at the abutment and is estimated by multiplying contraction scour with an amplification factor to consider the turbulent structures at the abutment, rather than adding contraction scour to abutment scour. This has been done in the abutment scour prediction formula by NCHRP project 24-20 (Ettema et al. 2010). This NCHRP abutment scour equation is the only equation to include a check of embankment stability in addition to scour depth prediction.

The objective of this research was to determine the scour limit or the maximum allowable depth of a scour hole at the abutment. The observed or predicted scour depth at the abutment can be contraction scour, abutment scour, or more commonly a combination of these two components. However, regardless the scouring process and the soil resistance to scour, the maximum allowable scour is based on stability criteria of the abutment foundation and embankment. Therefore, the

determination of the maximum allowable scour depth is not reliant upon differentiating the different components making up the total scour depth and the same allowable limit would be applied for a given abutment whether the scour is categorized as a contraction scour or an abutment scour. The determination of the allowable scour requires instead an estimation of the geotechnical strength of the approach embankment at the bridge. For this reason, guidelines for estimating the maximum allowable scour depths are based on effective stress and total stress slope stability analyses considering practical ranges of geometry and shear strength parameter. These limits are to be compared with observed or predicted scour depths to judge scour criticality at abutments and decide whether a plan of action should be implemented.

Since the scour limits are based on slope stability simulations, channel migration and stream widening processes involving the erosion of the embankment soils are not taken into account. These complex channel morphological changes can aggravate scour problems at abutments and cause abutment failures. However, preventing failures caused by meander migration can be done by locating bridge abutments outside zones of meander belts and braided stream paths.

5.3 Slope Stability Analysis

The determination of the failure scour depth, Z_{Fail}, controlled by failure mode 3 or slope stability failure of the abutment embankment is based on a series of slope stability analyses of different scour scenarios. In this context, Z_{Fail} is defined as the scour depth at which the FS against slope stability FS is equal to 1.0. Therefore, when Z_{Fail} is reached, a catastrophic slope stability failure of the abutment embankment would possibly occur. However, an FS of 1.1 or less translates into a stress ratio (mobilized shear stress/shear strength) greater than 0.9. If sustained for a long

enough period, such a high stress ratio would result in creep movements and would eventually lead to a long-term slope stability failure.

The slope stability analysis is performed using GEOSTASE, a 2D limit equilibrium slope stability program (Gregory 2018). A 2D idealization of the abutment cross-section, including geometry, soil profile, piezometric water surface and loads, is established. For each combination of input variables, the slope stability is analyzed using the Simplified Bishop Method and the Spencer Method. Both methods assume that the soil shear strength along the failure surface is governed by Mohr-Coulomb envelope. The two methods result in FS values within 5 percent difference. This difference can be explained by the different assumptions employed by each method to make the problem statistically determinate. Simplified Bishop Method assumes zero shear side forces and does not satisfy the horizontal forces equilibrium while Spencer Method assumes that the side forces are parallel and inclined at a constant angle θ (to be solved for) with respect to the horizontal and satisfies all equilibrium conditions.

The search parameters (i.e., start range, end range, and initiation angle) are selected and thousands trials of failure surfaces are generated and analyzed. The search parameters are then modified, and several independent searches are performed to ensure that the most critical failure surface, having the least FS, has been captured correctly. The search parameters are selected to capture the failure surfaces going beyond the abutment column. The slumping of the scour hole walls, in the case of cohesionless channel bed soil, is not considered critical and is not accounted for by the stability analysis.

The limit equilibrium methods assume that the mobilized stresses are reached at the same time at the base of all slices making up the potential failure surface and computes one FS for all slices. Therefore, when the failure surface passes through the concrete protection, the high concrete

shear strength will cause a significant increase in the FS. In reality, the concrete will not fail in shear. It could only be pushed away by the failing soil mass. To avoid inaccurate computations of the FS and numerical problems caused by the discontinuity in the strength parameters, the failure surface is prevented from intersecting the concrete layer using exclude lines (Figure 61). In this way, the presence of the concrete protection layer does not enhance geotechnical stability. On the other hand, this layer helps simulating realistic deep-seated slip surfaces going beyond the abutment column and prevents shallow raveling failures.

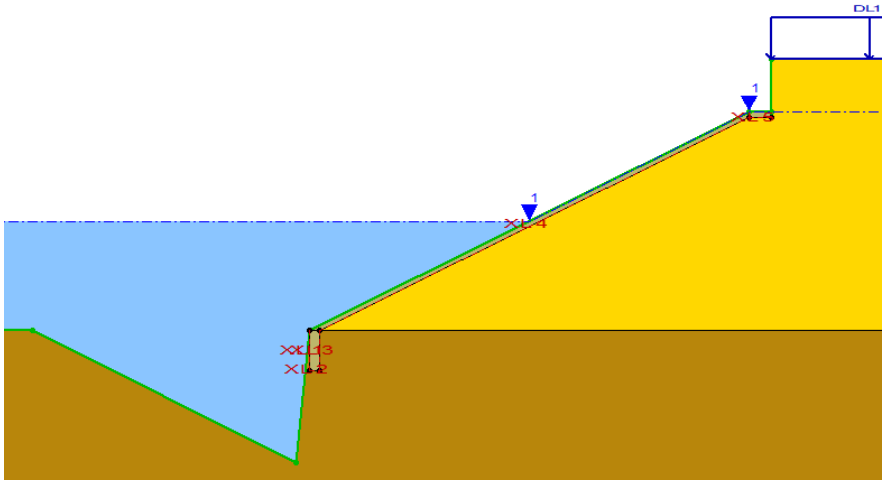

Figure 61-XCLUDE lines around the concrete protection

The use of Mohr-Coulomb failure envelope with a significant cohesion intercept results in tensile stress making the solution non-stable. Tension appears in the form of negative side and normal stresses acting on the slices located in the upper portion of the failing mass. Since soils do not possess significant tensile strength, the negative stresses should be eliminated by introducing a tension crack and consequently ignoring the soil upslope from the crack (Figure 62). Therefore, the performed slope stability analysis accounts for the effect of cracks or fissures in the soil. In

addition, the crack is conservatively assumed to be filled with water and the water force applied on the crack boundaries is accounted for in the FS computation. The required depth of the tension crack to remove all the tension from the failing mass is determined by trial and error until all tensile stresses are removed from the soil mass. The crack depth z_c can be well estimated by the Rankine earth pressure theory:

$$z_c = \frac{2c'}{\gamma \tan(45° - \frac{\varphi'}{2})} \qquad \text{(Eq. 5-1)}$$

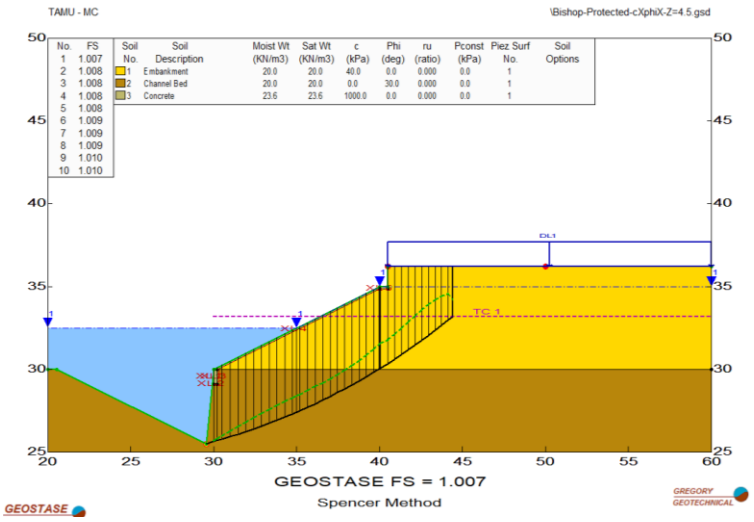

Figure 62- Tension crack used to suppress the tension in the embankment top

5.4 Abutment Model and Variables

Figure 63 illustrates the abutment cross-section used in the slope stability analyses. The abutment embankment is protected by concrete riprap of type RR8 including a 0.13 m (5-inch) thick facing and a 0.9 m (3-ft) deep toe-wall. The abutment slope is set to 2H:1V, which gives a slope angle β of 26.6°. This is representative of a typical slope of roadway embankments in Texas.

The abutment cap and back-wall dimensions are those corresponding to TxDOT pre-stressed concrete I girder, Tx34 or Tx40, typically used with an 8.5 m (28 ft) roadway. A slope height of 5 m is first considered. To cover the range of possible embankment heights, the stability analyses are repeated with a smaller slope height of 2 m and a lager slope height of 7.5 m. Adding the back-wall height of 1.2 m results in three total height H values of 3.2 m, 6.2 m, and 8.7 m. A uniform traffic surcharge of 12 kPa is placed on the approach roadway. The abutment model variables can be divided into four categories (Figure 64).

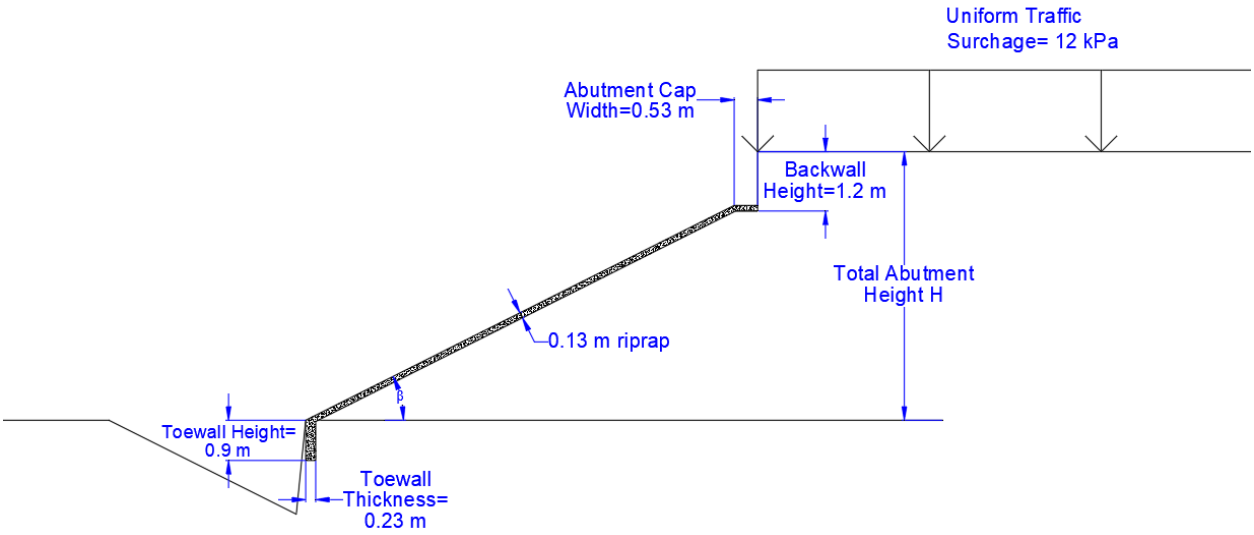

Figure 63- Abutment model

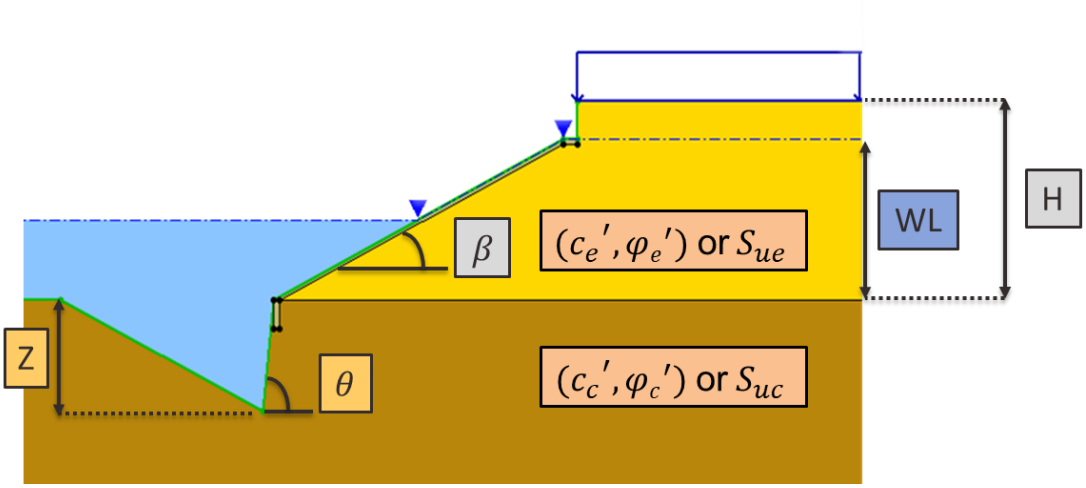

Figure 64- Abutment model variables

5.4.1 The Geometry Variable

The geometry variable consisting of the abutment total height H. H is the height to the roadway and is equal to the slope height plus the height of the backwall (1.2 m). Three values are assigned to this variable: 3.2 m, 6.2 m, and 8.7 m. The abutment slope is assumed to be 2H:1V, which gives a slope angle β of 26.6°.

5.4.2 The Scour Variable

The scour variable consisting of the depth Z of the scour hole located at the toe of the abutment embankment. Z is the difference in elevations of the abutment toe and the bottom of the scour hole. The slope angle of the scour hole wall adjacent to the abutment is conservatively assumed to be θ=84.3° corresponding to a nearly vertical slope of 1H:10V. The scour depth Z is increased from zero (initial condition) until reaching the value of Z_{Fail} (failure condition) at which the FS against slope stability FS is 1.0. The location of the scour hole defined as the distance

between the scour hole and the abutment toe, D, is conservatively set to zero to simulate scour directly located at the abutment toe.

5.4.3 The Hydraulic Condition

Slope stability failure of the abutment embankment is not likely to occur during a flood when the water level in the channel is high. In fact, the water forces have a stabilizing influence on the embankment and the slope stability simulations has shown that the slope becomes more stable as the water level in the channel increases. Failure mode 4 or lateral channel migration and erosion of the embankment soil, which is not captured by the slope stability analysis, could occur during high flow events due to the continuous water activity eroding the embankment soil under the water. Nevertheless, the most critical hydraulic condition for the slope stability of the abutment embankment is sudden drawdown after a long period of high water level in the river channel. Under such condition, appreciable positive water pressures remain in the embankment and underlying channel bed while the buttressing water forces are removed.

Slope stability analysis of a low permeability embankment under the sudden drawdown condition consists of three computation stages (Lowe and Karafiath 1960; Wright and Duncan 1987; Duncan et al. 1990). In the first stage, the initial water level (before drawdown) is maintained and the effective stress parameters (c' and φ') are used to compute the effective consolidation stresses and the shear stresses along the slip surface. In the second stage, the consolidation and shear stresses from the first stage are used to estimate the undrained shear strength during rapid drawdown. The second stage FS is based on the estimated undrained shear strength. The effective shear stress parameters are then used to compute the shear strength after drawdown with pore water pressure values corresponding to the lowered water level. For the slices where the effective stress

or drained shear strength is lower than the total stress or undrained shear strength, the calculation of a third stage FS is started by replacing the undrained shear strength by the drained shear strength for those slices. The FS due to the sudden drawdown is the one calculated by the second or the third stage.

Unfortunately, the second stage calculation of the undrained shear strength from the consolidation stresses require additional parameters, which are determined by conducting a consolidated undrained triaxial test. Since the test result cannot be predicted for the different possible types of embankment and channel bed soils, the use of a three-stage rapid drawdown analysis is not possible in this project.

For determining the failure scour depth Z_{Fail}, it is assumed that the embankment and channel bed soils have low permeability and therefore no drainage is allowed to occur during drawdown. In addition, positive excess pore water pressures are assumed to develop during the undrained condition. Under this assumption, the undrained condition is always more critical than the fully drained condition. In fact, the same effective stress envelope controls the undrained condition and the fully drained condition. The only difference between the two conditions is the pore water pressure used in the analysis. The fully drained is a steady state condition where the pore water pressures are estimated as the hydrostatic pressure and the excess pore pressure is zero. On the other hand, the undrained condition may involve positive or negative excess pore water pressures making it impossible to predict which condition controls the analysis. To find conservative values of Z_{Fail} during rapid drawdown after a high flow stage, the most critical case of undrained condition with positive pore water pressures in the embankment and channel bed is assumed.

Two analyses are performed to study the slope stability of the scoured abutment during sudden drawdown with undrained soils condition: an effective stress analysis and a total stress analysis.

A. Effective Stress Analysis

The analysis of an undrained condition using effective stresses requires the estimation of the excess pore water pressure along the failure surface during drawdown. Unsteady seepage analysis could be performed to predict the distribution of the pore water pressure caused by rapid drawdown. For simplicity, it is conservatively assumed that the piezometric line in the embankment is horizontal at the initial maximum elevation of the water in the river channel (i.e., no pore water pressure dissipation is allowed to occur). The piezometric line follows the embankment slope until reaching the steady-state seepage level in the channel after drawdown where it becomes horizontal again (Figure 64). This assumption implies that the flood would be sustained long enough to infiltrate and fully saturate the embankment and that the drawdown would occur fast enough to prevent any dissipation of the built-up pore water pressures. The WL parameter, defined as the percentage of the water height in the channel with respect to the embankment height, is used to describe the rapid drawdown condition. For example, Figure 64 shows the abutment under the sudden drawdown condition where the water dropped from the top of the embankment or WL=100 percent to half height of the embankment or WL=50 percent.

In reality, partial drainage would occur making the embankment more stable. In addition, the compacted and dense embankment soil is likely to exhibit a dilative behavior. Consequently, the shearing of the embankment soil would generate negative shear-induced pore water pressures, which are ignored by this analysis. Because of the high degree of

conservatism, using the effective analysis with a similar assumption for the pore pressures to analyze a complete rapid drawdown condition from WL=100 percent to WL=0 percent would result in an unrealistic failure of most of the embankments at their initial unscoured condition (Z=0). For this reason, the effective stress analysis is limited to the drawdown condition from the top of the embankment slope to half of the embankment height, which is a reasonable water level drawdown in the river between peak flow and normal flow conditions (Figure 64).

B. Total Stress Analysis

Because the pore pressure values for the undrained soil condition during sudden drawdown cannot be accurately estimated, a total stress analysis provides a simple alternative for the stability analysis. In addition to the condition of rapid drawdown to half of the slope height, the complete rapid drawdown condition, from WL=100 percent to WL=0 percent (Figure 65), can be analyzed in this case since the pore water pressure does not affect the computation of the FS. The total stress analysis requires that the determination of the undrained shear strength be accurate and consistent with the actual strength under the in-situ state of effective stress at a particular depth and the anticipated loading in the field.

Even with a complete rapid drawdown condition, the water in the scour hole is not likely to drain. A water condition where the scour hole walls are not supported by the water forces is a drought condition where water is suppressed from the entire problem. Since the soil under such condition would be dry, the slope stability of the abutment embankment should be analyzed using a long-term effective analysis. It has been proven that the effective analysis of dry conditions results in a higher FS against slope stability than that of the rapid drawdown condition. Although

the dry condition (no water) and other steady state conditions with WL=100 percent and WL=50 percent were simulated, the determination of the failure scour depth Z_{Fail} at or near the abutment is based on the rapid drawdown condition.

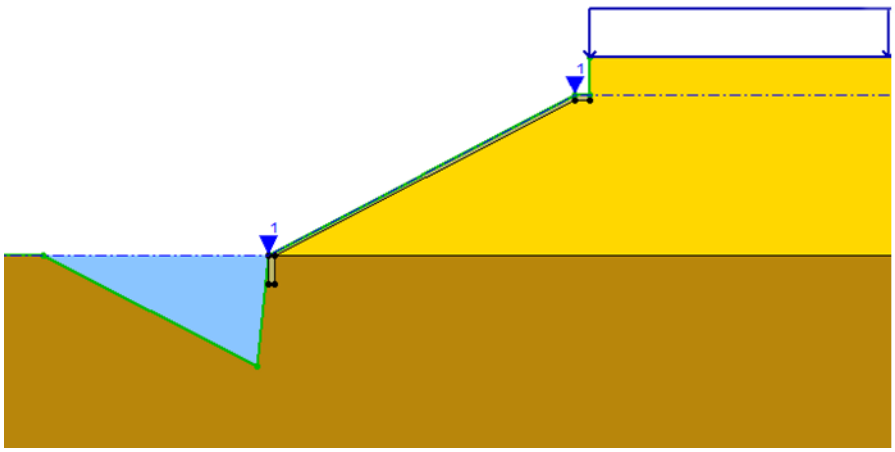

Figure 65- Complete rapid drawdown

5.3.4 The Geotechnical Variables

The geotechnical variables consisting of the shear strength parameters of the different model materials. The embankment and the channel bed soils are assumed isotropic and homogenous. The shear strength of these soils is computed using the linear Mohr Coulomb envelope. Consequently, the shear strength variables consist of:

- Effective Stress Strength Parameters:
  - Effective cohesion of the embankment soil, c'_e
  - Effective cohesion of the channel bed soil, c'_c
  - Effective friction angle of the embankment soil, φ'_e

- Effective friction angle of the channel bed soil, φ'_c

- Total Stress Strength Parameters:
  - Undrained shear strength of the embankment soil, S_{ue}.
  - Undrained shear strength of the channel bed soil, S_{uc}.

The analyses use a total unit weight γ= 20 kN/m^3 for all soil types of the embankment and channel bed regardless of their location with respect to the WL. This is because the variation of this parameter is found to have no significant effect on the slope stability analysis.

Concrete layer protection is given an equivalent undrained cohesion of 1 MPa. The shear strength of the concrete layer does not affect the analysis results as the failure surface is prevented from going through the concrete layer by the use of XCLUDE lines. The reason behind including the abutment protection is to obtain realistic deep-seated slip surfaces going beyond the abutment column and to prevent shallow raveling failures.

5.5 Effective Shear Strength Parameters

The effective stress analysis of the abutment slope stability employs low bound ranges of the effective shear strength parameters (c' and φ') for the different types of embankment and channel bed soils. Using low bound values allows applying the analysis results without having to accurately guess the in-situ values of these parameters. In addition, the conservative estimates of these parameters account for the fact that the peak strength would not likely be available along the entirety of the failure surface.

The low bound ranges of effective stress strength parameters for the compacted embankment soils are based on the U.S. Bureau of Reclamation (USBR) database published in the

book “Design of Small Dams” by the USBR (USBR 1987). This database is also cited by the Naval Facilities Engineering Command Design Manual 7.02 “Foundations and Earth Structures” (Naval Facilities Engineering Command 1982) and by the FHWA Geotechnical Engineering Circular GEC 5 “Geotechnical Site Characterization” (Loehr et al. 2016). It is based on 1500 soil tests performed between 1960 and 1982 on soil samples compacted to Proctor maximum dry density at the optimum water content using the USBR standard compaction method, which has similar compaction energy to AASHTO T99 and ASTM D698. Assuming a similar field compactive effort, low bound ranges, and values for the saturated effective cohesion c’ and effective friction angle φ’ for the soil types possibly used in the embankment are extracted from this database (Table 16). The embankment soil types considered are: CL (lean or low plasticity clay), CH (fat or high plasticity clay), SC (clayey sand), SM (silty sand), and ML (low plasticity silt). For each embankment soil type, the minimum value of the effective cohesion lower bound range is first considered. Whenever this minimum value results in initially unstable embankment, higher values within the range are considered. As a result, many combinations of the effective shear strength parameters c’ and φ’ are simulated for the same embankment soil type.

For the channel bed soil, three cohesionless soil types (gravel, sand, and silty sand) and four cohesive soil types (over-consolidated clay or OC Clay 1 through 4) are considered. Estimates of the effective shear stress strength parameters are assigned to each of these types (Table 17).

Table 16- Low bound ranges of embankment c’ and φ’

Soil Type	Saturated c’ (kPa)	φ’(°)
CL	6.2–11.0	26
CH	3.6–10.3	19
SC	4.8–6	27–28
ML	0.7–4.8	25–30
SM	1.4–4	27–32

Table 17- Channel bed c’ and φ’

Soil Type	c’ (kPa)	φ’(°)
	Cohesionless	
Gravel	0	35
Sand	0	30
Silty Sand	2	30
	Cohesive	
OC Clay 1	15	20
OC Clay 2	20	24
OC Clay 3	14	26
OC Clay 4	8	28

5.6 Total Shear Strength Parameters

The embankment and channel bed soils are conservatively assumed to be fully saturated. The total strength in this case is the undrained shear strength S_u, which can be expressed as $S_u = c' + (\sigma - u)\tan\varphi'$ where c’ and φ’ are the effective strength parameters; σ is the total normal stress and u is the pore water pressure. It follows that S_u is not a property of the soil as it varies with the in-situ stress state. In addition, the loading path and the loading rate also affect the value

of S_u. Moreover, the undrained shear strength S_u of the compacted embankment soil depends on the compaction condition achieved in the field (dry or wet of the optimum). Therefore, the total stress strength parameter S_u cannot be estimated on the basis of the general soil type and classification as in the case of the effective shear strength parameters c' and φ'.

The relationship between the undrained shear strength S_u of saturated soils and the effective consolidation stress σ'_{vc} is described by the following equation:

$$\frac{S_u}{\sigma'_{vc}} = S(OCR)^m$$

where S and m are fitting parameters, which could be estimated for different soil types and the over consolidation ratio (OCR) values. However, this relationship is best suited for soft clays and silts and is not valid for stiff and heavily consolidated soils where values for S and m cannot be estimated. Therefore, it would be inappropriate to use this relationship to describe the undrained shear strength S_u of the compacted embankment soil. As for the channel bed soil, using the S_u ratio method has no significant effect on the slope stability computations. This is because the failure slip depth in the channel bed is limited to the few feet of scour in the channel surface. In addition, using a linearly increasing S_u with depth limits the application of the analysis results to channel beds having OCR values consistent with the ones used in the analysis. For all these reasons, the increase of S_u with depth is ignored. Values of S_u are selected to cover different possible consistencies of saturated soils in the embankment and the channel (Table 18).

Table 18- Simulated values of the undrained shear strength.

Consistency	S_u (kPa)
Soft	20
Medium	30
	40
Stiff	50
	60

5.7 Effective Stress Analysis Results

Four different hydraulic conditions are first simulated with an abutment model having a height H=6.2 m, embankment cohesion c'_e=0 kPa, embankment friction angle φ'_e=30°, and a low plasticity channel bed with c'_c=5 kPa and φ'_c=30°. These hydrologic conditions are: dry, steady state with a horizontal WL at half height of the slope (WL=50 percent), steady state with a horizontal WL at full height of the slope (WL=100 percent), and rapid drawdown from the top of the slope (WL=100 percent) to half height of the slope (WL=50 percent). The decrease in the FS with the increase in the scour depth Z follows the same pattern with all the four water conditions (Figure 66). For a scour depth Z less than the riprap toe wall length (0.9 m), the failure surface goes around the scour hole and consequently the FS is not controlled by the depth of the scour. For Z equal to the riprap toe wall depth (Figure 67), the most critical failure surface passes by the bottom of the scour hole. This change in the location of the failure surface explains the drop in the

FS at Z=0.9 m. For all Z greater than the riprap toe wall depth (Figure 68), the most critical failure surface goes from the bottom of the scour hole to the top of the cohesionless embankment and FS decreases linearly as Z increases. The failure scour depth Z_{Fail}, defined as the scour depth Z corresponding to FS=1, can then be determined by linear interpolation (Table 19). As can be seen in Figure 66 and Table 19, rapid drawdown is the most critical water condition and is therefore used to determine the failure scour depth Z_{Fail}.

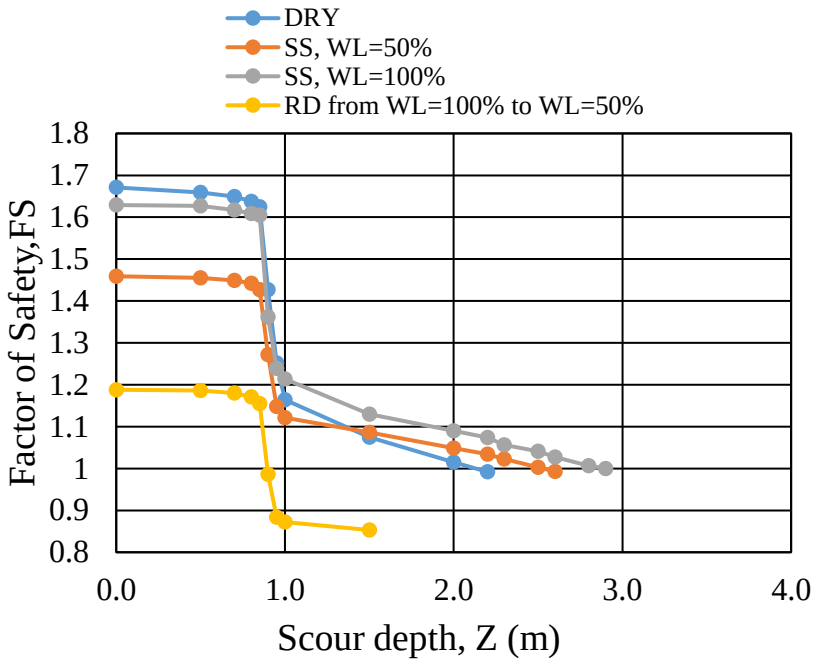

Figure 66- FS versus Z using effective stress analysis

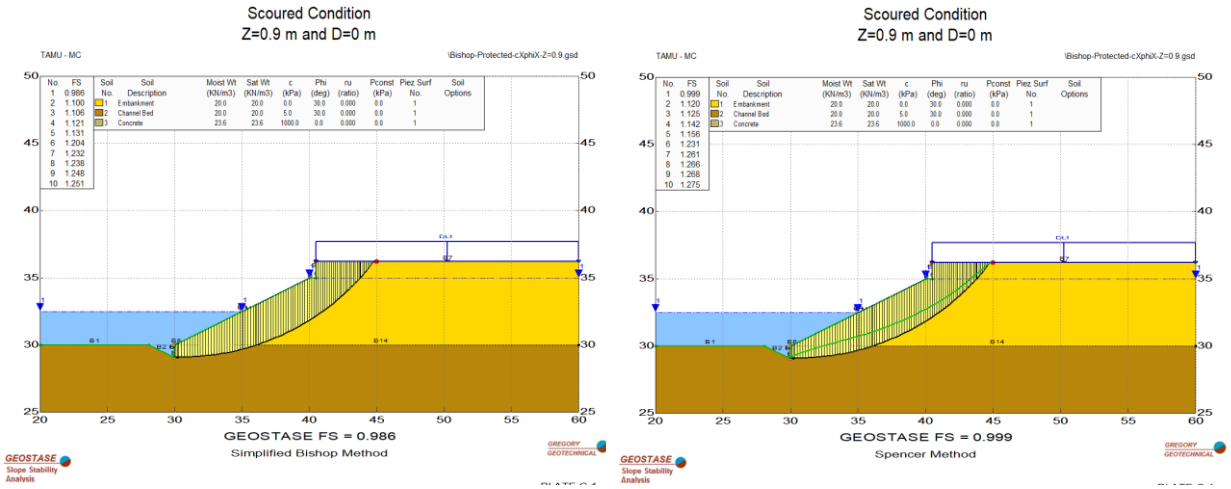

(a)Simplified Bishop Method

(a) Spencer Method

Figure 67- Failure surface location at Z equal to the toe-wall depth

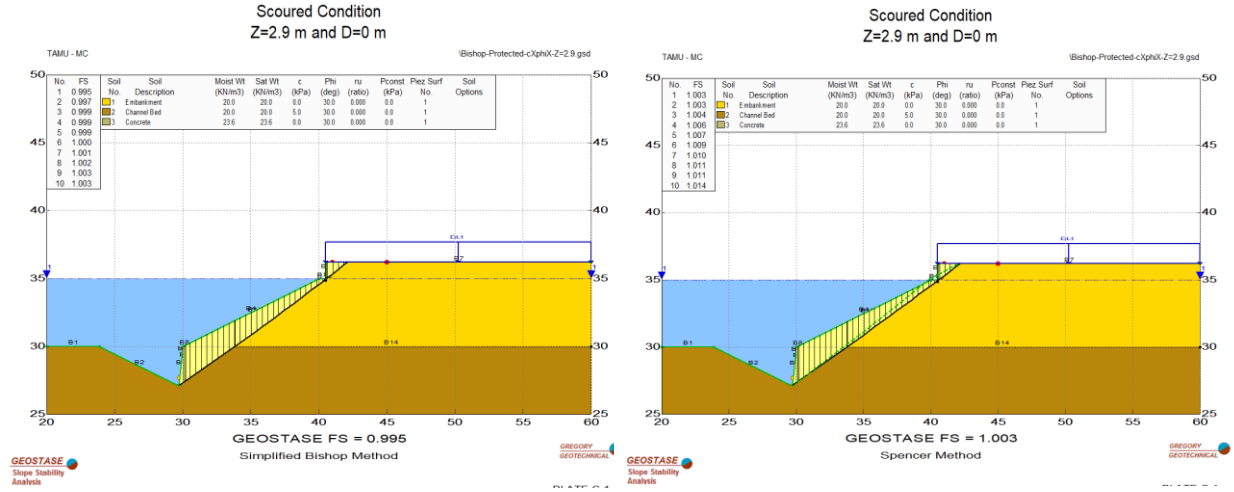

(a) Simplified Bishop Method

(b) Spencer Method

Figure 68- Failure surface location at Z greater than the depth of the toe-wall

Table 19- Z_{Fail} for different water conditions

Water Condition	DRY	SS, WL=50%	SS, WL=100%	RD from WL=100% to WL=50%
Failure Scour Depth, Z_{Fail} (m)	2.13	2.53	2.90	0.90
Z_{Fail}/H	0.34	0.40	0.46	0.14

The effective stress analysis of the abutment embankment stability under drawdown condition resulted in Z_{Fail} values for 105 model combinations of the various embankment and channel bed soil types and the three values of total height H (3.2 m, 6.2 m, and 8.7 m). For each embankment soil type (CH, CL, SC, SM, and ML), many sets of values for c'_e and φ'_e, falling within their respective ranges in Table 16 are simulated. Only one combination of c'_e and φ'_e values is selected to represent each embankment soil type (Table 20). This selection is based on the observation of the initial factor of safety, FS_0, with H=6.2 m. A reasonable initial FS against rapid drawdown ranges between 1.1 and 1.3. Therefore, each embankment soil type is represented by the most conservative combination of c'_e and φ'_e values that results in a reasonable FS_0 when combined with most of the channel bed soil types. This judgment is done for H=6.2 m, and the same c'_e and φ'_e values in Table 20 are used for H=3.2 m and H=8.7 m to determine the effect of abutment total height on the failure scour depth results.

Table 20- Effective shear strength parameters for each embankment soil type

Embankment Soil Type	Saturated Effective Cohesion c'_e (kPa)	Effective Friction angle φ'_e (°)
CH	10.3	19
CL	6.2	26
SC	4.8	28
SM	4	32
ML	2	30

Z_{Fail} results are normalized by the total abutment height H and presented in Table 21. The results are presented for all five embankment soil types and for four channel bed soil types. The selected channel bed soil types are gravel, sand, silty sand, and cohesive. Table 17 shows the

effective shear strength parameters of the different channel bed soil types. The over-consolidated clay (OC Clay 4 in Table 17) with $c'_c = 8$ kPa and $\varphi'_e = 28°$ is cautiously selected to represent the cohesive channel bed soil type. Table 21 also shows the values of FS_0, the initial FS before any scour occurs (i.e., FS at Z=0).

As expected, the value of Z_{Fail}/H decreases when the total abutment height is increased, and all other parameters are kept constant. Therefore, the determination of the failure scour depth at a certain abutment need to be based on the analysis of an abutment model of same or greater height. For H=8.7 m, Z_{Fail}/H of 0.10 is very common. This value corresponds to a failure scour depth equal to the length of the riprap toe wall (0.9 m). In fact, the selected cohesion values were too low for H=8.7 m that most failures occur when the scour reaches the bottom of the riprap toe wall, especially when the channel bed is cohesionless. All three heights gave a failure scour depth equal to the length of the riprap toe wall for the combinations where the channel bed is cohesionless sand or where the embankment is comprised of low cohesion ML. Therefore, the effective stress analysis results prove that cohesion is the most influential factor when it comes to the stability of scoured abutments and hence will play a major role in the determination of the failure scour depth. Failure scour depths equal to the length of the riprap toe wall translate to to Z_{Fail}/H of 0.28, 0.14, and 0.10 for abutments having with total height H of 3.2 m, 6.2 m, and 8.7 m, respectively.

Z_{Fail} results from all effective shear strength simulations are normalized by the total height of the abutment H and plotted against $S/\gamma H$ where S is a bulk shear strength expression. Many expressions are tested for S to find the best correlation between Z_{Fail}/H and $S/\gamma H$.

Table 21- Z_{Fail}/H results based on the effective stress analysis

		H= 3.2 m		H=6.2 m		H=8.7 m	
Embankment Soil Type	Channel Soil Type	Z_{Fail}/H	FS_i	Z_{Fail}/H	FS_i	Z_{Fail}/H	FS_i
CH	Gravel	0.42	1.29	0.32	1.161	0.10	1.057
	Sand	0.28	1.166	0.14	1.067	-	0.972
	Silty Sand	0.44	1.339	0.26	1.151	0.10	1.037
	Cohesive	0.84	1.730	0.51	1.354	0.27	1.189
CL	Gravel	0.37	1.306	0.24	1.155	0.10	1.075
	Sand	0.28	1.176	0.14	1.055	-	0.993
	Silty Sand	0.39	1.343	0.20	1.156	0.10	1.065
	Cohesive	0.82	1.744	0.47	1.376	0.28	1.222
SC	Gravel	0.30	1.295	0.18	1.151	0.10	1.077
	Sand	0.28	1.168	0.14	1.049	-	0.992
	Silty Sand	0.34	1.337	0.16	1.151	0.10	1.061
	Cohesive	0.78	1.738	0.44	1.379	0.27	1.229
SM	Gravel	0.32	1.337	0.26	1.2	0.19	1.137
	Sand	0.28	1.201	0.14	1.091	0.10	1.041
	Silty Sand	0.37	1.386	0.24	1.199	0.15	1.117
	Cohesive	0.81	1.789	0.48	1.432	0.35	1.283
ML	Gravel	0.28	1.231	0.14	1.088	0.10	1.07
	Sand	0.28	1.102	-	0.995	-	0.951
	Silty Sand	0.28	1.283	0.14	1.103	0.10	1.028
	Cohesive	0.62	1.696	0.31	1.349	0.10	1.198

At first, S was taken to be the bulk shear strength of the embankment S_e with $S_e = c'_e + \gamma H \tan\varphi'_e$, which results in $\frac{S_e}{\gamma H} = \frac{c'_e}{\gamma H} + \tan\varphi'_e$. Figure 69 shows that no correlation exists between Z_{Fail}/H and $S_e/\gamma H$. It was thought that including the channel bed shear strength parameters in the expression of S would improve the relationship between Z_{Fail}/H and $S/\gamma H$. Consequently, S_e was replaced by S_{avg} with $S_{avg} = c'_{avg} + \gamma H(\tan\varphi')_{avg}$ where $c'_{avg} = \frac{c'_e + c'_c}{2}$ and $(\tan\varphi')_{avg} = \frac{\tan\varphi'_e + \tan\varphi'_c}{2}$. However, no correlation is observed between Z_{Fail}/H and $S_{avg}/\gamma H$ neither (Figure 70).

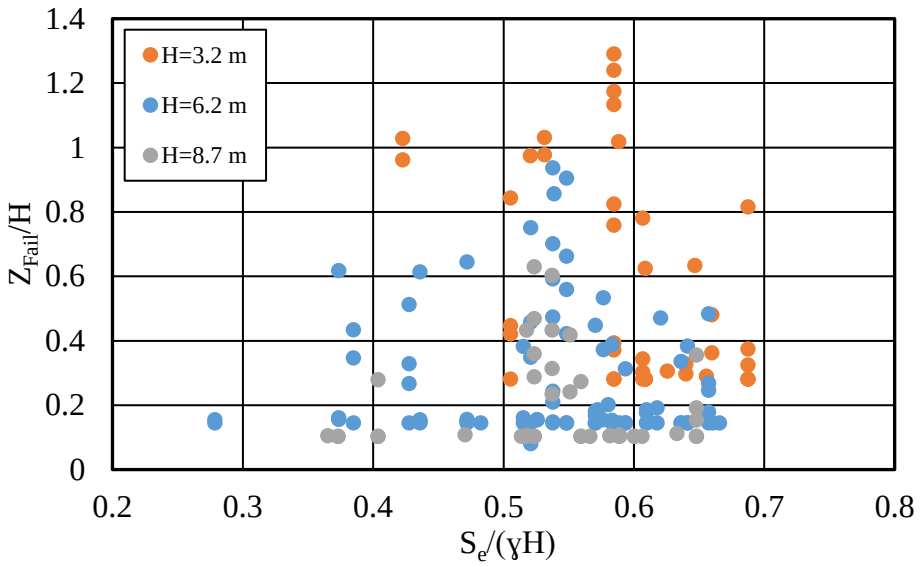

Figure 69- Z_{Fail}/H versus $S_e/\gamma H$

Given the importance of the traditional stability number $N=c'/\gamma H$ in slope stability analyses, Z_{Fail}/H results are plotted against $c'_e/\gamma H$, $c'_c/\gamma H$, and $c'_{avg}/\gamma H$ in Figure 71, Figure 72, and Figure 73, respectively. A general trend of increasing Z_{Fail}/H with increasing $c'_{avg}/\gamma H$ can be

observed despite the scatter in the data points for $c'_{avg}/\gamma H < 1$. This scatter is due to the variation of the embankment and channel bed effective friction angles, not captured in the independent variable $c'_{avg}/\gamma H$.

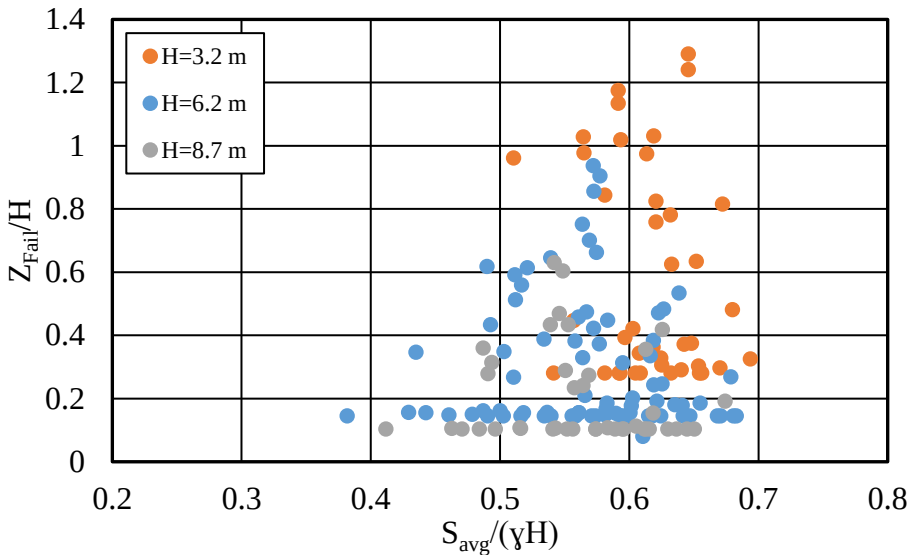

Figure 70- Z_{Fail}/H versus $S_{avg}/\gamma H$

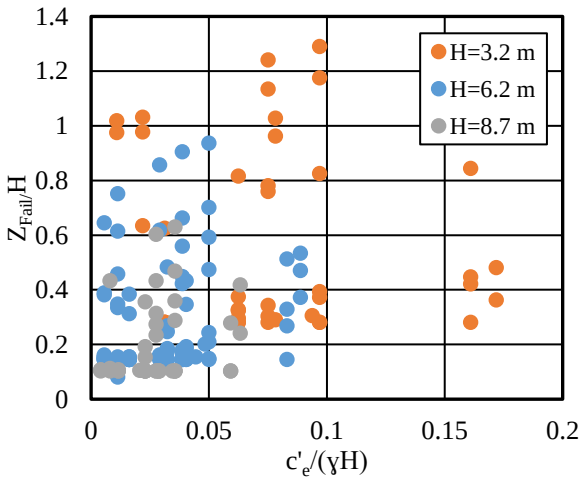

Figure 71- Z_{Fail}/H versus $c'_e/\gamma H$

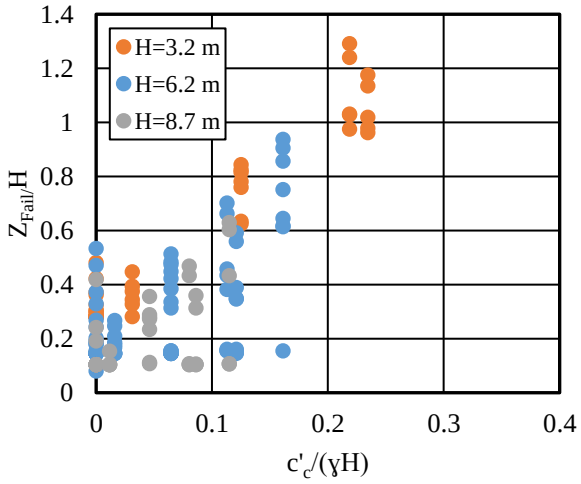

Figure 72- Z_{Fail}/H versus $c'_c/\gamma H$

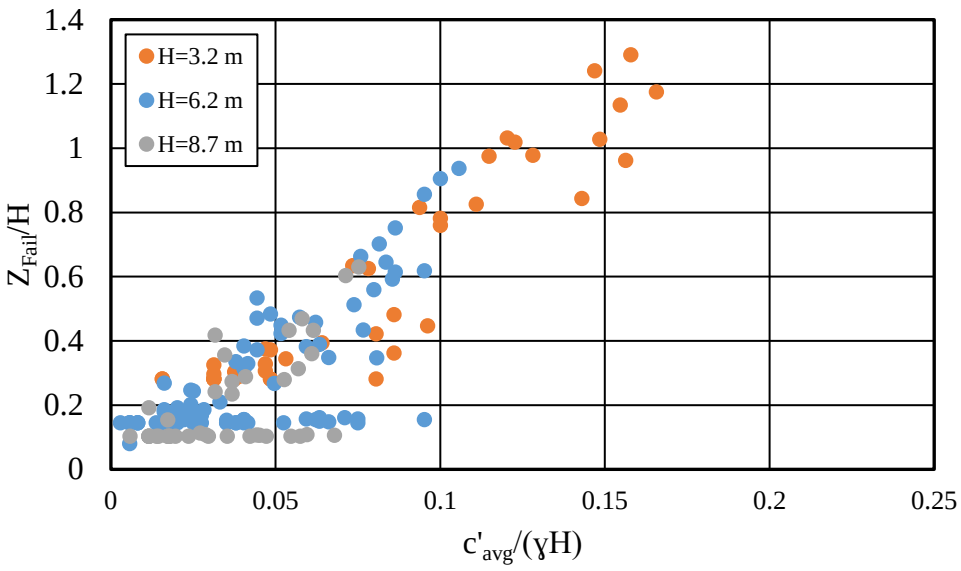

Figure 73- Z_{Fail}/H versus $c'_{avg}/\gamma H$

To include the effects of both effective shear strength parameters c' and φ' of the embankment and the channel bed, the shear strength expression S is assumed to be the average shear strength along the failure surface. Consequently, S is estimated as the shear strength at the average depth along the failure surface. An observation of the shape of the failure surface for the different combinations under the rapid drawdown condition indicates that the depth of the scour hole itself is a good estimation of the average depth of the most critical failure surface (Figure 74). Indeed, the abutment can handle deeper scour holes as the average shear strength along the failure surface increases, which in turn is directly proportional to the depth of the scour hole. It follows that S can be expressed as:

$$S = c'_{avg} + Z_{Fail}\gamma(\tan\varphi')_{avg} \quad \text{(Eq. 5-2)}$$

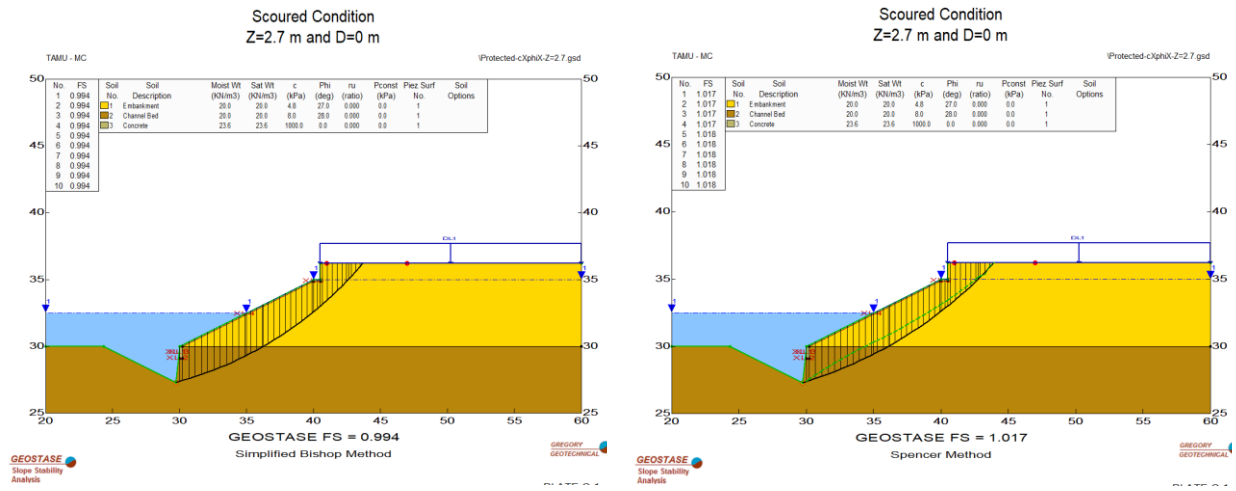

(a) Simplified Bishop Method (b) Spencer Method

Figure 74- Failure surface shape under rapid drawdown condition

Figure 75 shows Z_{Fail}/H is linearly dependent on $S/\gamma H$ with S calculated based on Eq. 5-2. A best estimate of this linear relationship is obtained from the least-squares linear regression through the simulation results, as follows:

$$\frac{Z_{Fail}}{H} = 1.72\frac{S}{\gamma H} - 0.046 \qquad \text{(Eq. 5-3)}$$

With the statistics:

Number of data points, n=164.

R squared, R^2=0.985.

Standard Error, S=0.033.

The data further show that the following provide a cautious lower bound estimate for Z_{Fail}/H:

$$\frac{Z_{Fail}}{H} = 1.55\frac{S}{\gamma H} - 0.1 \qquad \text{(Eq. 5-4)}$$

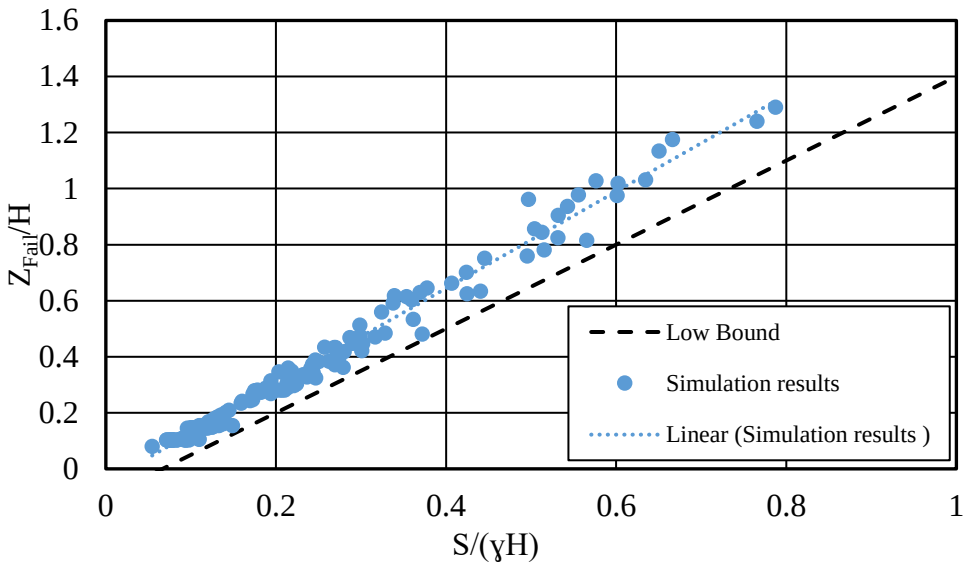

Figure 75- Z_{Fail} versus S/γH

5.8 Total Stress Analysis Results

To avoid assuming the pore water pressure distribution in the embankment and channel bed after sudden drawdown, the slope stability analysis is performed using a range of undrained shear strength values with the three abutment heights. This total stress analysis allowed the simulation of both complete and half rapid drawdown conditions. Figure 76 shows the relationship between FS against slope stability and Z for a single combination of input parameters where H=6.2 m, S_{ue}= 20 kPa, and S_{uc}= 30 kPa. Similarly to the results of the effective stress analysis, the FS decreases as Z increases and the relationship becomes linear for Z greater than the riprap toe wall length (0.9 m). As expected, the data points corresponding to the complete rapid drawdown condition are always below those corresponding to the half rapid drawdown condition (Figure 76). The failure scour depth Z_{Fail} associated with FS=1 is determined for each of the two rapid drawdown conditions by linear interpolation (Table 22- Z_{Fail} for complete and half rapid drawdown conditions).

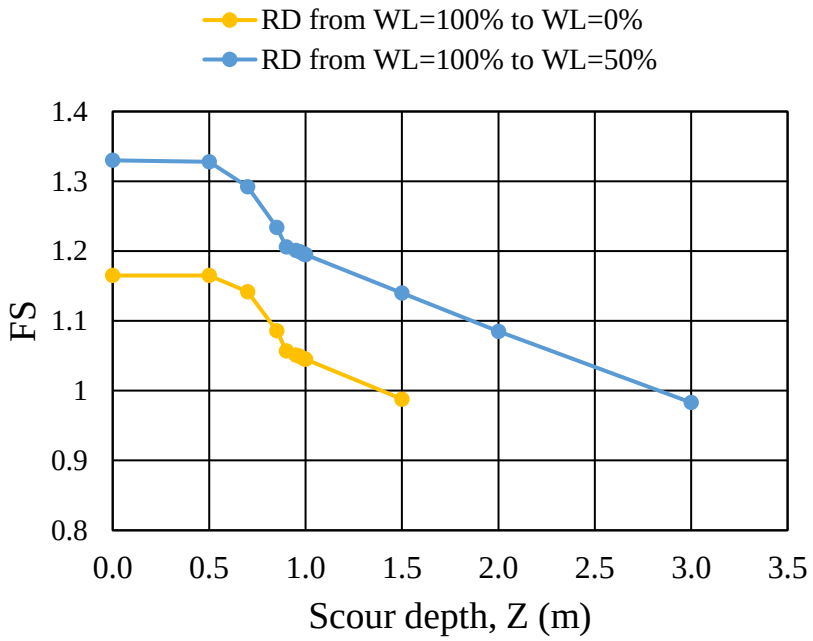

Figure 76- FS versus Z using total stress analysis

Table 22- Z_{Fail} for complete and half rapid drawdown conditions

Water Condition	RD from WL=100% to WL=0%	RD from WL=100% to WL=50%
Failure Scour Depth, Z_{Fail} (m)	1.39	2.83
Z_{Fail}/H	0.22	0.45

The total stress analysis of the abutment embankment stability under complete and half drawdown conditions is performed for abutment models with the three values of total height H. For the abutment models having H=6.2 m and H=8.7 m, each of the embankment undrained shear strength S_{ue} and channel undrained strength S_{uc} is varied over the range 20–60 kPa (Table 18). With H=3.2 m, S_{ue} values equal to or greater than 40 kPa would give the same Z_{Fail} as they result in a theoretical tension crack depth covering all the height of the embankment (Eq. 5-1). In addition, such small embankments laying on stiff channel beds with S_{uc} greater than 40 kPa are

found to be very stable and would not fail even when the scour depth at the abutment exceeds 2.5 H or 8 m. For these reasons, S_{ue} and S_{uc} are varied over the range 20–40 kPa with H=3.2 m. As a result, the total stress analysis includes a total 118 combinations of H, S_{ue}, and S_{uc}. Z_{Fail} results from these different combinations are normalized by the total height of the abutment H and plotted against $S_{ue}/\gamma H$ (Figure 77–Figure 79).

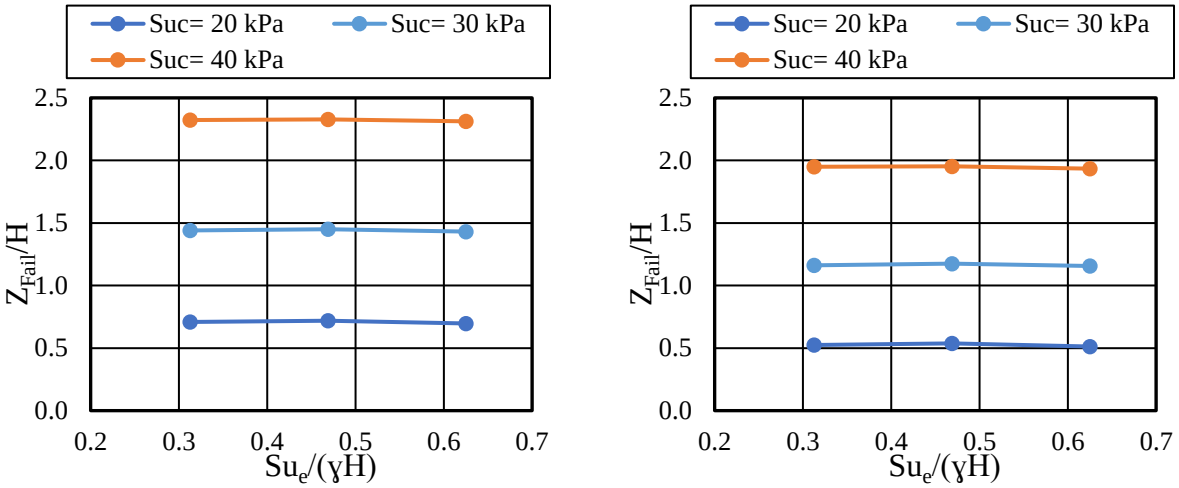

(a) Rapid Drawdown from WL=100% to WL=50%

(b) Rapid Drawdown from WL=100% to WL=0%

Figure 77- Z_{Fail}/H versus $S_{ue}/\gamma H$ with H=3.2 m

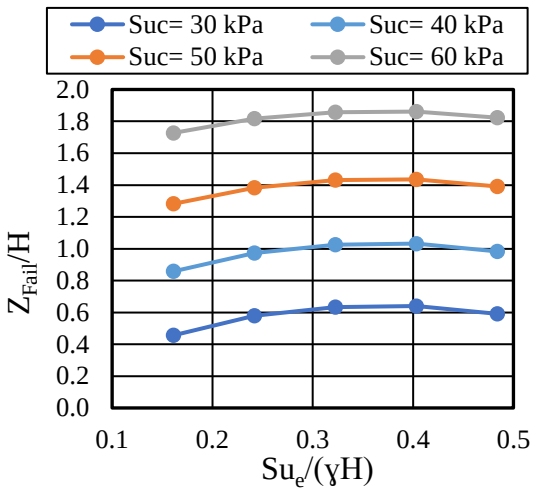

(a) Rapid Drawdown from WL=100% to WL=50%

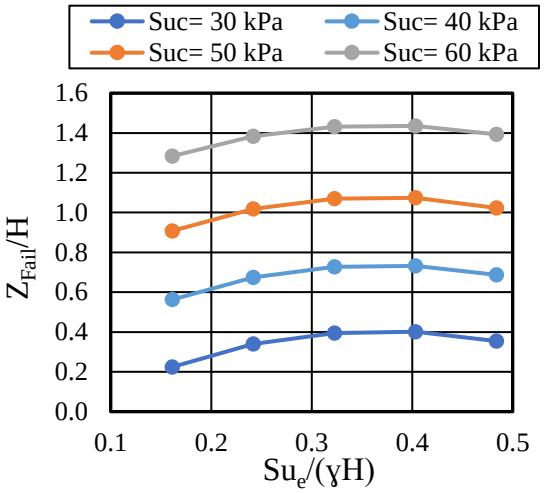

(b) Rapid Drawdown from WL=100% to WL=0%

Figure 78- Z_{Fail}/H versus $S_{ue}/\gamma H$ with H=6.2 m

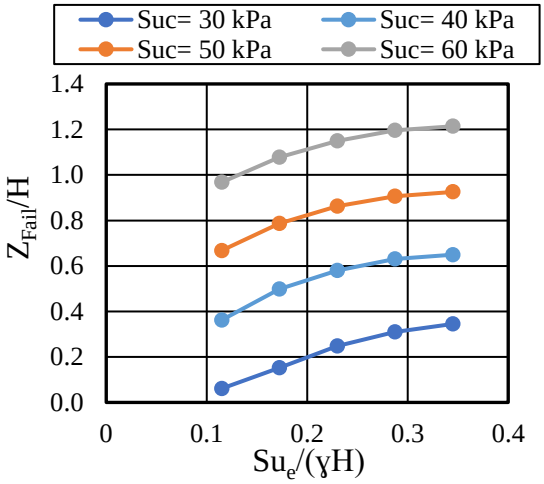

(a) Rapid Drawdown from WL=100% to WL=50%

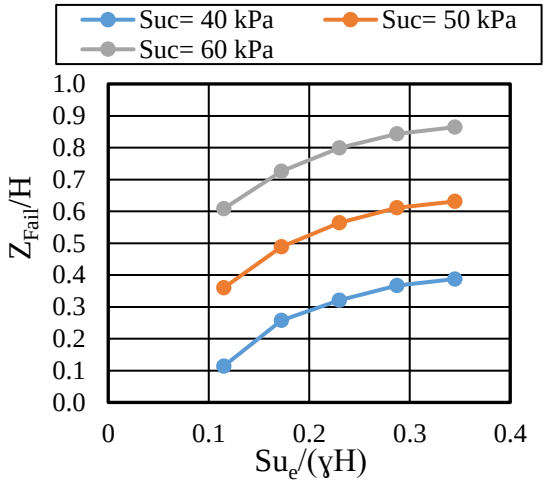

(b) Rapid Drawdown from WL=100% to WL=0%

Figure 79- Z_{Fail}/H versus $S_{ue}/\gamma H$ with H=8.7 m

For the slope stability simulations using total stress, the embankment cohesion c'_e is set to the value of the undrained shear strength Su_e and the embankment friction angle φ'_e is set to 0. Applying Eq. 5-1, the depth of the tension crack can be simply found as:

$$z_c = \frac{2S_{ue}}{\gamma} \quad \text{(Eq. 5-5)}$$

As a result, the embankment undrained shear strength S_{ue} has a double effect on the failure scour depth Z_{Fail}. As S_{ue} increases, the shear strength along the potential failure surface in the embankment increases but also the theoretical depth of the tension crack increases. Following Eq. 5-5, the ratio of the depth of the tension crack to the abutment total height $\frac{z_c}{H}$ is equal to $\frac{2S_{ue}}{\gamma H}$. This explains why Z_{Fail}/H is insensitive to $S_{ue}/\gamma H$ for H= 3.2 m, where the crack depth covers 60 percent to 100 percent of the embankment height with S_{ue} going from 20 kPa to 40 kPa. The effect of the embankment undrained shear strength S_{ue} becomes more noticeable as H increases and $\frac{z_c}{H}$ decreases (Figure 77–Figure 79).

Overall, the effect of the embankment strength on the failure scour depth is diluted because of the tension crack added in the embankment to eliminate the tension. The total stress stability analysis of a cohesive embankment on top of a cohesive channel bed shows that the failure scour depth is best correlated with the channel bed undrained shear strength S_{uc} (Figure 80). Despite the scatter in the data points, a trend of increasing Z_{Fail}/H with increasing $S_{uc}/\gamma H$ is generally observed. Some of the scatter may be the result of the variation of the embankment undrained shear strength S_{ue}. However, as previously explained, S_{ue} cannot be counted on because of the possible initiation of tension cracks, especially for high PI embankment soils.

Linear regression of these results showed the following:

Rapid drawdown to half of slope height (RD from WL=100 percent to WL=50 percent):

$$\frac{Z_{Fail}}{H} = 4.66\frac{S_{uc}}{\gamma H} - 0.55 \quad \text{(Eq. 5-6)}$$

With the statistics:

Number of data points, n=49.

R squared, R^2=0.960.

Standard Error, S=0.11.

Complete rapid drawdown (RD from WL=100 percent to WL=0 percent):

$$\frac{Z_{Fail}}{H} = 4.17\frac{S_{uc}}{\gamma H} - 0.68 \qquad \text{(Eq. 5-7)}$$

With the statistics:

Number of data points, n=44.

R squared, R^2=0.968.

Standard Error, S=0.084.

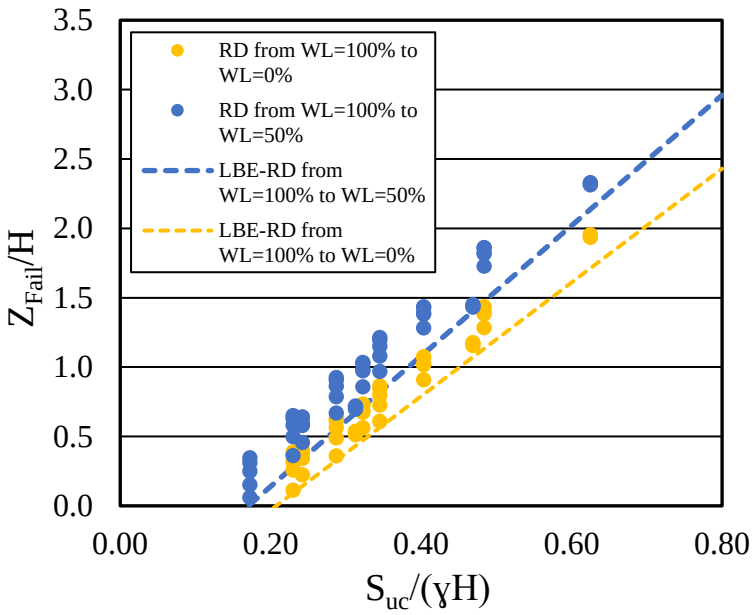

Figure 80- Z_{Fail}/H versus $S_{uc}/\gamma H$

Cautious lower bound estimates for Z_{Fail}/H would be:

Rapid drawdown to half of slope height (RD from WL=100 percent to WL=50 percent):

$$\frac{Z_{Fail}}{H} = 4.7\frac{S_{uc}}{\gamma H} - 0.8 \quad \text{(Eq. 5-8)}$$

Complete rapid drawdown (RD from WL=100 percent to WL=0 percent)

$$\frac{Z_{Fail}}{H} = 4.1\frac{S_{uc}}{\gamma H} - 0.85 \quad \text{(Eq. 5-9)}$$

A combination of total and effective stress shear strength parameters is used to analyze the slope stability of a cohesive embankment on top of a cohesionless channel bed. S_{ue} values of 20, 30, 40, 50, and 60 kPa are combined with two embankment friction angles for the channel bed φ_c'=35° (gravelly channel bed) and φ_c'=30° (sandy channel bed). The simulations were performed with the three heights (H=3.2 m, 6.2 m, and 8.7 m) for the abutment. With H=8.7 m, two higher values of S_{ue} (70 kPa and 80 kPa) are simulated to have $S_{ue}/\gamma H$ values over 0.4. Envelopes of Z_{Fail}/H versus $S_{ue}/\gamma H$ for the rapid drawdown condition from WL=100 percent to WL=50 percent with abutment heights H=6.2 m and H=8.7 m are presented in Figure 81 and Figure 82, respectively. In these sets of simulations, the theoretical crack depth is also used to prevent tensile stresses in the failing mass. Consequently, it can be seen how Z_{Fail}/H at first increases with the increase of $S_{ue}/\gamma H$ but then decreases as the tension crack covers around 80 percent of the embankment (i.e., $S_{ue}/\gamma H > 0.4$).

Figure 83 combines the results from the 21 combinations with H=6.2 m and H=8.7 m and presents a low bound envelope for Z_{Fail}/H corresponding to the rapid drawdown condition from WL=100 percent to WL=50 percent (Eqs. 5-10 and 5-11).

For $S_{ue}/\gamma H \leq 0.4$, $\frac{Z_{Fail}}{H} = 2.0\frac{S_{ue}}{\gamma H} - 0.3$ (Eq. 5-10)

For $S_{ue}/\gamma H > 0.4$, $\frac{Z_{Fail}}{H} = 0.3$ (Eq. 5-11)

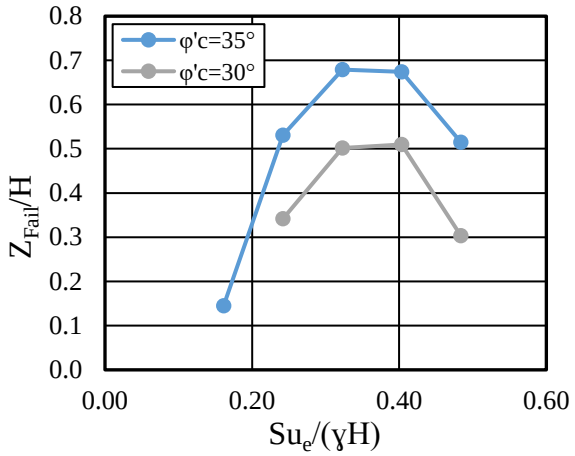

Figure 81- Z_{Fail}/H versus $S_{ue}/\gamma H$ for rapid drawdown to half slope height with H=6.2 m

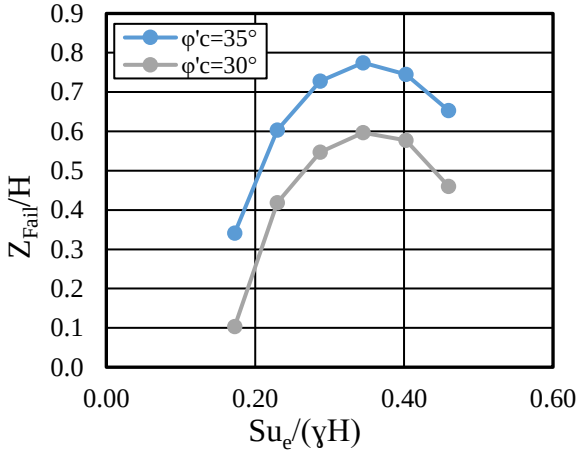

Figure 82- Z_{Fail}/H versus $S_{ue}/\gamma H$ for rapid drawdown to half slope height with H=8.7 m

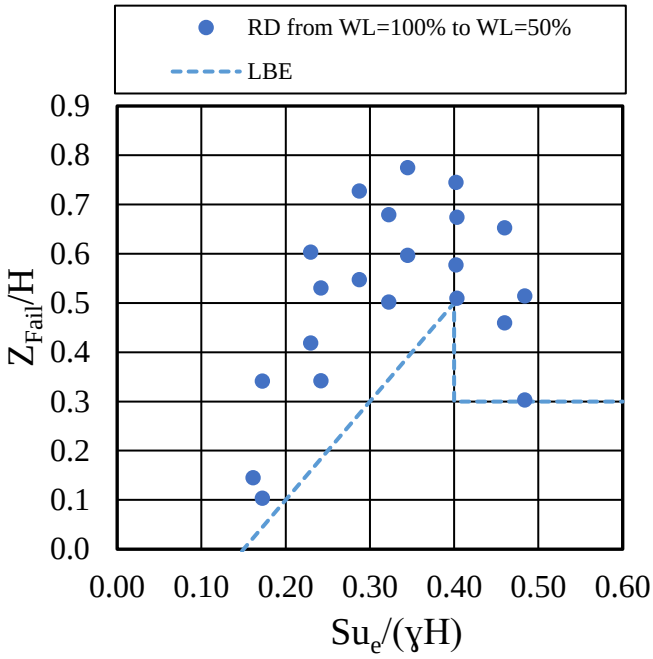

Figure 83- Z_{Fail}/H versus $S_{ue}/\gamma H$ for rapid drawdown to half slope height

The assumed piezometric line for the condition of complete rapid drawdown with a cohesive embankment on top of a cohesionless channel bed (Figure 65) results in extremely low Z_{Fail}/H results (Figure 84 and Figure 85), suggesting that the scour depth should be limited to the depth of the riprap toe wall whenever this condition is possible. However, as in the case of effective stress analysis, failure scour depth results based on this overly excessive assumption of piezometric surface with complete rapid drawdown analysis are not to be relied upon for the determination of the maximum allowable scour depth.

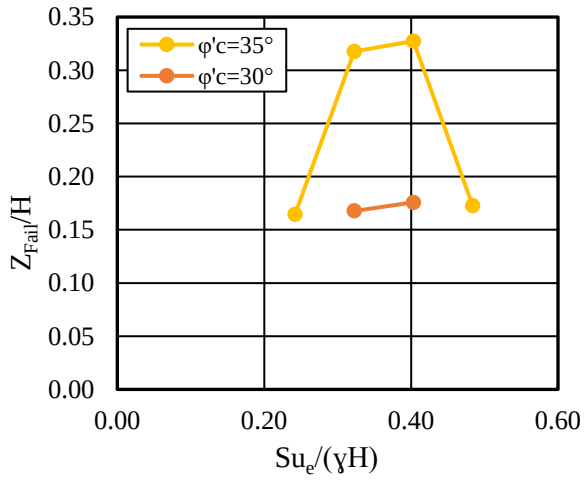

Figure 84- Z_{Fail}/H versus $S_{ue}/\gamma H$ for complete rapid drawdown with H=6.2 m

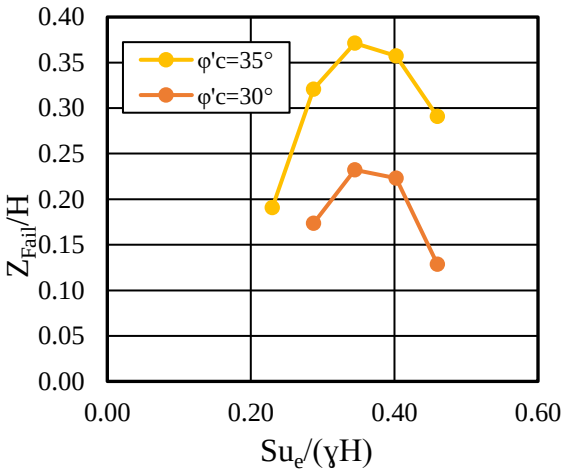

Figure 85-Z_{Fail}/H versus $S_{ue}/\gamma H$ for complete rapid drawdown with H=8.7 m

The simulations of the 3.2 m high abutment show that such a small embankment is initially unstable under complete rapid drawdown when it is underlain by sand and is failed by a scour depth less than the tow wall depth when it is underlain by gravel. On the other hand, the rapid drawdown to half of the embankment height resulted with Z_{Fail} equal to the depth of the riprap toe

wall, with both φ'_c=30° and φ'_c=35°. The low values of Z_{Fail} with H=3.2 m high can be explained by two facts:

- The embankment shear strength is not increasing the embankment stability because the tension crack depth corresponding to a certain S_{ue} covers a greater portion of the total height H as H decreases.
- The shear strength of the cohesionless channel bed is not enough to hold the embankment stable.

Whenever an abutment vulnerable to scour lies on a cohesionless channel bed, the abutment height should be increased enough to take into account the possible formation of tension cracks and to subsequently prevent slope stability failure of the embankment.

6. PROCEDURES AND RECOMMENDATIONS FOR CALCULATIONS OF SCOUR LIMITS AT/NEAR ABUTMENTS

To assist the judgement of bridge design engineers and bridge inspectors in evaluating the stability of scoured abutments, the results of the analyses detailed in Chapter 5 were used to develop practical guidelines for estimating the maximum allowable scour depth at abutments. These guidelines are applicable to bridges where the geometry, geotechnical, scour, and hydraulic parameters falls within the ranges considered in the analyses. When the application of these guidelines reveals a critical scour condition, a detailed numerical model becomes a readily justifiable and accessible option to further refine the scour condition and justify the need of implementing repair actions.

6.1 Guidelines Using Effective Shear Strength Parameters

Two forms of guidelines are established based on the results of the effective stress analysis. The first is a direct derivation of the failure scour depth Z_{Fail} at the abutment toe, under rapid drawdown to half slope height, from Eq. 5-4 of the low bound estimate line in Figure 75:

$$Z_{Fail} = \frac{1.55\frac{c'_{avg}}{\gamma} - 0.1H}{1 - 1.55(\tan\varphi')_{avg}} \quad \text{(Eq. 6-1)}$$

where c'_{avg} and $(\tan\varphi')_{avg}$ are the average effective cohesion and the average effective friction angle tangent of the embankment and channel bed, respectively, and H is the total height of the abutment.

This equation is applicable for abutments having a total height H in the range of 3.2–8.7 m, a slope of 2H:1V, and embankment and channel bed soil types falling within the ranges of soil types covered in Table 16 and Table 17, respectively.

A successful application of the above equation requires an accurate estimation of the shear strength parameters of the abutment embankment and river channel bed. This requires complex and costly laboratory testing (Consolidated Drained triaxial test, Consolidated Undrained triaxial test, or direct shear test). Empirical correlations related to soil type or routine index properties can also be used to estimate the effective friction angle of the soil φ′ (Kulhawy and Mayne 1990). For fine-grained soils, many correlations exist between the effective friction angle φ′ and the plasticity index PI as both parameters are linked to soil mineralogy and composition. Correlations estimating the effective cohesion of clays as a function of the plasticity index PI are not appropriate to use as the PI does not capture the soil structure and dilative tendencies to which the cohesion is linked (Sorensen and Okkels 2013).

Further filtering Z_{Fail}/H results presented in Table 21 leads to a second form of guidelines for maximum allowable scour depth at abutments. This filtering is based on the following considerations:

1. Embankment fills in Texas are required to have a plasticity index PI between 15 and 35 (TxDOT 2014; Item 132). This range of PI translates empirically to an effective friction angle φ' between 28° and 32° (Holtz and Kovacs, 1985). Therefore, it can be assumed that abutment embankments in Texas are mostly composed of silts (ML), clayey sand (SC), and/or silty sand (SM).
2. The ML embankments could not handle a scour depth going beyond the depth of the riprap toe wall (0.9 m), except when underlain by a cohesive channel bed. The study of case

histories and field scour measurements reveals that limiting scour to the depth of the tow wall would be too conservative. As a result, it is assumed that embankment soils have a saturated effective cohesion greater than 2 kPa and the ML embankment type is ruled out.

3. The same reasoning in 2 applies for the cohesionless sandy channel bed. Hence, a purely sandy channel bed is eliminated from consideration.
4. The two channel bed soil types, gravel and silty sand, result in very close values of Z_{Fail}/H. Both channel bed types are lumped into one group named "cohesionless" of which Z_{Fail}/H values corresponds to the least of the two channel bed types.
5. The performed slope stability simulations cannot be the basis for Z_{Fail}/H guidelines for an embankment having a height much greater than 6.2 m. Although simulations were performed with an abutment model having H=8.7 m, the input values for effective cohesion were the least values leading to a reasonable initial safety factor for the abutment model having H=6.2 m. Such cohesion values are found to be too low when used with H=8.7 m that the majority of the cases resulted in $Z_{Fail}/H=0.1$, which corresponds to a failure scour depth equal to the length of the riprap toe wall (0.9 m).

Following the above considerations, the maximum allowable scour depth at abutments based on the effective stress analysis of the embankment stability under rapid drawdown condition from WL=100 percent to WL=50 percent are presented in Table 23. Z_{Fail}/H corresponding to H=6.2 m can be used to limit the scour depth at the toe of abutments having a total height between 3.2 m and 6.2 m while Z_{Fail}/H corresponding to H=3.2 m can be used to limit the scour depth at the toe of abutments having a total height of 3.2 m and lower.

Table 23- Maximum allowable scour depth based on the effective stress analysis

		Z_{Fail}/H	
Embankment Soil Type	Channel Soil Type	H=3.2 m	H=6.2 m
SC	Cohesionless	0.3	0.16
	Cohesive	0.78	0.44
SM	Cohesionless	0.32	0.24
	Cohesive	0.81	0.48

The advantage of using Table 23 rather than Eq. 6-1 is that the classification of the embankment and channel bed soils can be done by a visual or a manual examination without the need for laboratory testing. Table 23 can be used for bridge inspection and prioritization at sites where the embankment and channel bed soils can be properly classified. Overall, a reasonable and conservative estimate of the maximum allowed scour depth at abutments would be 0.24 times the embankment height.

6.2 Guidelines Using Total Shear Strength Parameters

A low bound estimate of the failure scour depth at the toe of an abutment embankment laying on a cohesive channel bed is derived for the conditions of rapid drawdown to half and full slope height from Eqs. 5-8 and 5.9, respectively:

Rapid drawdown to half of slope height (RD from WL=100 percent to WL=50 percent)

$$Z_{Fail} = 4.7\frac{S_{uc}}{\gamma} - 0.8H \qquad \text{(Eq. 6-2)}$$

Complete rapid drawdown (RD from WL=100 percent to WL=0 percent)

$$Z_{Fail} = 4.1\frac{S_{uc}}{\gamma} - 0.85H \qquad \text{(Eq. 6-3)}$$

where S_{uc} is the channel bed undrained shear strength and H is the total abutment height.

Eqs. 6-2 and 6-3 are applicable for abutments having a total height H in the range of 3.2–8.7 m, and a slope of 2H:1V, laying on a channel bed with undrained shear strength in the range 20–60 kPa.

A low bound estimate of the failure scour depth at the toe of an abutment embankment laying on a cohesionless channel bed is derived from Eqs. 5-10 and 5-11, for the condition of rapid drawdown to half embankment height:

For $S_{ue}/\gamma H \leq 0.4$, $Z_{Fail} = 2.0\frac{S_{ue}}{\gamma} - 0.3H$ (Eq. 6-4)

For $S_{ue}/\gamma H > 0.4$, $Z_{Fail} = 0.3H$ (Eq. 6-5)

where S_{ue} is the embankment undrained shear strength, and H is the total abutment height.

Eqs. 6-4 and 6-5 applicable for an abutment having a total height H in the range of 6.2–8.7 m, a slope of 2H:1V, and an embankment with undrained shear strength falling in the range 20–80 kPa laying on a sandy or gravelly channel bed.

Whether the embankment is laying on a cohesive or cohesionless channel bed, the total stress analysis correlates the failure scour depth Z_{Fail} with the undrained shear strength of either the channel bed, S_{uc}, or the embankment, S_{ue}. The determination of the undrained shear strength requires less complex testing than that of the effective shear strength parameters. Easy and fast laboratory tests such as the Unconsolidated Undrained (UU) triaxial test or the unconfined compression test and field tests such as the Vane Shear Test or the TCP test can be used to estimate the undrained shear strength S_u. However, the measurements of the undrained shear strength are not as reliable as those of the effective strength parameters since the undrained shear strength is affected by many variables. Therefore, the measurements of the channel bed undrained shear strength S_{uc} obtained from the TCP testing during the geotechnical investigation before the bridge

construction may not be representative of the value of S_{uc} during rapid drawdown. For the determination of Z_{Fail}, it is recommended to obtain conservative S_u estimates of embankment or channel bed soil samples under conditions mimicking the field conditions during rapid drawdown. For this purpose, UU triaxial tests can be performed on different possible embankment and channel bed soil types to relate conservative estimates of S_{uc} and S_{ue} to the respective soil classification of the embankment and channel bed. For the embankment, samples can be collected from the borrow source and then compacted to reach the dry density and water content anticipated to be achieved in the field. These samples should be saturated to measure the lowest S_{ue} that can be reached during sudden drawdown. For the natural soil of the channel bed, undisturbed samples can be extracted, saturated, and then tested for S_{uc}.

7. VALIDATION AND APPLICATION OF THE PROPOSED GUIDELINES

7.1 CASE NO.1: CR 22 over Pomme De Terre River

Using the case geometry, scour and geotechnical information presented in Table 9, the guidelines in Table 23 based on the effective stress analysis can be applied to find the failure scour depth under rapid drawdown condition. The channel bed type is silty sand SM and has a friction angle of $\varphi'_c = 30°$. Therefore, the channel bed is considered to be cohesionless for the determination of the maximum allowable scour depth from Table 23. No information is given about the embankment soil type. However, using Eq. 7-1, a minimum value of c'_{avg} can be estimated knowing that the embankment must have been designed to survive rapid drawdown conditions, (i.e., $Z_{Fail} \geq 0$ in Eq. 6-1):

$$(c'_{avg})_{min} = \frac{0.1\gamma H}{1.55} \qquad \text{(Eq. 7-1)}$$

with H=5 m, $(c'_{avg})_{min} = 6.5$ kPa.

Given that the channel bed is non cohesive silty sand, most of this average cohesion can be attributed to the embankment. Therefore, the embankment soil type is assumed to be either SC or SM corresponding to Z_{Fail}/H values of 0.16 and 0.24, respectively (Table 23). Applying these guidelines results in scour limit depths of 0.8 m in the case of an SC embankment and 1.2 m in the case of a SM embankment. Both these limits would have prevented the failure of the right abutment where the observed scour causing failure is estimated to be 3 m. The observed scour at the left abutment of 0.46 m is below the scour limits and would have been considered acceptable. Indeed, no failure occurred at the left abutment. The actual limits are slightly underestimated since the

limits correspond to an abutment having a total height H=6.2 m, 1.2 m greater than the actual total height of the abutments in this case.

The scour limits based on Table 23 corresponds to the rapid drawdown to half embankment height. This is the most critical condition that should be used to limit scour depths wherever a rapid drawdown condition is possible. However, the right abutment of CR 22 over Pomme De Terre River failed during the flood event, while the WL was found to submerge the abutment embankment (WL=100 percent). As previously explained, this water condition is much safer than the rapid drawdown condition as the water in the channel has a buttressing effect. Therefore, Z_{Fail}/H corresponding to the steady state water condition with WL=100 percent would be higher than the limits of 0.16 and 0.24 from Table 23. Table 19 indicates that the failure scour depth Z_{Fail} (Z at FS=1) for WL=100 percent with H=6.2 m, c'_e= 0 kPa, c'_c= 5 kPa, and $\varphi'_e = \varphi'_c = 30°$ is Z_{Fail}=2.9 m. Therefore, even under the safest hydraulic condition, the analysis confirms that a scour depth exceeding 2.9 m would fail the abutment embankment.

The case information and the failure scour limits from Table 23 are summarized in Table 24.

Table 24- Application of failure scour guidelines to case no. 1

Abutment	H (m)	β (°)	Z (m)	Channel Bed Soil Type	Embankment Soil Type	Z_{Fail} (m)	Predicted Failure	Actual Failure
Right	5	26.6	3	SM	SC or SM	0.8 or 1.2	YES	YES
Left			0.46				NO	NO

7.2 CASE NO.2: SR 37 over James River

No failure occurred in this case but the case information is used to apply the guidelines in Table 23 and find the failure scour depth under rapid drawdown condition. The resulting failure scour depth at the right abutment would be overestimated as the guidelines in Table 23 are abutments with total height H less than 6.2 m while the total height of the right abutment for SR 37 over James River is 9.8 m. On the other hand, the failure scour for the left abutment would be underestimated as the guidelines are based on a 2H:1V slope, which is steeper than the actual slope of the left embankment. The channel bed type is mildly cohesive sandy silt. No information is given about the embankment soil type. However, using Eq. 7-1, a minimum value of c'_{avg} can be estimated knowing that the embankment must have been designed to survive rapid drawdown conditions (i.e., $Z_{Fail} \geq 0$ in Eq. 6-1):

$$(c'_{avg})_{min} = \frac{0.1\gamma H}{1.55} \quad \text{(Eq. 7-1)}$$

with H=9.8 m, $(c'_{avg})_{min} = 12.6$ kPa.

Given that the channel bed is only mildly cohesive, the embankment must have been cohesive clay to result in a minimum saturated effective cohesion that can handle the rapid drawdown condition. Therefore, assuming an SC or SM embankment would be safe. Table 23 shows that Z_{Fail}/H is 0.16 or 0.24 with SC or SM embankment soils, respectively, and H=6.2 m. These scour limits can be applied to the left abutment to give 1 m or 1.5 m for SC or SM embankment soil, respectively. In reality, the failure scour must be greater than these values from Table 23 because the left abutment slope angle β is 18.4° and not 26.6° and the slope angle of the scour hole θ is 29.1° well below the slope angle of 84.3° used in the analyses. Consequently, the

observed scour at the left abutment of 1.2 m is expected to be below the actual value of failure scour depth. Indeed, no failure occurred at the left abutment.

Table 21 shows that Z_{Fail}/H for the combination of silty sand channel and SC/SM embankment with H=8.7 m is between 0.1 and 0.15 corresponding to a failure scour depth in the range of 1–1.5 m. However, no scour protection or riprap toe wall is present at SR 37 over James River, which means that Z_{Fail}/H at the right abutment where H=9.8 m could be even less than the results in Table 21. Nonetheless, no scour was observed at the right abutment.

Table 25 summarize the case information and the failure scour limits from Table 21 and Table 23.

Table 25- Application of failure scour guidelines to case no. 2

Abutment	H (m)	β (°)	Z (m)	Channel Bed Soil Type	Embankment Soil Type	Z_{Fail} (m)	Predicted Failure	Actual Failure
Right	9.8	26.6	0	Sandy silt	SC or SM	<1 or <1.5	NO	NO
Left	6.3	18.4	1.2			>1 or >1.5	NO	NO

7.3 CASE NO.3: FM 692 over McGraw Creek

This case can be used to apply Eqs. 6-2 and 6-3 since the undrained shear strength values of the channel bed S_{uc} at the right and the left abutment are found based on the TCP test results. Table 26 presents the resulting failure scour depths at the right and left abutments under complete and half drawdown conditions. Eqs. 6-2 and 6-3 fail to predict the failure of the left abutment under the rapid drawdown condition to half slope height and to full slope height, respectively. While the application of these equations gives a failure scour depth at the left abutment greater than 5 m, this

abutment has failed during Hurricane Harvey when the observed scour was 2.3 m. This can be justified by the fact that the S_{uc} values used in Eqs. 6-2 and 6-3 (Table 26) are derived from the TCP results obtained during the geotechnical investigation before the bridge construction. However, as explained in section 5.6, the undrained shear strength is not a property of the soil and is dependent on many variables (in-situ stress state, degree of saturation, pore water pressure, loading path, loading rate, etc). Therefore, the available S_{uc} values obtained from TCP testing prior to bridge construction are not representative of the true S_{uc} values during failure. Indeed, the channel bed soil may become fully saturated. The transition from partially to fully saturated state decreases the channel bed undrained shear strength S_{uc} and consequently the calculated failure scour depths Z_{Fail}. Conservative S_{uc} estimates under conditions mimicking the field conditions during rapid drawdown can be obtained by dividing the value of S_{uc} from TCP tests of partially saturated channel bed soils by a certain factor. This factor may be obtained by conducting UU triaxial tests on undisturbed channel bed samples in their native saturation state and their fully saturated state. Another reason behind the failure of Eqs. 6-2 and 6-3 to reflect the critical condition at the left abutment may be that this condition was actually aggravated by the erosion of the embankment soil (failure mode 4), not accounted for by the slope stability analysis and the developed equations.

Table 26- Application 1 of failure scour guidelines to case no. 3

Abutment	H (m)	β (°)	Z (m)	S_{uc} (kPa)	Z_{Fail} (m) under complete rapid drawdown	Z_{Fail} (m) under half rapid drawdown	Predicted Failure	Actual Failure
Right	2.8	26.6	0	23.9	2.5	3.4	NO	NO
Left	2.5		2.3	35.9	5.2	6.4	NO	YES

The channel bed soil type is clayey silt at the right abutment and silty sand at the left abutment. To apply the guidelines in Table 23 to this case, the channel bed soil is assumed to be cohesive at the right abutment and cohesionless at the left abutment. The embankment is conservatively assumed to be SC. For this combination of channel bed and embankment types with H=3.2 m, Table 23 gives $Z_{Fail}/H=0.78$ at the right abutment and $Z_{Fail}/H=0.3$ at the left abutment, for the rapid drawdown condition to half embankment height. This results in failure scour depths of 2.2 m at the right abutment and 0.75 m at the left abutment. The observed scour at the left abutment (2.3 m) exceeds the failure scour depth (0.73 m). The failure of the left abutment validates the guidelines of Z_{Fail}/H based on the effective stress analysis (Table 27).

Table 27- Application 2 of failure scour guidelines to case no. 3

Abutment	H (m)	β (°)	Z (m)	Channel Bed Soil Type	Embankment Soil Type	Z_{Fail} (m)	Predicted Failure	Actual Failure
Right	2.8	26.6	0	Clayey silt	SC	2.2	NO	NO
Left	2.5		2.3	Silty sand		0.75	YES	YES

7.4 CASE NO.4: FM 937 over Montgomery Creek

Eqs. 6-2 and 6-3 are first applied to this case to evaluate their ability to predict the slope stability failure that occurred at the left abutment, after the 2013 Halloween flood. Table 28 presents the resulting failure scour depths at the right and left abutments under complete and half drawdown conditions. For this case, the failure of the left abutment can be predicted by applying Z_{Fail} equations based on the total stress analysis, even though the S_{uc} values used in the equations are inaccurate since they are based on TCP results prior to bridge construction. The reason may be

the low S_{uc} value at the right abutment (22.3 kPa). These equations predict the right embankment to stay stable as long as the scour depth at the abutment is less than 5.9 m. The high value of the calculated Z_{Fail} at the right abutment is due to the relatively high value of Suc (51.1 kPa).

Table 28- Application 1 of failure scour guidelines to case no. 4

Abutment	H (m)	β (°)	Z (m)	S_{uc} (kPa)	Z_{Fail} (m) under complete rapid drawdown	Z_{Fail} (m) under half rapid drawdown	Predicted Failure	Actual Failure
Right	5.3	26.6	1.7	51.1	5.9	7.7	NO	NO
Left			2.4	22.3	0.066	1.0	YES	YES

Case 4 can also be used to verify Z_{Fail} guidelines based on the effective stress analysis. The channel bed is assumed to be cohesive since it is comprised of silty clay. The embankment is a mixture of silty sand SM and clayey sand SC. Table 23 indicates that Z_{Fail}/H under the condition of rapid drawdown to half slope height is 0.44 for the combination of cohesive channel bed with an SC embankment and H=6.2 m. As a result, the failure scour depth Z_{Fail} is 2.3 m, just below the observed scour at the left abutment (Table 29). Again, the validity of the effective stress analysis is confirmed by this case.

Table 29- Application 2 of failure scour guidelines to case no. 4

Abutment	H (m)	β (°)	Z (m)	Channel Bed Soil Type	Embankment Soil Type	Z_{Fail} (m)	Predicted Failure	Actual Failure
Right	5.3	26.6	1.7	Silty clay	SM-SC	2.3	NO	NO
Left			2.4				YES	YES

7.5 CASE NO.5: CR 309 over Rocky Creek

The channel bed undrained shear strength estimated from the TCP blow counts at the locations of the right and left abutments are used to apply Eqs. 6-2 and 6-3. Table 30 presents the resulting failure scour depths at the right and left abutments under complete and half drawdown conditions.

Table 30- Application 1 of failure scour guidelines to case no. 5

Abutment	H (m)	β (°)	Z (m)	S_{uc} (kPa)	Z_{Fail} (m) under complete rapid drawdown	Z_{Fail} (m) under half rapid drawdown	Predicted Failure	Actual Failure
Right	2	26.6	0	41.5	6.8	8.1	NO	NO
Left			0.9	28.7	4.2	5.1	NO	YES

For the application of the effective stress analysis guidelines, the channel bed soil, described as sandy clay, is assumed to be cohesive and the embankment is assumed to be SC. Table 23 with H=3.2 m gives Z_{Fail}/H=0.78, which translates to a failure scour depth of 1.56 m (Table 31).

Table 31- Application 2 of failure scour guidelines to case no. 5

Abutment	H (m)	β (°)	Z (m)	Channel Bed Soil Type	Embankment Soil Type	Z_{Fail} (m)	Predicted Failure	Actual Failure
Right	2	26.6	0	Sandy clay	SC	1.56	NO	NO
Left			0.9				NO	YES

Both analyses indicate that the failure of the left abutment is not a slope stability failure as the failure scour is greater than the observed scour at the left abutment. In fact, pictures of the failed abutment confirm that the abutment embankment did not experience a slope stability failure. However, the erosion of the embankment material itself formed large voids beneath the approach slab and exposed the drilled shafts at the abutment (Figure 50). This mode of failure is caused by the lateral erosion of the embankment soil rather than the vertical scour at the abutment toe. Therefore, preventing such failure can be achieved by appropriately protecting the embankment soils against erosion and not by limiting the scour depth at the abutment toe.

7.6 CASE NO.6: SH 105 over Rocky Creek

Table 32 presents the results of applying Eqs. 6-2 and 6-3 to this case. Table 33 presents the results of using Table 23 with H=6.2 m and the combination of cohesive channel bed and silty sand (SM) embankment. Both the effective and total shear stress guidelines underestimate the actual failure scour depth as the embankment slope β is 18.4° and not 26.6° as assumed in the analyses. The failure scour depth at the right abutment under rapid drawdown to half embankment height is 3.6 m by the total stress analysis and 2.35 m by the effective stress analysis.

In this case, both the total and effective analyses indicate that if the failure occurred at Z=1.2 m, it is attributed to erosion of the unprotected embankment soil rather than slope stability failure. A combination of both modes of failure is also possible. However, the reported scour depth of 1.2 m is estimated by the bridge inspector by recalling the case and looking and the pictures as measurements of the post-flood channel profile were not made.

Table 32- Application 1 of failure scour guidelines to case no. 6

Abutment	H (m)	β (°)	Z (m)	S_{uc} (kPa)	Z_{Fail} (m) under complete rapid drawdown	Z_{Fail} (m) under half rapid drawdown	Predicted Failure	Actual Failure
Right	4.9	18.4	1.2	31.9	> 2.4	> 3.6	NO	YES
Left	4.4		-	54.3	> 7.4	> 9.2	-	NO

Table 33- Application 2 of failure scour guidelines to case no. 6

Abutment	H (m)	β (°)	Z (m)	Channel Bed Soil Type	Embankment Soil Type	Z_{Fail} (m)	Predicted Failure	Actual Failure
Right	4.9	18.4	1.2	Clay with some sand	SM	> 2.35	NO	YES
Left	4.4		-			> 2.1	-	NO

7.7 CASE NO.7: US 90 over Nueces River

Although not all the required parameters are available, the case is used to apply Eqs. 6-4 and 6-5 as it is the only available case of a cohesive embankment on top of a cohesionless channel bed. For this purpose, two values of embankment undrained shear strength S_{ue}, both falling in the medium consistency range, are assumed: 30 kPa and 40 kPa. The failure scour depth under rapid drawdown from WL=100 percent to WL=50 percent is determined for each case as follows:

For S_{ue} = 30 kPa, $S_{ue}/\gamma H = 0.35 < 0.4$,

$$Z_{Fail} = 2.0\frac{S_{ue}}{\gamma} - 0.3H \qquad \text{(Eq. 6-4)}$$

$$Z_{Fail} = 1.71 \text{ m.}$$

For S_{ue} = 40 kPa, $S_{ue}/\gamma H$ =0.46> 0.4,

$$Z_{Fail} = 0.3H \quad \text{(Eq. 6-5)}$$

$$Z_{Fail} = 1.29 \text{ m.}$$

For both S_{ue} considered, the failure scour depth is below the observed scour of 2.1 m at the right abutment (Table 34). Consequently, the slope stability failure of the right abutment can be predicted by applying the Z_{Fail} guidelines for a cohesive embankment on top of a cohesionless channel bed.

Table 34- Application of failure scour guidelines to case no. 7

Abutment	H (m)	β (°)	Z (m)	Channel Bed type	S_{ue} (kPa)	Z_{Fail} (m)	Predicted Failure	Actual Failure
Right	4.3	26.6	2.1	Cohesionless (gravel)	30	1.7	YES	YES
					40	1.3	YES	

8. CONCLUSIONS AND RECOMMENDATIONS

8.1 Background Knowledge

Based on the literature review and the survey of the DOTs, the following conclusions are advanced:

- The review of existing soil and rock erosion tests reveals that the idea of the proposed Borehole Erosion Test is a novel idea.
- The maximum allowable scour depth needs to be incorporated in the states scour evaluation programs. The last step of the evaluation should compare the predicted scour depth to the maximum allowable scour depth to determine future action.
- The stability of the abutment is affected by both local abutment scour and contraction scour. Contraction scour is expected to be much higher than local abutment scour when the flow is severely contracted at the bridge section.
- The maximum allowable scour depth is based on the stability of the bridge piers and abutments, regardless of the scour process and the scour components involved.
- Most of the states have guidelines on the estimation of the maximum allowable scour depth at piers supported by deep foundations. In this case, the scour is limited to satisfy the foundation bearing capacity and lateral stability criteria. On the other hand, there is a lack of well-defined recommendations for allowable scour depth at abutments.
- Guidelines on maximum allowable scour at piers can be used to limit scour at vertical wall abutments where the abutment embankment is confined and protected against slope stability failures by the vertical and wing walls.

- Most of the abutments have spill through embankments where scour at/near the abutments affects not only the foundations stability but also the spill through slope stability. Therefore, guidelines on the maximum allowable scour depth at/near spill through abutments should satisfy the slope stability criterion in addition to the foundations structural stability criteria.
- The scour depth causing the slope stability failure of the spill through slope is known as the limiting scour depth or the geotechnical limit to scour because when this depth is reached and the slope fails, the flow area is increased and the extent and depth of scour is limited. A simplistic formulation of the geotechnical limit to scour has already been developed for uniform cohesionless soils based on the embankment equilibrium slope. Nonetheless, this limiting scour depth is found to be highly dependent on the embankment soil shear strength.
- Slope stability analyses using 2D limit equilibrium methods can be performed to develop guidelines for the determination of the maximum allowable scour depth at abutments while accounting for possible ranges of variables related to soil shear strength, abutment geometry, and hydraulic conditions.

8.2 The Borehole Erosion Test

A new in situ erosion test called the borehole erosion test or BET is proposed. It consists of circulating water in an open borehole using conventional drilling equipment and a set of calipers. The flow duration for each velocity is suggested to be 10 minutes. The lateral increase in diameter is recorded after each 10 minute flow period and a corresponding erosion rate is obtained as the

increase in radius divided by the time of flow application. By repeating the BET for different velocities, the erosion function is obtained point by point at any depth along the depth of the boring. Early tests are very encouraging. The comparison between the BET results and the EFA results indicates that comparable values are obtained; however further testing is desirable. The results of the numerical simulations indicate that the water flow becomes a steady flow after about 0.6 m above the drill bit for a 100 mm diameter borehole. They also show that the surface roughness can have a major impact on the interface shear stress and that the shear stress is about 10 times higher on the bottom of the borehole than it is on the walls of the borehole.

Future BET research should include additional BET tests while incorporating the lessons learned from the previous testing. The ultimate deliverable of the BET research would be a new and simple BET tool to facilitate the testing procedure. The tool to be developed records the increase in diameter of the borehole while measuring the drilling fluid velocity. In this way, the steps consisting of repeatedly taking out and placing back the drilling bit and rods and the mechanical caliper, after each fluid run, are avoided.

8.3 Case Histories of Bridges with Scour at Abutments

The study of sources and references of field scour measurements revealed many cases of bridge sites that have experienced abutment failure due to embankment washout and mass failures in Texas, Minnesota, and South Carolina. Therefore, such cases are not infrequent. However, failure case histories for which scour data were recorded are very scarce. This might be caused by the difficulties of accessing the bridge during a flooding event and by the pressing need to quickly repair and stabilize the abutment after a scour failure. In addition, accessible field scour databases are primarily established to verify the scour prediction equations based on the laboratory scour

data and to develop new prediction methods based on the field data. Since prediction equations for pier scour are more frequently used than those for abutment scour, most of the field data focus on pier scour. Indeed, FHWA does not require the abutment scour to be computed where appropriate scour protection measures are provided, which makes the validation of abutment scour prediction equations of a lesser importance. In addition, where field abutment scour investigations are performed, the reported parameters are limited to those needed for the application of the prediction equations being validated (i.e., hydraulic variables, mean grain size, and scour depth). Therefore, most of the cases do not present information on abutment geometry, scour location, shear strength parameters, and the water conditions in the channel. As a result, those cases could not be used to apply and validate the proposed guidelines for the determination of maximum allowable scour depths. For all these reasons, the collection of quality case histories was challenging.

Four sources of scour measurements near/at the abutments were found and studied. These are: NBSD, SCBSD, abutment scour data in Maine, and contraction scour data in Alabama. These four sources are not consistent with the way scour is reported. In the NBSD and Maine database, the abutment scour depth needs to be added to the average contraction scour depth to find the total scour depth at/near the abutment, whereas the contraction and abutment are considered mutually exclusive in the South Carolina and Alabama databases. Actually, the scour depth Z, of interest to our project, is the total depth of the scour hole at the abutment regardless the components (contraction or abutment) making up the scour. Therefore, the best way of finding Z is by using the channel cross-section measurements records of the bridge.

Seven case histories are presented and analyzed. Case No. 1 and Case No. 2 are NBSD cases for which the channel profiles are supplied. Cases No. 3–7 are cases of bridges in Texas for

which the required information is provided by TxDOT. Table 35 summarizes all the seven case histories and their parameters. All cases except for Case No. 2 experienced abutment failure.

The study of case histories revealed two possible modes of abutment embankment failures. The first is slope stability failure due to vertical scour near/at the abutment toe (Case 1, 3, 4, 7 and possibly 6), and the second is embankment soil washout due to lateral erosion of the embankment soil (Cases 5 and possibly 6). The two modes can occur simultaneously, especially in the case of unprotected abutment (Case 6). The end result is large voids under the bridge ends and ultimately the failure of the approach slab or first bridge span. The approach developed by this project considers the first failure mode and limit the vertical scour depth at/near the abutment to prevent a stability failure of the spill-through abutment.

In addition, the study of case histories showed the lack of characterizing and reporting the embankment and channel bed shear strengths at bridge sites. There is a great need to investigate strength parameters given their importance to the stability of spill-through abutments. This importance has already been recognized in the literature (Ettema et al., 2016; Ng et al., 2015; Feliciano Cestero et al., 2014; Wagner et al., 2006; Bennedict 2016). In particular, NCHRP project 24-14 (Wagner et al., 2006) stresses the importance of three properties of the stream bed soils affecting the resistance to erosion and mass failure:

- True cohesion: due to cementation and attractive forces between clay minerals.
- Apparent cohesion: due to suction or negative pore water pressure.
- Vegetation: providing a tensile reinforcement to the soil particles, developing suction in soils, and reducing pore water pressure.

These factors do not only affect the strength of the soil to resist failure but also influence the scouring process, particularly the location and the depth of the scour hole. Scour holes typically begin in unvegetated locations (areas shadowed by the bridge) or locations of coarse cohesionless soils (streambank toes located near the abutments in the zone of high-velocity flow). The scour then extends by undermining the stability and causing mass failures of the more erosion resistant soils layers.

As cohesion is proven to be the most important variable when analyzing the stability of the abutment exposed to scour, there will be a commensurate need to measure and record channel bed cohesion or any representative characteristic of the abutment embankments and channel bed at bridge sites. For bridge sites in Texas, TCP blow count are used to estimate the undrained shear strength of the channel bed S_{uc}. This estimation is not accurate as S_{uc} is not a soil property and S_{uc} values measured before construction are not representative of S_{uc} values during slope stability failure of the abutment embankment. For bridge sites retrieved from the NBSD, the description of soil type is used to estimate the effective cohesion of the channel bed. In both cases, no information on the embankment soil type or shear strength is available.

Table 35- Summary of the selected case histories

					Abutment Geometry			Scour Data			Channel Bed Info		Hydraulic Information
Case No.	**Bridge Name**	**State**	**Right/Left Abutment?**	**Failure?**	**H (m)**	**β (°)**	**Protection**	**Z (m)**	**D (m)**	**θ (°)**	**Soil type**	**Shear Strength**	**Flood event, WL**
1	CR 22 over Pomme De Terre River	MN	Left	No	5	26.6	Stone Riprap	0.46	0	-	SM	non-cohesive $\varphi'_c = 30°$	April 1997 Flood, WL=100%
1			Right	Yes				3.0	0	-			
2	SR 37 over James River	SD	Left	No	6.3	18.4	None	1.2	0	29.1	Sandy silt	mildly cohesive	April 2001 Flood, WL=81%
3	FM 692 over McGraw Creek	TX	Left	Yes	2.5	26.6	Concrete Riprap	2.3	0	-	SM	S_u=35.9 kPa	Hurricane Harvey
4	FM 937 over Montgomery Creek	TX	Left	Yes	5.3	26.6	Concrete Riprap	2.4	0	-	CL	S_u= 22.3 kPa	2013 Halloween Flood
4			Right	No				1.7	0	-		S_u= 51.1 kPa	
5	CR 309 over Rocky Creek	TX	Left	Yes	2.0	26.6	Concrete Riprap	0.9	0	-	CL	S_u= 28.7 kPa	2016 Tax Day Flood
6	SH 105 over Rocky Creek	TX	Right	Yes	4.9	18.4	None	1.2	0	-	CL	S_u= 31.9 kPa	2017 Tax Day Flood
7	US 90 over Nueces River	TX	Right	Yes	4.3	26.6	Concrete Riprap	2.1	0	-	Gravel	non-cohesive	1998 Flood

8.4 Maximum Allowable Scour Depth at Bridge Abutments

Current guidelines for maximum allowable scour are applicable only to piers as they are based on stability criteria of the bridge foundations. An additional criterion must be considered when limiting scour at abutments where scour may also affect the stability of the approach embankment. This is especially true in the case of spill-through abutments supported by deep foundations. As evident from case histories in Texas, scour at the abutment is expected to cause slope stability failure of the spill-through embankment before reaching the depth causing bearing capacity or lateral stability failure of the foundation. Equations and practical guidelines are developed for the determination of the maximum allowable scour depth at or near spill-through abutments based on the slope stability criteria of the abutment embankment.

The approach selected to develop practical guidelines for allowable scour depth is based on a combination of review of the existing knowledge, a DOT survey, study of case histories, analyses of different scour failure scenarios, and slope stability simulations accounting for possible ranges of influential variables. The proposed equations and guidelines are verified against collected case histories.

The review of existing knowledge proves that this research project is needed since very little information was found on allowable scour depths. The DOT survey identifies the current DOT practices about scour limits and shows the lack of well-defined recommendations for allowable scour depth at abutments. The analyses of possible scour failure scenarios result in four possible failure modes that a bridge can experience due to scour at its abutment: foundation failure due to vertical loading, foundation failure due to lateral loading, embankment slope failure, and lateral erosion of embankment soils. The controlling failure mode of bridge abutments in Texas is slope stability failure of the spill-through embankment. For this reason, over 50,000 slope stability

simulations are performed using two 2D limit equilibrium methods: Simplified Bishop method and Spencer method. A slope of 2H:1V is used for the abutment embankment and the three values are used for the total abutment height: 3.2 m, 6.2 m, and 8.7 m. Low bound ranges are assigned to the shear strength parameters of the different possible soil types composing the embankment and the channel bed. The scour depth at the abutment toe is increased until reaching the failure scour depth at which slope stability failure occurs. The failure scour depth is defined as the scour depth when the FS against slope stability reaches a value of 1. Failure scour depths at abutments with different geometries and soil types are found under the condition of rapid drawdown. As a result, linear relationships between failure scour depth and soil shear strength parameters are developed. Additionally, practical recommendations for the immediate determination of the scour limit at or near spill-through abutments as a function of the abutment total height, and embankment and channel bed soil types are established. Case histories of bridges with significant scour at the abutments are collected and used for the application and validation of the developed equations and proposed guidelines.

Because the analyses leading to the failure scour depth are based on conservative assumptions, the maximum allowable scour depth is taken to be equal to the failure scour depth. In other words, no FS is applied to the failure scour depth found from the analyses to give the maximum allowable scour depth that would be used to judge the criticality of the scour at bridge abutments. However, the resulting recommendations and guidelines do not account for the lateral erosion of the embankment soils nor for mender migration, which also cause slope instabilities and failures. Hence, when applicable, an FS needs to be applied on the proposed failure scour depths to obtain the maximum allowable scour depths accounting for the destabilizing effects of these

erosion processes. Alternatively, these processes can be prevented by protected the embankments soils against erosion and locating bridges outside meander migration zones.

Two types of analyses are performed to study the slope stability of the scoured abutment under sudden drawdown from top to half slope height, with undrained soils condition: an effective stress analysis and a total stress analysis.

The effective stress analysis leads to an equation for the low bound estimate of the failure scour depth, Z_{Fail}, as a function of the embankment and channel bed average effective cohesion, c'_{avg}, and average effective friction angle tangent, $(\tan\varphi')_{avg}$, and the total abutment height, H (Eq. 8-1).

$$Z_{Fail} = \frac{1.55\frac{c'_{avg}}{\gamma} - 0.1H}{1 - 1.55(\tan\varphi')_{avg}} \quad \text{(Eq. 8-1)}$$

where γ is the soil total unit weight assumed to be 20 kN/m^3 in the analysis. Eq. 8-1 is applicable for abutments having a total height H in the range of 3.2-8.7 m. It is based on the linear relationship between Z_{Fail}/H and $S/\gamma H$ (Figure 86), where S is the average effective stress along the failure surface.

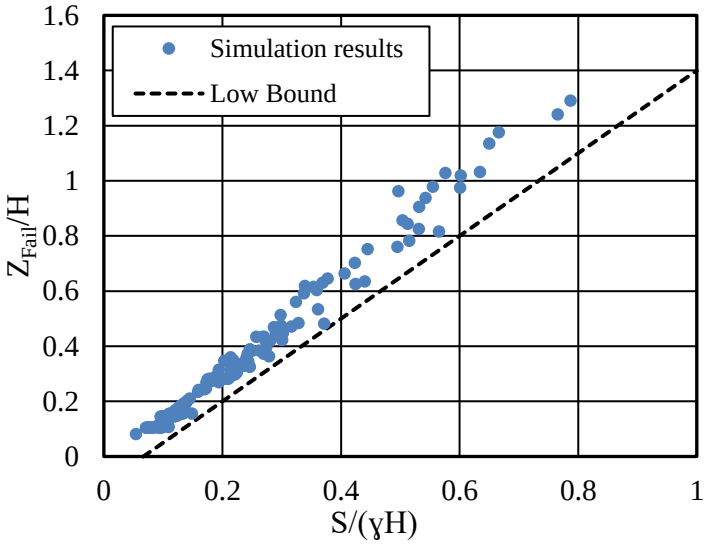

Figure 86- Effective stress analysis results

A successful application of Eq. 8-1 requires an accurate estimation of the effective shear strength parameters (c' and φ') of the abutment embankment and river channel bed. This makes the application of Eq. 8-1 unpractical. To avoid the need for laboratory testing, Z_{Fail}/H results are filtered and conservatively assigned to combinations of embankment and channel bed soil types (Table 36).

Table 36- Maximum allowable scour depth based on embankment height and soil type

Embankment Soil Type	**Channel Soil Type**	**Z_{Fail}/H**	
		H = 3.2 m	**H = 6.2 m**
Clayey sand, SC	Cohesionless	0.3	0.16
	Cohesive	0.78	0.44
Silty sand, SM	Cohesionless	0.32	0.24
	Cohesive	0.81	0.48

Overall, a reasonable and conservative estimate of the maximum allowed scour depth at abutments in Texas would be 0.24 times the embankment height. This corresponds to the case of an abutment having a total height of 6.2 m with a silty sand embankment fill on top of a cohesionless channel bed.

The total stress analysis leads to an equation for the low bound estimate of the failure scour depth, Z_{Fail}, as a function of the channel bed undrained shear strength, S_{uc}, and the abutment height H (Eq. 8-2):

$$Z_{Fail} = 4.7\frac{S_{uc}}{\gamma} - 0.8H \qquad \text{(Eq. 8-2)}$$

where γ is the soil total unit weight assumed to be 20 kN/m^3 in the analysis. Eq. 8-2 is applicable for abutments having a total height H in the range of 3.2-8.7 m, laying on a channel bed with undrained shear strength in the range 20-60 kPa. It is based on the linear regression of the simulation data points presented in Figure 87. Figure 87 shows that conservative maximum allowable scour depth of 0.24 times the embankment height, found by the effective analysis, falls well below the majority of the data points obtained from the total stress analysis.

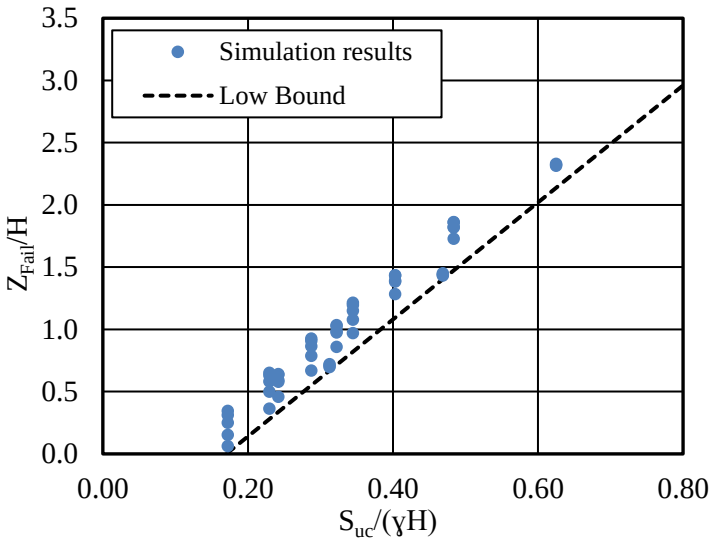

Figure 87- Total stress analysis results

In the case of an abutment embankment laying on a cohesionless channel bed, it is found that a low bound estimate of the failure scour depth, Z_{Fail}, can be estimated as a function of the embankment undrained shear strength, S_{ue}, and the abutment height, H (Eqs. 8-3 and 8-4):

For $S_{ue}/\gamma H \leq 0.4$,

$$Z_{Fail} = 2.0\frac{S_{ue}}{\gamma} - 0.3H \qquad \text{(Eq. 8-3)}$$

For $S_{ue}/\gamma H > 0.4$,

$$Z_{Fail} = 0.3H \qquad \text{(Eq. 8-4)}$$

where γ is the soil total unit weight assumed to be 20 kN/m^3 in the analysis. Eqs. 8-3 and 8-4 are applicable for an abutment having a total height H in the range of 6.2-8.7 m, and an embankment with undrained shear strength falling in the range 20-80 kPa laying on a sandy or gravelly channel bed. They are based on the linear regression of the simulation data points presented in Figure 88.

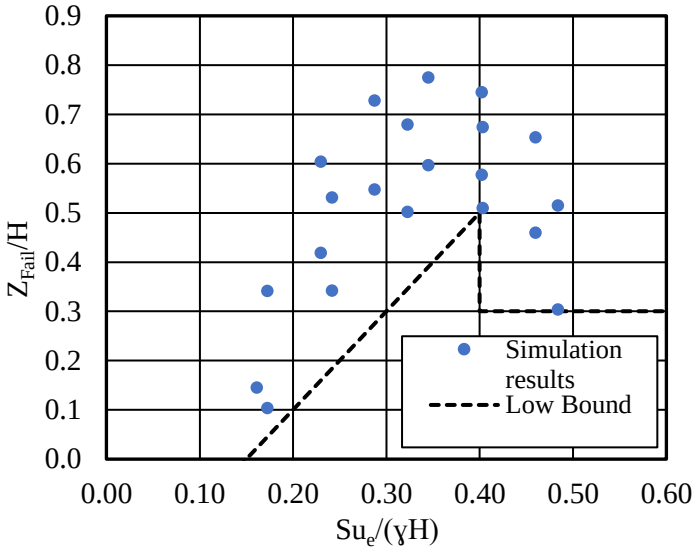

Figure 88- Total stress analysis results with cohesionless channel bed

The determination of soils undrained shear strength involves less complex testing than that of the effective shear strength parameters and can be done by field tests such as the Vane Shear Test or the TCP. However, undrained shear strength results are less reliable than those of drained shear strength. This is because the undrained shear strength is sensitive to many variables.

The results of the application of the guidelines from Eqs.8-1 through 8-4 are as good as the input shear strength parameters used in these equations. In the presence of estimates of both drained and undrained shear strength parameters, the equation using the parameter with the highest geotechnical confidence should be used to predict the maximum allowable scour depth. Eq. 8-1 is not be validated because information on the effective shear strength parameters of the embankment and the channel bed is not available for any of the collected cases. Alternatively to using Eq. 8.1, Table 36 is used to find conservative estimates of maximum allowable scour depth at abutments since it is based on low ranges of effective shear strength parameters for different embankment

and channel bed soil types. Where possible, the failure scour depth should be the lesser depth found by the application of the effective stress analysis guidelines (Table 36) and total stress analysis guidelines (Eqs. 8-2 through 8-4). Attention should be made when selecting the value of the undrained shear strength S_u to be used in Eqs. 8-2 through 8-4. The application of the guidelines to the collected case histories revealed that S_u values based on TCP testing before the bridge construction may overestimate the calculated failure scour depth (e.g., case 3). For this reason, it is recommended to perform Triaxial UU tests on partially saturated and fully saturated channel bed samples to estimate the reduction in S_u when the soil goes from the partially saturated state (before construction of the bridge, when the TCP was performed) to the fully saturated state (during the flood or during rapid drawdown).

In the absence of any data, 0.24H can be used as a quick conservative estimate of the maximum allowable scour depth at abutments with total height H. This limit falls under the failure scour depth results obtained from both the total and effective stress analyses. In addition, the limit of 0.24H is smaller than the actual failure scour depths observed in the collected case histories.

The proposed equations and guidelines for the determination of the maximum allowable scour depth are based on detailed slope stability analyses, yet are practical and easily used by bridge engineers and inspectors. They complement the existing guidelines on maximum allowable scour depth based on foundation stability criteria to determine. The maximum allowable scour depth satisfying both the foundation and the embankment stability criteria is compared to the measured or predicted total scour at the abutment, including contraction and local scour. Consequently, the criticality of the scour condition can be quickly evaluated and a plan of action can be implemented only if necessary.

The research findings also provide a geotechnical approach to improving scour prediction at abutments. The slope stability failure of the abutment embankment increases the flow area and relieves the flow. Therefore, the existing abutment scour prediction equations that ignore this geotechnical failure are likely to overestimate the scour depth at abutments. Scour depths predicted using these equations can be limited by a maximum depth equal to the failure scour depth determined following the proposed guidelines by this project.

Finally, the findings of the research on maximum allowable scout depth at abutments highlight the following research needs:

- Measurement and characterization of the abutment embankment and channel bed shear strength parameters are extremely important since these parameters are the basis for applying the proposed guidelines. The lack of information about the effective cohesion prevents the validation of Eq. 8-1 and makes its application impossible. Since cohesion is proven to be the most important variable when analyzing the embankment stability, there is a commensurate need to measure and record channel bed and embankment cohesion or any representative characteristic. There is also a need to measure the undrained shear strength of channel bed and embankment soils after the bridge construction and under saturated conditions. TCP results performed during the geotechnical investigation cannot be relied upon to estimate the channel bed undrained shear strength during sudden drawdown condition at the bridge. Having better estimates of shear strength parameters at bridge sites may improve the analyses and further refine the proposed guidelines that are currently based on low bound estimates of these parameters.
- In Texas, channel profile measurements are taken every two years at each bridge site as part of a routine inspection. The objective of this inspection is to compare channel profiles

from different years, evaluate scour, and detect potential scour problems. If the collected scour measurements at abutments are organized in a single database along with some other variables such as stability condition of the abutment embankments and the geometry, geotechnical and hydraulic parameters defined by this research, an envelope of failure scour depth can be developed based on the actual field measurements. Such envelope can be used to increase the confidence in the developed guidelines based on slope stability simulations.

- The relationship between the erosion of the embankment material and slope stability failure of the embankment should be investigated. This project assumes that the slope failure of the embankment is solely attributed to vertical scour at the abutment. In reality, the embankment slope stability failure can be accelerated by the erosion and washout of the embankment soils. Future research may address the combination of both vertical and lateral erosion processes to result in a maximum allowable scour depth at abutments accounting for the possibility of embankment soils erosion.
- A more accurate determination of the failure scour depths can be done if the conservatively assumed piezometric line is replaced by the actual distribution of pore pater pressure immediately after rapid drawdown. For the purpose of advancing the guidelines for maximum allowable scour depth at abutment, rigorous transient combined seepage and slope stability analyses can be investigated.
- Risk-informed guidelines for the maximum allowable scour depth at abutments can be developed by varying the allowable depth as a function of the bridge failure consequences.

REFERENCES

1. Arneson, L.A., Zevenbergen, L.W., Lagasse, P.F., and Clopper, P.E. (2012). "Evaluating scour at bridges." Hydraulic Engineering Circular No. 18, *Publication No. FHWA-HIF-12-003*, U.S. Dept. of Transportation, Federal Highway Administration, Washington, DC.
2. ASTM. (2006). "Standard Test Method for Identification and Classification of Dispersive Clay Soils by the Pinhole Test." *ASTM D4647-93*, West Conshohocken, PA.
3. Benahmed, S. and Bonelli S. (2012). "Internal erosion of cohesive soils: laboratory parametric study." *6th International Conference on Scour and Erosion*, SHF (Société Hydrotechnique de France), Paris.
4. Benedict, S. T. (2016). "Clear-water abutment and contraction scour in the Coastal Plain and Piedmont Provinces of South Carolina, 1996-99." US Department of the Interior, US Geological Survey, Reston, VA.
5. Bishop, A. W. (1955) "The use of the slip circle in the stability analysis of slopes." *Geotechnique*, 5(1), 7-17.
6. Bloomquist, D., Sheppard, D. M., Schofield, S., and Crowley, R.W. (2012). "The rotating erosion testing apparatus (RETA): A laboratory device for measuring erosion rates versus shear stresses of rock and cohesive materials." *Geotech. Test. J.*, 35(4). 641-648.

7. Briaud, J.-L. (1997). “The national geotechnical experimentation sites at Texas A&M University - Clay and sand: A Summary.” Zachry Dept. of Civil Engineering, Texas A&M Univ., College Station, TX.
8. Briaud, J.-L., Chen, H.-C., Chang, K.A., Oh, S.J., Chen, S., Chen, Wang, J., Li, Y., Kwak, K., Nartjaho, P., Gudaralli, R., Wei, W., Pergu, S., Cao, Y.-W., and Ting, F. (2011). “The Sricos – EFA method.” Summary Report, Texas A&M Univ., College Station, TX.
9. Briaud J.-L. (2008). “Case histories in soil and rock erosion: Woodrow Wilson Bridge, Brazos River Meander, Normandy Cliffs, and New Orleans Levees.”, J. Geotech. Geoenviron. Eng., 10.1061/(ASCE) 1090-0241 (2008) 134:10(1425), 1425-1447.
10. Briaud, J.-L. (2013). *Geotechnical engineering: Unsaturated and saturated Soil*, Wiley, New York.
11. Briaud J.-L. (2014). “Disclosure of invention: The borehole erosion test.”, *Rep. to the Intellectual Property Committee of the Texas Transportation Institute*, Texas A&M Univ., College Station, TX.
12. Briaud J.-L., Bernhardt M., and Leclair M. (2012). “The pocket erodometer test: Development and preliminary results.” *Geotech. Test. J.*, 35 (2), 342-352.
13. Briaud, J.-L., Chedid, M., Chen, H.-C., and Shidlovskaya A. (2017). “Borehole erosion test”. *J. Geotech. Geoenviron. Eng*., 143(8). http://doi.org/10.1061/(ASCE)GT.1943-5606.0001712.
14. Briaud, J.-L., Chedid, M., and Shidlovskaya A. (2016). “The borehole erosion test.” *Proc., 8th Int. Conf. on Scour and Erosion*, CRC Press/A.A. Balkema, Leiden, Netherlands, 12-15.
15. Briaud, J.-L., Chen, H.-C., Kwak, K., Han, S., and Ting, F. (2001a). “Multi-flood and multilayer method for scour rate prediction at bridge piers.” *J. Geotech. Geoenviron. Eng*., 10.1061/(ASCE) 1090-0241 (2001) 127:2(114), 114-125.

16. Briaud J.-L., Ting F., Chen H.C., Cao Y., Han S.-W., and Kwak K. (2001b), "Erosion function apparatus for scour rate predictions". *J. Geotech. Geoenviron. Eng.,* 10.1061/(ASCE) 1090-0241 (2001) 127:2(105), 105-113.
17. Chapuis, R. P., and Gatien, T. (1986). "An improved rotating cylinder technique for quantitative measurements of the scour resistance of clays." *Can. Geotech. J.*, 23(1), 83-87.
18. Chen, H.C. (2002). "Numerical simulation of scour around complex piers in cohesive soil." *Proc., First Int. Conf. on Scour of Foundations*, Texas Transportation Institute, Texas A&M Univ., College Station, TX, 14-33,
19. Chen, H.C., and Patel, V.C. (1988). "Near-wall turbulence models for complex flows including separation." *AIAA J.*, 26(6), 641-648.
20. Chen, H.C., Patel, V.C., and Ju, S. (1990). "Solutions of Reynolds-averaged Navier-Stokes equations for three-dimensional incompressible flows." *J. Comput. Phys.*, 88(2), 305-336.
21. Crowley, R. W., Bloomquist, D. B., Shah, F. D., and Holst, C. M. (2012). "The sediment erosion rate flume (SERF): A new testing device for measuring soil erosion rate and shear stress." *ASTM Geotech. Test. J.*, 35(4), 649-659.
22. Delphia, J. (n.d.). "Bridge Scour Coding and Documentation." [PowerPoint Slides]
23. Duncan, J. M., Wright, S. G., and Wong, K. S., 1990, "Slope Stability During Rapid Drawdown." H. Bolton Seed Symposium, Vol. 2, University of California at Berkeley, pp 253-272.
24. Ettema, R., Bergendahl, B. S., Yorozuya, A., and Idil-Bektur, P. (2016). "Breaching of Bridge Abutments and Scour at Exposed Abutment Columns." *J. Hydraul. Eng.*, 142(10).

25. Ettema, R., Nakato, T., and Muste, M. (2010). “Estimation of scour depth at bridge abutments.” National Cooperative Highway Research Program, *Final Report for NCHRP Project 24-20,* National Academy of Science, Washington, DC.
26. Feliciano Cestero, J. A., Imran, J., and Chaudhry, M. H. (2014). “Experimental investigation of the effects of soil properties on levee breach by overtopping.” *J. Hydraul. Eng.*, 141(4).
27. Federal Highway Administration. (2004). “National bridge inspection standards.” *23 CFR Part 650,* U.S. Dept. of Transportation, Washington, DC.
28. Federal Highway Administration. (1995). “Recording and coding guide for the structure inventory and appraisal of the nation's bridges,” *Report No. FHWA-PD-96-001,* U.S. Dept. of Transportation, Washington, DC.
29. Federal Highway Administration. (1991). “Evaluating scour at bridges.” *Technical Advisory T5140.23*, U.S. Dept. of Transportation, Washington, DC.
30. Fredlund, D. G., and Krahn, J. (1977). “Comparison of slope stability methods of analysis.” *Can. Geotech. J.*, 14(3), 429-439.
31. Gabr, M. A. (2014) “In situ erosion evaluation probe (ISEEP).” ⟨http://coastalhazardscenter.org/dev/wp-content/uploads/2012/05/GABR-ISEEP-2014-Annual-Meeting.pdf⟩ (May 20, 2016).
32. Gregory, G. (2018). GEOSTASE Program Manual.
33. Haas, C., Weissmann, J., and Groll, T. (1999). “Remote bridge scour monitoring: A prioritization and implementation guideline.” *Report No. TX-00/0-3970-1*, Texas Department of Transportation Research and Technology Transfer Section- Construction Division, Austin, TX.

34. Hanson, G. J. (1990). “Surface erodibility of earthern channels at high stresses. Part I – Open channel testing.” *Trans. ASAE*, 33(1), 127-131.

35. Hanson, G. J. and Cook, K. R. (2004). “Apparatus, test procedures and analytical methods to measure soil erodibility in situ”, *Appl. Eng. Agric*., 20(4), 455-462.

36. Holtz, R., and Kovacs, W. (1985). *An introduction to geotechnical engineering*. Prentice Hall, New Jersey.

37. Kim, H.S. and Chen, H.C. (2014). “Three-dimensional numerical analysis of sediment transport around abutments in channel bend.” *Int. Conf. on Coastal Engineering*, ASCE, Reston, VA.

38. Kim, H.S., Chen, H.C. and Briaud, J.L. (2016). “Numerical simulation of scour infilling in overset grid.” *8th Int. Conf. on Scour and Erosion*, CRC Press/A.A. Balkema, Leiden, Netherlands.

39. Kulhawy, F. H., and Mayne, P. W. (1990). “Manual on estimating soil properties for foundation design.” *Publication No. EPRI-EL-6800*, Electric Power Research Institute, Palo Alto, CA.

40. Lee, K. G., and Hedgecock, T. S. (2008). “Clear-water contraction scour at selected bridge sites in the Black Prairie Belt of the Coastal Plain in Alabama.” *Report No. 2007-5260*, US Geological Survey, Reston, VA.

41. Lefebvre, G., Rohan, K., and Douville, S. (1985). “Erosivity of natural intact structured clay: Evaluation.” *Can. Geotech. J*., 22(4), 508-517.

42. Loehr, E., Lutenegger, A., Rosenblad, B., and Boeckmann, A. (2016). “Geotechnical Site Characterization.” Geotechnical Engineering Circular No.5, *Report No. FHWA NHI-16-072,* U.S. Dept. of Transportation, Washington, DC.
43. Lombard, P., and Hodgkins, G. (2008). “Comparison of observed and predicted abutment scour at selected bridges in Maine.” *Report No. 08-04,* US Geological Survey, Reston, VA.
44. Lowe, J., and Karafiath, L. (1960). “Stability of earth dams upon drawdown.” *Proc., First Pan American Conf. on Soil Mechanics and Foundation Engineering,* Mexican Society of Soil Mechanics, Mexico D.F., pp 537-552.
45. McNeil, J., Taylor, C., and Lick, W. (1996). “Measurements of erosion of undisturbed bottom sediments with depth.” *J. Hydraul. Eng*., 10.1061/(ASCE) 0733-9429 (1996) 122:6(316), 316-324.
46. Melville, B., Van Ballegooy, S., Coleman, S., and Barkdoll, B. (2006). “Scour countermeasures for wing-wall abutments.” *J. Hydraul. Eng*., *132*(6), 563-574.
47. Minnesota Department of Transportation. (2009). “Bridge Scour Evaluation Procedure For Minnesota Bridges.” Minnesota Bridge Scour Task Force, MN.
48. Moody, L.F. (1944). “Friction factors for pipe flow.” *Trans. ASME,* 66(8), 671-684
49. Moore, W.L., and Masch, F.D. (1962). “Experiments on the scour resistance of cohesive sediments.” *J. Geophys. Res*., 67(4), 1437-1446.
50. Morgenstern, N. R., and Price, V. E. (1965). “The analysis of the stability of general slip surfaces.” *Geotechnique, 15*(1), 79-93.
51. Mueller, D. S., and Wagner, C. R. (2005). “Field observations and evaluations of streambed scour at bridges.” *Publication No. FHWA-RD-03-052*, U.S. Dept. of Transportation, Federal Highway Administration, Washington, DC.

52. Mueller, D. S., and Hitchcock, H. A. (1998). "Scour measurements at contracted highway crossings in Minnesota, 1997." Proc., *1998 International Water Resources Engineering Conf.*, Part 2 (of 2) pp. 210-215.

53. Munson, B.R., Young, D.F., Okiishi, T.H., and Huebsch, W.W. (2009). *Fundamentals of fluid mechanics*, Wiley, New York.

54. Naval Facilities Engineering Command. (1982). "Foundations and Earth Structures." *Design Manual DM-7.02*, Dept. of the Navy, Alexandria, VA.

55. Ng, K., Ettema, R., Kempema, E., Chakradhar, R., and Fuller, J. (2015). "Geotechnical limit to scour at spill-through bridge abutments: Laboratory investigation." *Report No. MPC-15-280*, Mountain-Plains Consortium, Dept. of Civil and Architectural Eng., Univ. of Wyoming, Laramie, WY.

56. Patel, V. C., and Yoon, J.Y. (1995). "Application of turbulence models to separated flow over rough surfaces." *J. Fluid Eng.*, 117(2), 234-241.

57. Pontaza, J.P., Chen, H.C., and Reddy, J.N. (2005). "A local-analytic-based discretization procedure for the numerical solution of incompressible flows." *Int. J. Numer. Methods Fluids*, 49(6), 657-699.

58. Roberts, J. D., Jepsen, R.A., and James, S.C. (2003). "Measurements of sediment erosion and transport with the adjustable shear stress erosion and transport flume." *J. Hydraul. Eng.*, 10.1061/(ASCE) 0733-9429 (2003) 129:11(862), 862-871.

59. Shan, H., and Kerenyi, K. (2014). "Scour in cohesive soils.", *Proc., National Hydraulic Engineering Conf.*, Federal Highway Administration, Washington, DC.

60. Shan, H., Shen, J., Kilgore, R., and Kerenyi, K. (2015). "Scour in cohesive soils." *Publication No. FHWA-HRT-15-033*, U.S. Dept. of Transportation, Federal Highway Administration, Washington, DC.
61. Sorensen, K. K., and Okkels, N. (2013). "Correlation between drained shear strength and plasticity index of undisturbed overconsolidated clays." *Proc., 18th International Conf. on Soil Mechanics and Geotechnical Engineering*, Paris, pp. 1-6.
62. Spencer, E. (1967). "A method of analysis of the stability of embankments assuming parallel inter-slice forces." *Geotechnique*, *17*(1), 11-26.
63. Sturm, T., Melville, B.W., and Ettema, R. (2011). "Evaluation of bridge-scour research: Abutment and contraction scour processes and prediction." National Cooperative Highway Research Program, *Final Report for NCHRP Project 24-27(02)*, Transportation Research Board, Washington, DC.
64. Texas Department of Transportation. (2018). "Geotechnical manual." Texas Dept. of Transportation Bridge Division, Austin, TX.
65. Texas Department of Transportation. (2014). "Standard specifications for construction and maintenance of highways, streets, and bridges."
66. Texas Department of Transportation. (1993). "Texas secondary evaluation and analysis for scour (TSEAS)." Texas Bridge Scour Program, Division of Bridges and Structures, Austin, TX.
67. Trammell, M. (2004). "Laboratory apparatus and methodology for determining water erosion rates of erodible rock and cohesive sediments". M.S. thesis, Dept. of Civil Engineering, Univ. of Florida, Gainesville, FL.

68. U.S. Bureau of Reclamation. (1987). "Design of small dams." *Water Resources Technical Publication*, US Dept. of the Interior, Washington, DC.

69. US Geological Survey. "National Bridge Scour Database." Accessible through https://water.usgs.gov/osw/techniques/bs/BSDMS/BSDMS_1.html.

70. USSD (U.S. Society on Dams). (2011). "21st century dam design- Advances and adaptations." *Proc., 31st Annual USSD Conf.*, U.S. Society on Dams, Denver, 1023-1032.

71. Wagner, C. R., Mueller, D. S., Parola, A. C., Hagerty, D. J., and Benedict, S. T. (2006). "Scour at contracted bridges." National Cooperative Highway Research Program, *Final Report for NCHRP Project 24-14*, Transportation Research Board, Washington, DC.

72. Wahl, T. L. (2010). "A comparison of the hole erosion test and jet erosion test." *Joint Federal Interagency Conf. on Sedimentation and Hydrologic Modeling*, Advisory Committee on Water Information, Washington, DC.

73. Wan, C.F., and Fell, R. (2004). "Investigation of rate of erosion of soils in embankment dams." J. Geotech. Geoenviron. Eng., 10.1061/(ASCE) 1090-0241 (2004) 130:4(373), 373-380.

74. Wright, S. G., and Duncan, J. M. (1987). "An examination of Slope stability computation procedures for sudden drawdown." *Miscellaneous Paper GL-87-25*, U. S. Army Engineer Waterways Experiment Station, Vicksburg, MS.

75. Yorozuya, A., and Ettema, R. (2015). "Three abutment scour conditions at bridge waterways." *J. Hydraul. Eng.*, *141*(12), 04015028.

APPENDIX

SURVEY RESPONSES

Table 37- Maximum allowable abutment scour depth

State / Answer	Mentioned site-specific factors	Foundation exposure	Piles embedment length	Roadway embank-ment	Damage to abutment protection features	Abutment protection per HEC-23 without scour evaluation
Alaska	risks and vulnerabilities, structure stability			☑ erosion		
California	structure stability	☑any footing exposure	☑			
Colorado	foundation depth	☑				
Delaware	piles length, sheeting, scour history, streambed material	☑substantial exposure of footing	☑			
Illinois	structure stability					
Indiana						☑
Iowa						☑
Maine	stream material, potential to flood	☑footing bottom exposed				
Maryland		☑footers exposed				
Michigan	footing type, pile depth, debris, geotechnical conditions					
Missouri	abutment and embankment stability			☑stability		☑
Nebraska			☑ 2/3 down the length of the steel sheet pile			
New Mexico		☑ bottom exposed	☑	☑erosion	☑	
New York		☑footing bottom exposed, scour not addressed previously and top exposed			☑	
Ohio	action is taken when hole threatens the bridge					
Oklahoma	subjective evaluation by the hydraulic engineer					
Pennsylvania	foundation type	☑>20% of the length of the footing or >20% of the area under the footing	☑			
Rhode Island						
South Dakota	structure/abutment details	☑piling or spread footing on the verge of exposure				
Utah		☑				
Virginia	case-by-case analysis					

Table 37- Continued

State / Answer	Mentioned site-specific factors	Foundation exposure	Piles embedment length	Roadway embank-ment	Damage to abutment protection features	Abutment protection per HEC-23 without scour evaluation
Wyoming	foundation type and depth	☑				
Vermont		☑moderate undermining of footing				
Wisconsin	foundation type, soil characteristics	☑		☑stability and erosion	☑	
Wyoming	foundation type and depth	☑				

Table 38- Maximum allowable contraction scour depth

State / Answer	Same as answer#1	Total scour depth triggering action	Take action only when contraction scour impacts abutments or piers foundations	Contraction scour classified as either abutment or pier scour
Alaska	☑			
California	☑			
Colorado	☑			
Delaware	☑			
Illinois	☑			
Indiana		☑within 10ft. of the pile tip		
Iowa		☑exceeding 50% of pile embedment under footing or maximum unbraced length for pile bent		
Maine	☑			
Maryland	☑			
Michigan	☑			
Missouri	☑			
Nebraska	☑			
New Mexico			☑	☑
New York				☑
Ohio	☑			
Oklahoma	☑			
Pennsylvania	☑			
Rhode Island	☑			

Table 38- Continued

State / Answer	Same as answer#1	Total scour depth triggering action	Take action only when contraction scour impacts abutments or piers foundations	Contraction scour classified as either abutment or pier scour
South Dakota			☑if contraction scour is "considerable," protection is provided well before foundation exposure.	
Utah	☑			
Virginia	☑			
Vermont			☑	
Wisconsin	☑			
Wyoming			☑	

Table 39- Maximum allowable pier scour depth

State / Answer	Same as answer#1	Same as answer#2	Allowable pier scour depth
Alaska			☑maximum scour depth such as embedment depth is at least equal to 3*ls where ls can be calculated using the 5th Root equation for granular soils (ls=1.8*(EI/nh)^(1/5)
California	☑		
Colorado	☑		
Delaware	☑		
Illinois	☑		
Indiana		☑	
Iowa		☑	
Maine	☑		
Maryland	☑		
Michigan	☑		
Missouri			☑for pile cap bents: least (depth causing maximum unsupported length, depth causing minimum pile embedment depth) for pile footings: depth exposing the piles
Nebraska			☑scour depth below the braced point on the pier pile
New Mexico			☑for shallow pier foundation: depth exposing the footing for deep foundation piers: depth reducing the embedment length to around 5 ft.

Table 39- Continued

State / Answer	Same as answer#1	Same as answer#2	Allowable pier scour depth
New York	☑		
Ohio	☑		
Oklahoma	☑		
Pennsylvania	☑		
Rhode Island	☑		
South Dakota	☑		
Utah	☑		
Virginia	☑		
Vermont	☑		
Wisconsin			☑depth exposing the piles on non-pile bent foundations
Wyoming	☑		

Table 40- Additional information and references

State	Answer
Alaska	FHWA online hydraulics publications
California	NONE
Colorado	CO specific guidance, sent over mail
Delaware	N/A
Illinois	http://www.idot.illinois.gov/Assets/uploads/files/Doing-Business/Manuals-Guides-&-Handbooks/Highways/Bridges/Inspection/Structural%20Services%20Manual%202015.pdf
Indiana	http://www.in.gov/indot/design_manual/files/Part_2_2013.pdf
Iowa	No answer
Maine	No answer
Maryland	There is no set standard depth that would apply to all structures
Michigan	Respondent skipped this question
Missouri	NA
Nebraska	N/A
New Mexico	No answer
New York	All of our new or replacement bridges require piles unless founded on bedrock. We also protect all new or replacement bridges with stone protection.
Ohio	N/A

Table 40- Continued

State	Answer
Oklahoma	I can upload our countermeasure book to Box for you if you would like. Please email me a request at llewis@odot.org
Pennsylvania	1. Pub 238, Bridge Safety Inspection Manual: http://www.dot.state.pa.us/public/PubsForms/Publications/PUB%20238.pdf 2. Bridge Management System 2 (BMS2) Coding Manual: http://www.dot.state.pa.us/public/PubsForms/Publications/PUB%20100A.pdf
Rhode Island	No answer
South Dakota	The structure response to scour varies widely from site to site depending on many variables in foundation and substructure details. In addition, the site hydraulics and subsurface materials vary widely in SD, making a standard scour depth triggering action difficult, if not impossible, to determine.
Utah	FHWA Recording and Coding Guide for the Structure Inventory and Appraisal of Nation's Bridges. UDOT Bridge Management Manual.
Virginia	N/A
Vermont	We use the standards FHWA documents, HEC18, HEC20, and HEC23.
Wisconsin	None.
Wyoming	Nothing to share.